Government of **Western Australia**
Department of **Mines and Petroleum**

RECORD 2014/16

STRUCTURAL EVOLUTION OF THE YALGOO DOME, YILGARN CRATON, WESTERN AUSTRALIA: A CORE PERSPECTIVE

by
Michael James Fenwick



Geological Survey of Western Australia

Government of **Western Australia**
Department of **Mines and Petroleum**

Record 2014/16

STRUCTURAL EVOLUTION OF THE YALGOO DOME, YILGARN CRATON, WESTERN AUSTRALIA: A CORE PERSPECTIVE

by

Michael James Fenwick

MONASH University

Perth 2014

Geological Survey of Western Australia

MINISTER FOR MINES AND PETROLEUM
Hon. Bill Marmion MLA

DIRECTOR GENERAL, DEPARTMENT OF MINES AND PETROLEUM
Richard Sellers

EXECUTIVE DIRECTOR, GEOLOGICAL SURVEY OF WESTERN AUSTRALIA
Rick Rogerson

REFERENCE
The recommended reference for this publication is:
Fenwick, MJ 2014, Structural Evolution of the Yalgoo Dome, Yilgarn Craton, Western Australia: A Core Perspective: Geological Survey of Western Australia, Record 2014/16, 93p.

National Library of Australia Card Number and ISBN 978-1-74168-602-9

Grid references in this publication refer to the Geocentric Datum of Australia 1994 (GDA94). Locations mentioned in the text are referenced using Map Grid Australia (MGA) coordinates, Zones 50 and 51. All locations are quoted to at least the nearest 100 m.

About this publication
This Report is an Honours thesis researched, written and compiled through an ongoing collaborative project between the Geological Survey of Western Australia (GSWA) and Monash University, Victoria. Although GSWA has provided field support for this project, the scientific content of the Record, and the drafting of figures, has been the responsibility of the author. No editing has been undertaken by GSWA.

Published 2014 by Geological Survey of Western Australia
This Record is published in digital format (PDF) and is available online at <www.dmp.wa.gov.au/GSWApublications>.

Further details of geological products and maps produced by the Geological Survey of Western Australia are available from:
Information Centre
Department of Mines and Petroleum
100 Plain Street
EAST PERTH WESTERN AUSTRALIA 6004
Telephone: +61 8 9222 3459 Facsimile: +61 8 9222 3444
www.dmp.wa.gov.au/GSWApublications

Structural Evolution of the Yalgoo Dome, Yilgarn Craton, Western Australia: A Core Perspective

Michael James Fenwick

School of Earth, Atmosphere and Environment

Monash University

Submitted as a requirement for the fulfilment of a Bachelor of Science Honours Degree,

Monash University

Submitted October 31st 2014

TABLE OF CONTENTS

DECLARATION

This thesis contains no material which has been accepted for the award of any other degree or diploma in any university and that, to the best of the candidate's knowledge and belief, the thesis contains no material previously published or written by another person, except when due reference is made in the text.

Signature: Date:

ACKNOWLEDGEMENTS

My sincere thanks and appreciation are extended to

Prof. Roberto Weinberg for guidance and contributions as a supervisor and for introducing me to the intricate world of migmatites.

Dr Ivan Zibra for support and guidance in the field, and continued support at the Geological Survey.

Fred Clos

Aaron Tomkins

The Geological Survey of Western Australia

Thankyou to my fellow honours colleagues.

Thankyou to Monash University, School of Earth, Environment and Atmosphere staff in particular Dr. Massimo Raveggi, Junnel Alegado and Dr. Rachelle Pierson for assistance in the laboratory.

STRUCTURAL EVOLUTION OF THE YALGOO DOME, YILGARN CRATON, WESTERN AUSTRALIA: A CORE PERSPECTIVE

M.J. Fenwick[1]

[1]*School of Earth, Atmosphere and Environment, Monash University, Victoria 3800, Australia*

ABSTRACT

How Archean granite domes form is a key question in understanding Archean tectonic processes. The Yalgoo Dome is a 90 x 30km Archean granitic dome in the North East Murchison province consisting of a 2.96 Ga migmatitic tonalite core surrounded by a 2.65 Ga monzogranite mantle. The dome is flanked by 2.95 Ga greenstone belts. This study focuses on the structural evolution of the older migmatitic tonalite core. Previous studies proposed broad scale dome formation models including fold interference and diapirism, and only briefly considered how the older core was emplaced. Magnetic anomalies in a geophysical image of the core define a large scale fold with a northern apex. Detailed structural mapping was conducted in three domains that correspond to a hinge zone and two limb zones of the large scale fold. The N-S axial planar foliation of the large scale fold overprints two earlier foliations that formed during emplacement. The earliest fabric recognisable in the migmatitic tonalite is melanocratic leucocratic banding formed through water-fluxed partial melting of a tonalite protolith. The migmatitic tonalite was then subject to a diapiric ascent phase indicated by a pervasive radially distributed sub-vertical stretching lineation, sheath folds with a sub-vertical solid-state axial planar foliation, and variations in migmatite morphology that can be correlated to strain regimes in an ascending diapir. An E-W compressional event subsequently folded the two early foliations and formed the large scale fold.

KEY WORDS: Archean, granite-greenstone, Yalgoo dome, tonalite, migmatite, sheath fold, diapirism.

1. INTRODUCTION

Granite-greenstone terranes are characteristic of Archean cratons but are rare in younger parts of the crust. The broad, elliptical granite bodies surrounded by linear synclinal greenstone belts lack a modern analogue, and their origin is an evolving discussion amongst researchers (Van Kranendonk et al., 2004). The debate is categorised into two opposing principles: "uniformitarianism" describes models that are consistent with today's notion of plate tectonics of crustal growth through horizontal accretion and collision (De Wit, 1998). Non-uniformitarianism describes processes distinct from modern styles and explains crustal growth through mechanisms that operated in the hotter Archean

geodynamic environment (Condie and Benn, 2006; Gerya, 2014). This principle focuses on vertical tectonics, and prescribes models that incorporate diapirism and convective overturn (Collins et al., 1998; Van Kranendonk et al., 2007).

On average Archean crust is composed of 90% granitoid gneiss and granite and 10% greenstone rocks (Goodwin, 1996). Identifying how granite became emplaced within greenstone belts is therefore the key to understanding Archean tectonic processes. The Yilgarn Craton of Western Australia displays a typical Archean granite-greenstone pattern (Fig. 1.1A). The origin of granite-greenstone terranes within the Yilgarn have been explained through a number of mechanisms, including interference folding (Myers and Watkins, 1985), crustal extension and metamorphic core complexes (Williams and Whitaker, 1993; Swager and Nelson, 1997; Rosenbaum et al., 2008), and diapirism (Archibald et al., 1978; Gee, 1979).

The Yalgoo Dome is an elliptical Archean granitic dome in the northeast Murchison Province of the Yilgarn Craton (Fig. 1.1B). It is approximately 90 x 30km, and composed of an inner core of migmatitic tonalite orthogneiss surrounded by a monzogranite mantle (Fig. 1.1B). Synclinal greenstone belts flank the dome and host base metal deposits (e.g. Gold Grove Fig 1.1B)(Refer to section 2: Local geology for a detailed description). The dome is a well-exposed complex and provides a particular relevant case study for testing models of granite emplacement. Three studies have been completed on the dome, resulting in two contrasting models. The first study by Myers and Watkins (1985) proposed an uniformitarian model. Foley (1997) proposed an alternate non-uniformitarian model, which was further substantiated by Caudery (2013).

Myers and Watkins (1985) explained the dome was the result of superposed folding, consisting of two perpendicular compression events. Their model was based on observations of large- and small-scale dome-and-basin interference patterns (type-one of

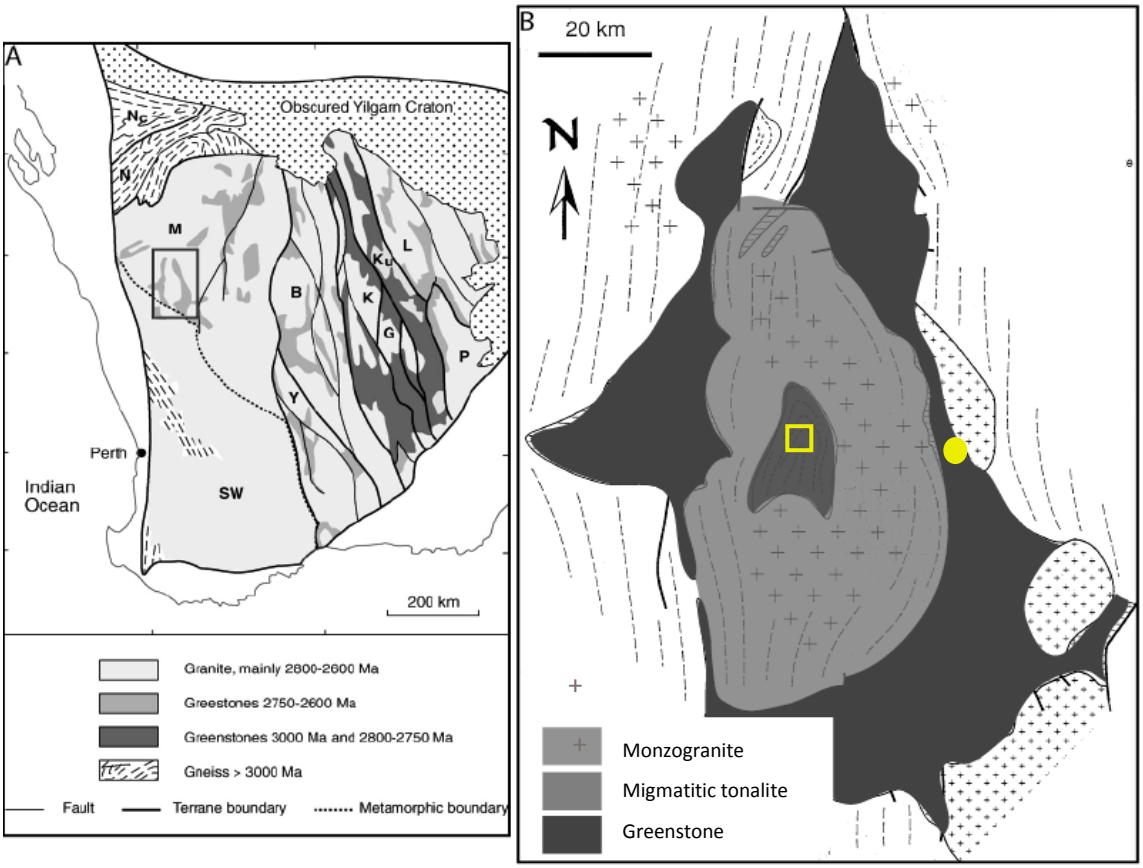

Figure 1.1: A) Yilgarn Craton: The Yalgoo dome is in the grey square Modified from Chen et al., (2003) **B)** Simplified lithological map of the Yalgoo Dome: white areas are granite bodies outside of the dome. Yellow square: core mapping area of Myers & Watkins (1985) (Figure 1.2), Yellow circle: Golden Grove base metals deposit and greenstone geochronology site. Modified from Watkins & Hickman (1990).

Ramsay 1980) in the migmatitic core of the dome (Fig. 1.2). They also suggested greenstone rafts in the core might be analogous to an older volcanic sequence found in greenstones belts that flanks the dome. They explained D3 upright folds with a N-S axial hinge overprinted D2 upright folds with an E-W axial hinge. These observations for the Yalgoo dome led them to apply a fold interference model to the entire Yilgarn craton.

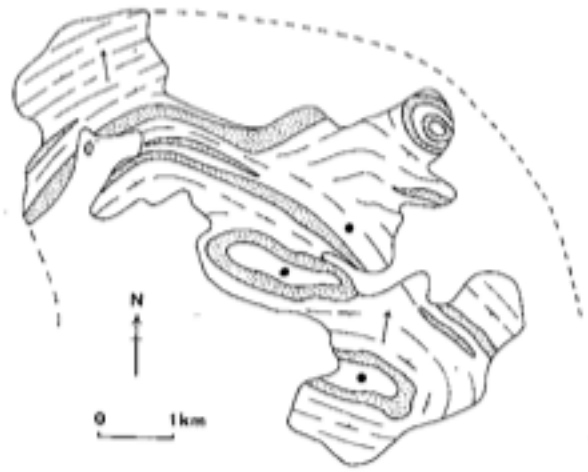

Figure 1.2: Map of core area from Watkins and Myers (1985) (area corresponds to the yellow box in Figure 1.1B). Grey bands are greenstone and BIF rafts, dashed white is migmatitic tonalite. Circular greenstone rafts were interpreted as dome-and-basin interference patterns. The central elliptical greenstone raft was remapped during this study (Refer to section 5.2: Central Domain).

Foley (1997) conducted a more detailed structural investigation close to the granite-greenstone margin of the Yalgoo dome. His study found internal fabrics of the granite dome trend parallel to the greenstone margin. This contradicts Myers & Watkins (1985) hypothesis because the fold interference model predicts axial planar foliations will be continuous through the granite-greenstone contact. He also observed a sub-vertical stretching lineation near the greenstone margin and interpreted it to represent the downward displacement of greenstones relative to granitoids. Foley (1997) proposed a diapiric model for the Yalgoo dome and included a brief explanation of the *'migmatite core',* suggesting a number of alternatives for its formation:

a) The result of the rising tail of a diapir
b) A sagducted triple point between minor uprising granitoid plutons
c) Partially convected greenstones drawn in by convective flow
d) A product of thicker greenstone crust where melt has not fully penetrated

Caudery (2013) found the dome-and-basin interference patterns were the result of sheath folding during an early deformation event. A N-S foliation was observed overprinting dome-and-basin patterns described in Myers and Watkins (1985). Caudery (2013) concluded that the patterns could not have formed form fold interference.

In 2013, the Geological Survey of Western Australia (GSWA) conducted a preliminary U-Pb SHRIMP geochronology analysis on the granitoids of the dome and confirmed that the inner core is older than the outer monzogranite mantle (Fig. 1.1B). The crystallisation age of the migmatitic tonalite protolith from the core was interpreted to be 2960 +/- 10Ma and crystallisation age of the monzogranite mantle was interpreted to be 2749 +/- 4Ma. Formation of the original tonalite core was followed by a hiatus of ~150Ma in intrusive activity. Geochronology information was not available to Foley (1997) and the implications of the 150Ma hiatus between emplacement of the inner core and the

surrounding granitoids were not considered.

In the aeromagnetic images of the Yalgoo dome and surroundings (Fig. 1.3), there are a number of smaller anomalies that are confined to the migmatitic tonalite core (Fig. 1.3B). The distribution of anomalies resembles a large-scale fold with a N-S trending axial plane and with limbs in the east and west (Fig. 1.3C). These high magnetic responses correspond to the greenstone and BIF lenses mapped by Myers and Watkins (1985) (Fig. 1.2).

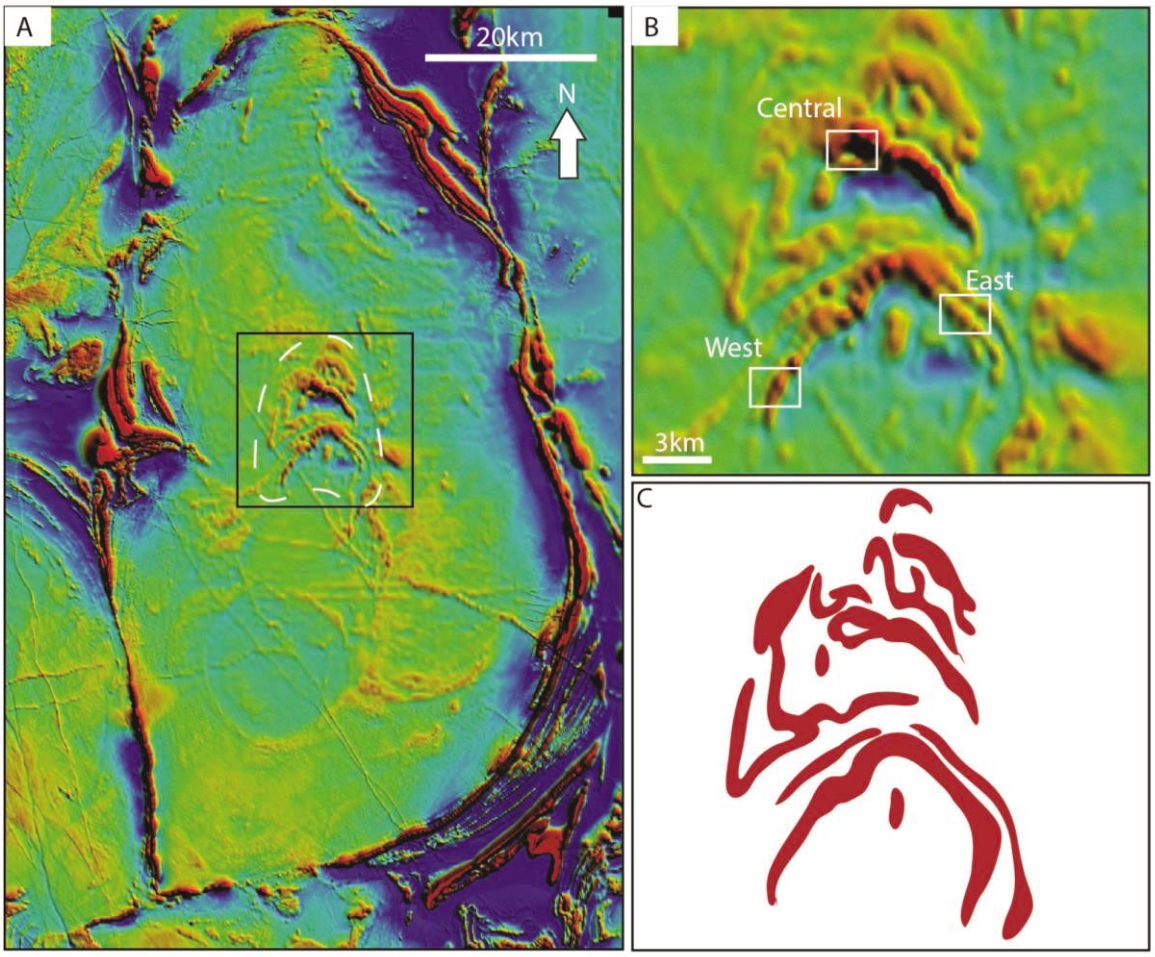

Figure 1.3: A) Aeromagnetic image of the Yalgoo dome from the 2013 GSWA geophysical survey: greenstone belts are clearly distinguishable by their strong red magnetic response. The monzogranite and migmatitic tonalite have a lower response, and are blue and yellow. The white dashed line is the approximate boundary between the migmatitic tonalite core and the monzogranite mantle (from Fig. 1.1B). **B)** Zoom in of A). The study area was divided into 3 domains indicated by the white boxes. The central domain corresponds to Figure 1.2 previously mapped by Myers and Watkins (1985). **C)** Schematic representation of B) highlighting magnetic anomalies defining a large-scale fold. The three domains mapped here were chosen to represent the two limbs and hinge a zone of this fold pattern.

This study revisited the Yalgoo dome to investigate the structural origin of the 2950Ma core. Detailed structural mapping was conducted in three domains corresponding to a different structural part of the large-scale fold interpreted on the aeromagnetic image (Fig. 1.3): a western 'limb', a central 'hinge', and an eastern 'limb'. A detailed description of lithologies is first presented, followed by a detailed description of three early deformation fabrics. These descriptions apply to the entire study area because deformation fabrics and rock lithologies are similar in each domain. We then describe the structural characteristics of each domain and draw on field observations to explain how the early deformation fabrics were formed. Our observations are then tied together to propose a structural history of the core. A collation of maps and structural data for each study area is provided in Appendix 2.

2. LOCAL GEOLOGY

Synclinal greenstone belts flank the dome to the east, west and south (Fig. 1.1B). They are composed of two stratigraphic sequences that are separated by an unconformity. The lower sequence is a thick succession of felsic and intermediate volcanics, felsic volcaniclastic and chemical sedimentary rocks. The upper sequence is composed of banded iron formation (BIF) and volcaniclastics. The upper package has been dated (U-PB SHRIMP) at 2945+/- 4Ma and 2809+/-5Ma in the Golden Grove area (Fig. 1.1B)(Van Kranendonk et al., 2013, Watkins & Hickman 1990)

A monzogranite mantle separates the core from the greenstone belts. It is composed of three distinct textural types: porphyritic, medium grained equigranular and fine-grained equigranular. Numerous felsic dykes cross-cut the monzogranite (Caudery 2013).

The core of the dome consists of migmatitic tonalite intruded into BIF and amphibolite units (greenstone sequence)(Myers & Watkins 1985). It is around 20 x 20km and has an arch shape with an apex to the north. A geochronology analysis on core

greenstones has not been performed, however similar interbedded amphibolite and BIF sequences occur in the greenstone belts surrounding the dome (Myers & Watkins 1985; Watkins and Hickman, 1990), which have been analysed by the Geological Survey of Western Australia. U-Pb SHRIMP analysis of zircons from a meta-dacite sample (203701) interlayered with these rock types yielded a crystallisation age of 2958Ma +/- 6Ma, not unlike the ages of the tonalite core.

3. NATURE AND TERMINOLOGY OF PARTIALLY MOLTEN ROCKS

We use the nomenclature set out in Sawyer (2008) to describe migmatitic tonalite. A migmatite is comprised of a 'neosome' and a 'paleosome'. The neosome is formed through partial melting of a rock (protolith). The 'paleosome' remains unaffected by partial melting and preserves structures that are older than the melting event. The neosome is further divided into a leucosome and melanosome. The leucosome is lighter coloured and derived from the segregation of partial melt, it consists predominantly of quartz and feldspars. The melanosome (residuum) is the darker coloured, solid residual fraction remaining after the segregation of partial melt. It consists of more mafic minerals such as biotite and hornblende. If the rock preserved its coherence during partial melting, the migmatite is called a 'metatexite' migmatite. A 'diatexite' migmatite refers to a rock that has lost its coherence during melting and started to flow 'en masse' as a magma, and is dominated by leucosome, with melanosome present as narrow rafts and 'ghost like' schlieren, or lost altogether.

During early stages of partial melting, the rock remains coherent and the solid framework of interlocking grains accommodates deformation. As partial melting progresses the rock becomes weaker and viscosity decreases because continuity of the solid framework is lost. Deformation becomes accommodated by the liquid (melt) phase. The change from dominantly solid phase deformation to liquid phase deformation marks

the transition from metatexite migmatite to diatexite migmatite.

4. LITHOLOGIES

The core is defined by a large migmatitic tonalite body that hosts rafts and xenoliths of greenstone (Fig. 1.1 & 1.2). 70% of rock outcrops are composed of migmatitic tonalite orthogneiss (migmatitic tonalite) with distinctive melanocratic-leucocratic banding (Fig. 4.1A). The remaining 30% is composed of greenstone rafts and xenoliths of amphibolite and metamorphosed banded iron formation (BIF)(Fig 4.1B,C). Outcrops exhibit various degrees of weathering from large fresh platforms and smaller sub-crops to lateritic rubble. Up to four generations of granitic and pegmatitic dykes crosscut the main units. During this study, geochronology samples were prepared from two granitic dykes that cross cut early fabric within the migmatitic tonalite. The data will be used to constrain an upper emplacement age for the core area but results of the analysis were not available before the submission date of this thesis.

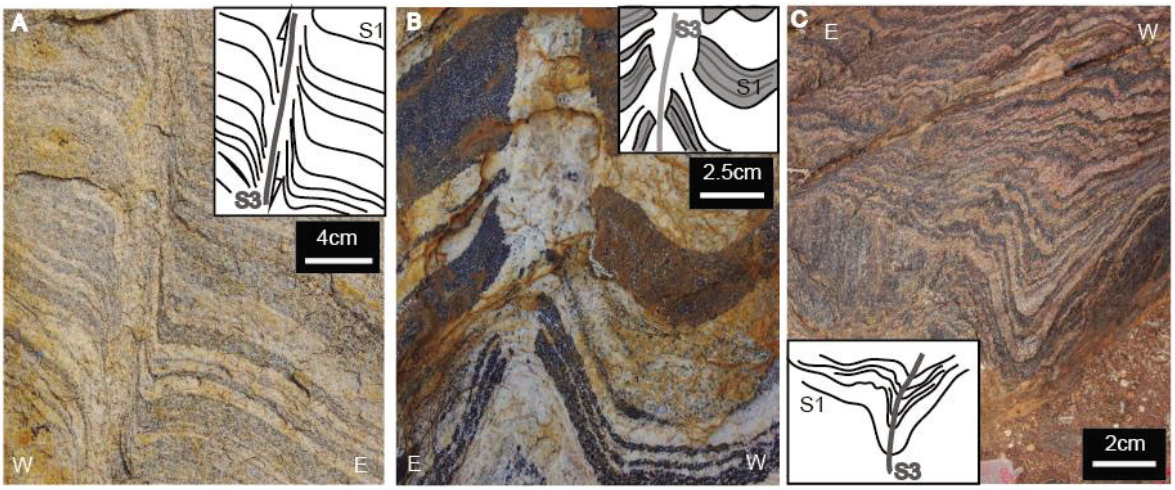

Figure 4.1: A) Migmatitic tonalite: medium-grade stromatic migmatite with characteristic leucocratic-melanocratic banding (S1), S1 fabric is deflected into a N-S melt-filled dextral shear band (S3). **B)** Amphibolite: thick felsic veins (S1) are truncated by a N-S leucocratic band linked directly with layer-parallel (S1) leucocratic bands and interpreted to represent melt-filled shear zones (S3). **C)** BIF: interlayered ferruginous and siliceous bands (S1), crenulated by N-S axial plane interpreted as S3.

4.1 Migmatitic tonalite

The migmatitic tonalite ranges in colour from light to dark grey depending on the amount of leucocratic (leucosome) material present (Fig. 4.1A). It is fine to medium

grained (<4mm), composed of plagioclase (50-60%), quartz (20-30%), biotite (10-15%) with minor K-feldspar (<5%), hornblende (<5%), magnetite (<1%) and epidote (<1%). Titanite, zircon and monazite are present as accessory minerals.

Quartz grains are either large and elongate (1-4mm) with straight or lobate boundaries, or small (<1mm) with rounded or polygonal boundaries. Smaller grains (<1mm) exist on the edges of large grains, or form aggregates (1-3mm).
Quartz grains within the leucosome have irregular stepped and bulging boundaries indicative of dynamic recrystallization through grain boundary migration (Vernon 2004). Grains within the aggregates contain polygonal and rounded boundaries and lack undulose extinction, also indicative of dynamic recrystallization through grain boundary migration (Fig. 4.2A-E).

Large plagioclase grains are equant and subhedral (2-3mm) with corroded edges. Smaller aggregates (with individual grains <0.8mm) of plagioclase have irregular, angular shapes. Larger grains of plagioclase contain sub-grains indicative of dynamic recrystallization through grain boundary migration. Some boundaries between plagioclase and quartz contain smaller trains of recrystallised grains consistent with the 'string of beads' microstructure described of Vernon (2004)(Fig. 4.2A, B, C, E & F).

Biotite is scarce in the leucosome, sometimes appearing as inclusions within larger grains of quartz and plagioclase (Fig. 4.2D). In the melanosome, aggregates form schlieren and trend parallel to the main foliation. Individual grains within the schlieren have sharp edges and appear to be broken from larger grains indicative of brittle deformation (Fig. 4.1A-D).

Grains of magnetite (<2mm) occur as dark spots in the leucosome. Its occurrence is discussed in section 7.1: Anatexis.

Caudery (2013) conducted a preliminary U-Pb SHRIMP analysis of zircons from a

core migmatitic tonalite sample (209689), yielded a crystallisation age of 2960Ma +/- 10Ma.

4.1.1 Migmatitic tonalite morphology

There are two generations of leucosome in migmatitic tonalite (Fig. 4.1A). The earliest leucosome forms a pervasive melanocratic-leucocratic banding (described in this section) forming a stromatic metatexite migmatite morphology (defined in Sawyer 2008). A later stage leucosome deflects and sometimes truncates earlier banding and trends predominantly N-S (described in section 5). At outcrop scale, leucosomes are distinguished by their light colour and coarser grain size. They are and composed predominantly of quartz and feldspar and lack mafic minerals. Melanosomes are distinguished by their dark grey colour, finer grain size and presence of mafic minerals such as biotite. These features are also seen in thin section (Fig. 4.2A,B & C).

In areas of high strain, typically near greenstone contacts, the migmatitic tonalite has a strong foliation and contains more leucosome than melanosome; away from the greenstone contacts and in areas of lower strain, the foliation is weaker and the melanosome predominates. Stromatic migmatites are divided into high-, medium- and low-grade based on the amount of leucosome present and preservation state of the melanosome (Appendix A, Table 1). Low-grade is dominated by melanosome, with leucosome present in thin, coarser grained bands. High-grade is strongly foliated and dominantly leucocratic, with melanosome present in only thin finer-grained schlieren.

4.2 Greenstones

Greenstone consist of around 50% amphibolite and 50% metamorphosed banded iron formation (BIF). They range in size from large supracrustal rafts up to 2km in length and up to 100m thick that bound large migmatitic tonalite outcrops to small xenoliths (50cm to 5m) in migmatitic tonalite. These smaller xenoliths comprise only one rock type,

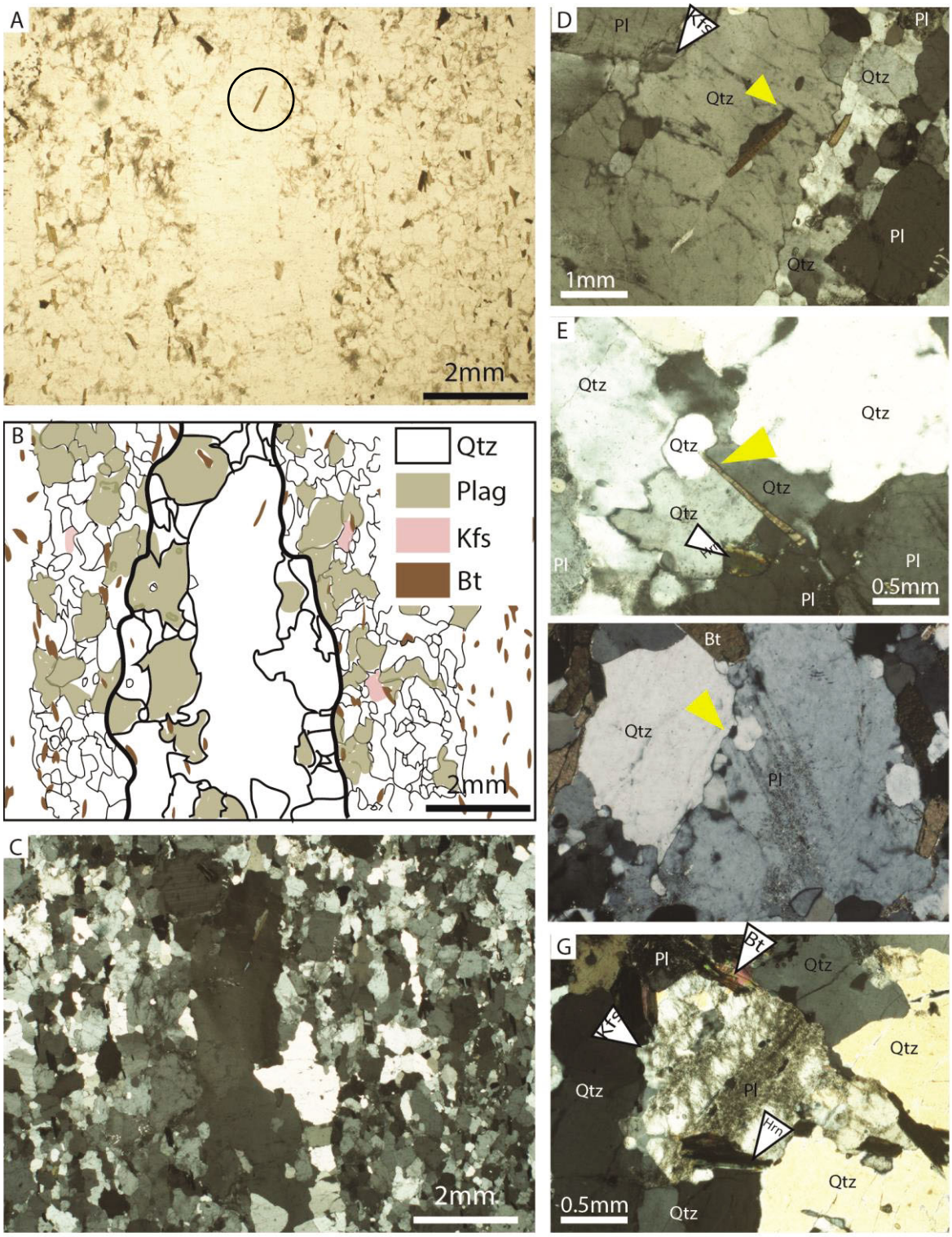

Figure 4.2: Photomicrographs of sample MZF214318 from the migmatitic tonalite A) PPL S1 leucosome (XZ section) **B)** Schematic representation of A - C, S1 leucosome contained between bold lines – note the larger grain size compared to melanosome and rarity of Kfs grains. Quartz grains have lobate boundaries indicative of grain boundary migration recrystallisation **C)** XPL - same field as A). Note undulose extinction in large quartz grain in leucosome. **D)** Leucosome: biotite inclusion in quartz grain (gold arrow)(circled in A). **E)** Leucosome: quartz recrystallised around the end of biotite grain indicating pinning. **F)** Melanosome: String of beads structure and bulging recrystallisation (gold arrow). **G)** Melanosome: Large plagioclase grain with corroded boundaries, surrounded by recrystallised quartz.

larger supracrustal regions contain interbedded amphibolite and BIF. Previous studies suggested the xenoliths are the remnants of an interbedded supracrustal sequence intruded by the original tonalite (Myers & Watkins 1985, Caudery 2013).

4.2.1 Amphibolite

Fresh amphibolite is fine grained (1-3mm) composed of hornblende (60-65%) and plagioclase (35-40%). Clinopyroxene was also observed in some field areas. Colour ranges from dark-grey with a salt and pepper texture, to a homogenous black (Fig. 4.1B). Most outcrops contain felsic veins between 2mm and 20mm thick, composed of quartz (45%), plagioclase (30%) and K-feldspar (15%) (Fig. 4.3; Caudery 2013). Adjacent to the veins, the modal content of plagioclase in the amphibolite drops, forming a melanocratic rim. The leucocratic veins contain two types of hornblende inclusions, fragments of host rock and large hornblende grains. Fragments of host rock typically have fine-grained hornblende (<2mm) and occur as either discrete fragmented blocks (<4mm) or long, narrow discontinuous laminations (Fig. 4.3A). Large hornblende grains occur isolated within leucocratic veins. The composition of the veins suggests that the adjacent amphibolite has undergone partial melting and the melt has been segregated into the felsic bands (veins), leaving a dark hornblende-rich rim. Inclusions and laminations suggest that melt within the veins was mobile and caused the host rock to break apart. In this case, veins represent leucosomes, and their associated darker rim the melanosome, morphology characteristic of vein metatexite migmatites (Sawyer 2008). The large hornblende grains are interpreted to be peritectic and to have been suspended in or carried by the melt.

Some areas within large bodies of migmatitic tonalite contain amphibolite that has been progressively disaggregated. Preservation ranges from fresh blocks (1-5m) that have sharp contacts with the migmatitic tonalite, to trails of disaggregated clasts in leucosomes that are interpreted to have been ingested by melt. In disaggregated areas, small boudin (3-

20cm in length) trains and brecciated clasts are entrained in the neosome (Fig. 4.3A). Breccia is composed of coarse-grained hornblende aggregates (0.5-4mm). The aggregates have been partitioned into dark bands that are interlayered with leucocratic bands and resemble melanocratic-leucocratic banding of the stromatic migmatites (Fig. 4.3A). In thin section (Fig. 4.3B) hornblende aggregates have an irregular shape with straight or serrated boundaries, and appear alongside biotite and quartz. They are around 1-4mm in diameter and contain euhedral crystals. Biotite occurs as single, highly fractured and splintered grains that are surrounded by plagioclase and quartz, in contact with hornblende aggregates or other singular biotite grains.

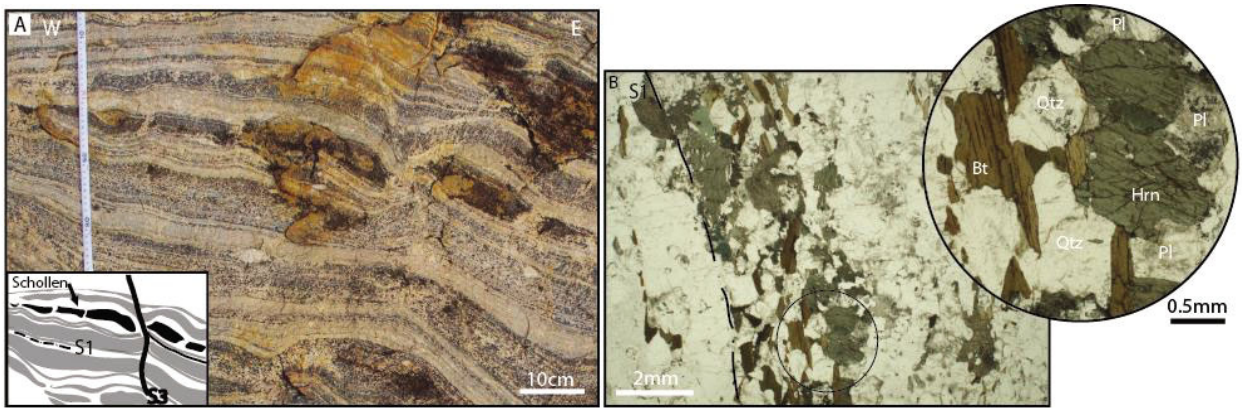

Figure 4.3: A) High grade stromatic migmatite with amphibolite layer broken down into angular boudins, the adjacent bands contained coarse-grained hornblende aggregates. **B)** Photomicrograph of sample MZF214321 from magmatic tonalite, PPL S1 XZ thin section showing composition and texture of the darker melanocratic banding. Inset: euhedral hornblende and broken biotite.

4.2.2 Banded Iron Formation (BIF)

BIF is composed of interlayered ferruginous and siliceous aphanitic bands, between 1 and 4mm thick (Fig. 4.1C). Ferruginous bands are more abundant and comprise between 60 and 70 vol. % of rock. Fresh outcrops are dark grey and weakly magnetic. Weathered outcrops are brown, lacking siliceous layering and are not magnetic. BIF is most abundant in lateritic form, it is a medium brown colour and occurs in-situ or as loose, dense rubble. In-situ, it has a distinct cleavage where siliceous layering has weathered away.

5. DEFORMATION

The two earliest recognisable deformation events in the migmatitic tonalite (D1 and

D2) produced the melanocratic-leucocratic banding (S1) and an overprinting foliation (S2) that is axial planar to F2 folds. S2 is deflected and sometimes truncated by shear zones filled with leucocratic granite (melt filled) and trending N-S (S3)(Fig. 4.1A). Due to rheological differences, deformation is expressed differently in amphibolite and BIF. Deformation in the migmatitic tonalite is expressed through folding and migmatisation. Amphibolite has smaller volumes of leucosomes suggesting that it generated less melt than the migmatitic tonalite. It is also more competent than the migmatitic tonalite, deforming through boudinage and fragmentation into angular blocks. BIF is folded and crenulated. Boudinage and brecciation is completely absent indicating it had low viscosity during deformation.

5.1 First foliation, S1

The leucocratic-melanocratic banding in migmatitic tonalite is interpreted to be S1 (Fig. 4.1A). Proximal to greenstones, S1 is sub-vertical and trends parallel to the contact. It has thin banding (5 – 40mm). Away from greenstones, S1 has a more variable orientation, and has thicker banding (10 – 50mm).

In amphibolite S1 trends parallel to the migmatitic tonalite contact and is defined by plagioclase and hornblende alignment and parallel felsic veins (Fig. 4.1B). Angular boudins also form trains that are parallel to S1 (Fig. 4.3A). S1 in BIF is defined by parallel siliceous and ferruginous layering (Fig. 4.1C), which is also parallel to the tonalite contact.

5.2 First lineation, L1

Migmatitic tonalite has a sub-vertical lineation, defined by biotite preferred orientation and elongate quartz and feldspar aggregates (Fig. 5.1A & B) and interpreted to be a stretching lineation. It has a radial orientation (Fig. 5.1C). If it was an intersection lineation between the N-S vertical S3 (described below) and earlier foliations, we would expect the lineations to be along a N-S vertical great circle, and not radial as shown in

Figure 5.1C..

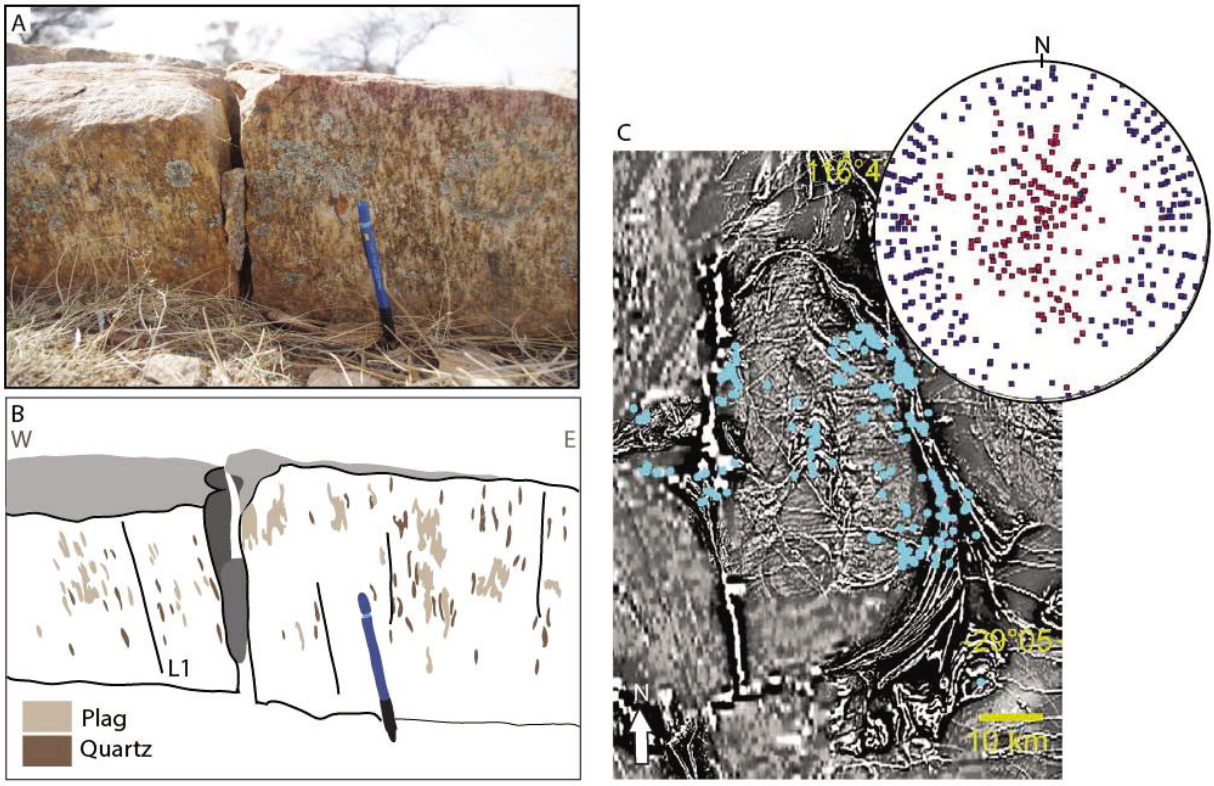

Figure 5.1: A) First lineation, migmatitic tonalite: Sub-vertical L1 defined by elongate aggregates of quartz and plagioclase (pencil for scale) **B)** Schematic drawing of A). **C)** A preliminary report completed by Zibra, 2014 collated all lineation and foliation measurements taken during previous studies. Measurements were taken from the core, monzogranite mantle and surrounding greenstone belts. Dome-wide lineation measurements display a sub-vertical radial pattern. In the aeromagnetic map of the dome, blue dots show location of structural data that is displayed in top right inset. **Inset:** collation of dome-wide structural data from previous studies (equal area projection): red dots: stretching lineation, mineral and magmatic lineation and fold axes. Blue dots: gneissic and magmatic foliation in granitoids; metamorphic foliation in greenstones (modified from Zibra 2014).

5.3 Second foliation, S2

S1 melanocratic-leucocratic banding is overprinted by a sub-vertical foliation defined by alignment of elongate grains and aggregates of quartz and plagioclase, and the preferred orientation of biotite. At the greenstone contact, S2 trends parallel to S1 and is difficult to distinguish. Away from the contact, where S1 has a variable orientation and becomes folded, S2 defines an axial planar foliation (Fig. 5.2) of sheath folds found in migmatitic tonalite (discussed in section 6.2). At fold hinges, quartz and feldspar aggregates are continuous through and cross cut the boundary between leucosome and melanosome (Fig. 5.2C). Biotite grains have two different orientations: their long axis is

either aligned parallel to the S2 foliation that crosses through fold hinges, or parallel to S1. Axial planar biotite alignment is more pervasive than S1 alignment.

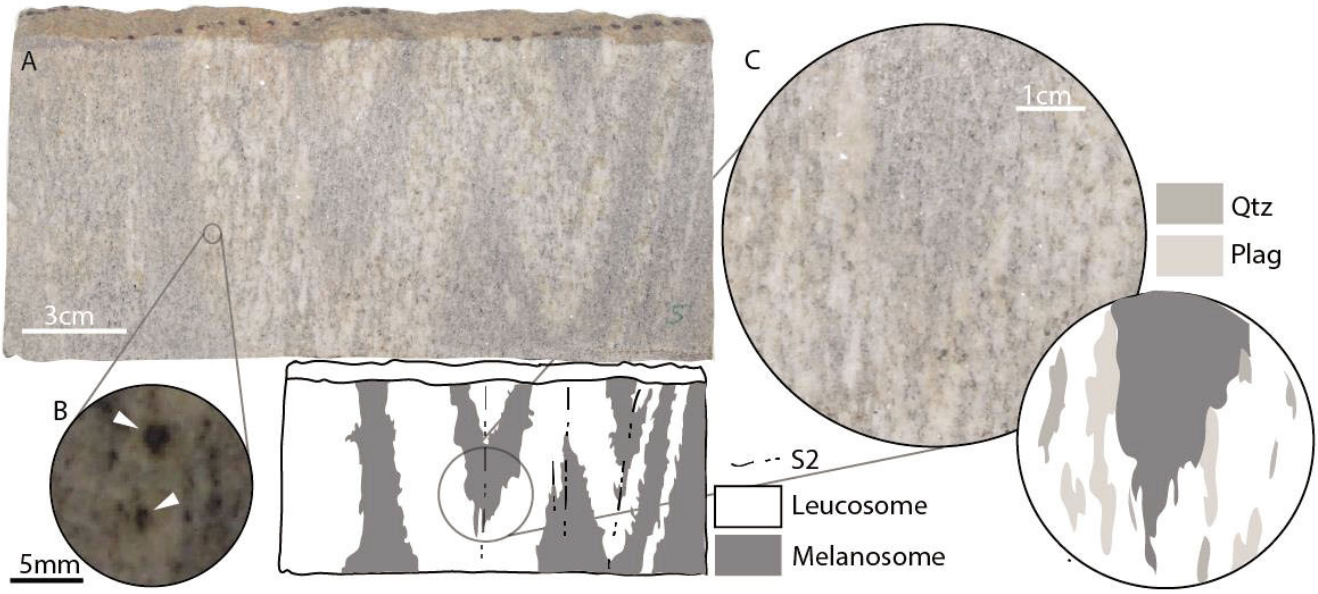

Figure 5.2: Migmatitic tonalite section through a sheath fold sliced parallel to S2, perpendicular to L1: A) Slab section: schematic diagram below highlights melanosome and leucosome (S1) and axial planar S2. Note: continuity of S2 foliation through leucosome-melanosome contact. **B)** Zoom in: Magnetite in S1 leucosome. **C)** Zoom in of hinge zone: Elongate plagioclase and quartz aggregates (S2) create an irregular margin between melanosome and leucosome. **Inset:** schematic diagram, the melanosome is dark grey, quartz grains are medium grey and plagioclase is light grey.

Thin section analysis revealed quartz grains have undergone grain boundary migration recrystallization. The two orientations of biotite suggest they were originally aligned to S1 and have been subsequently rotated towards S2. However this is uncertain as S1 biotite alignment in fold hinges is only very weak. Elongation of recrystallised aggregates with evidence of grain boundary migration and alignment of euhedral crystals (biotite) are diagnostic of solid-state ductile deformation (Paterson et al., 1989). S2 in the greenstones is difficult to distinguish. S1 was predominantly sub-vertical in greenstones, making it difficult to see a sub-vertical overprint. In summary S2 is solid-state foliation in the migmatitic tonalite and is axial planar to F2 folds.

5.4 Third foliation, S3

The S3 foliation is interpreted to be axial planar to the large scale fold system described in the aeromagnetic image of Fig. 1.3. S1 melanocratic-leucocratic banding and S2 axial planar foliation are deflected and sometimes truncated by N-S trending shear zones that display apparent dextral and sinistral sense on the horizontal plane (Fig. 4.1A; discussed in Fig. 6.1A,B). Due to poor 3D exposure on most outcrops it was difficult to determine the dip, and vertical component of the sense of shear, however some sub-vertical dip measurements were recorded (Map: Fig. 6).

Shear zones are filled with leucocratic material composed of quartz, plagioclase and minor K-feldspar. They vary in intensity, from a slight undulating deflection of host rock fabric, to a more pronounced deflection that displaces S1 and S2 on either side. The composition of the leucocratic material and its diffuse relationship with the host rock is evidence for in-situ partial melting of the migmatitic tonalite, characteristic of metatexite migmatites (Sawyer 2008).

Quartz grains within the leucosome are elongate (2-4mm) with long axis parallel to the sub-vertical host rock contact. Grain boundaries are straight, with only minor bulging. Plagioclase grains are euhedral (2-3mm) with slightly corroded edges. K-Feldspar is subhedral and displays microcline twinning. Compared to the S1 leucosome, the S3 leucosomes has a coarser grainsize and contain more euhedral plagioclase grains, quartz displays larger sub-grains and weaker grain-boundary migration crystallisation (Fig. 5.3).

S3 in amphibolite is defined by N-S melt filled shear bands that cross cut S1 leucocratic veins (Fig. 4.1B). Crenulations of S1 siliceous and ferruginous layers, with a predominantly N-S axial plane are interpreted to be S3 in BIF (Fig. 4.1C). In weathered outcrops and large supracrustal rafts, S3 is interpreted to be a N-S trending dissolution cleavage that cross-cuts S1 layering.

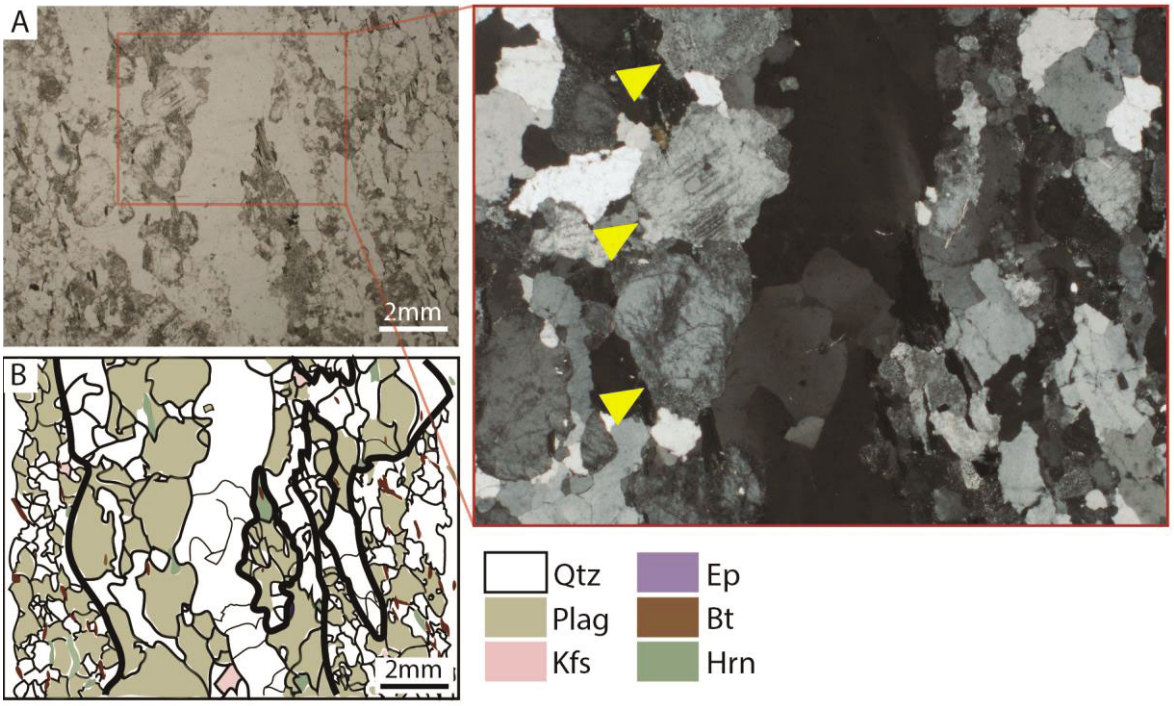

Figure 5.3: Photomicrographs of sample of MZF214311, S3 leucosme in migmatitic tonalite: A) PPL S3 leucosome (XZ section). **B)** Schematic representation of A - C, S3 leucosome contained between bold lines – note the larger grain size compared to melanosome. **C)** XPL S3 leucosome (XZ section), euhedral plagioclase grains indicated by gold arrows. Note plagioclase is more abundant and equant compared to S1 leucosome. A large quartz grain transects the centre. Note straight edged subgrains and contacts with plagioclase, bulging recrystallisation is not as apparent compared to S1.

6. STRUCTURAL DOMAINS

This section contains structural observations and measurements that were taken during fieldwork. Each mapping domain is described separately. A preliminary interpretation is given after the description of each domain. A collation of maps and measurement data is provided in Appendix 4.

6.1 Western domain

The western domain is approximately 1km from the monzogranite contact and encompasses a 1km N-S by 500m E-W area of migmatitic tonalite (Map: Fig. 3). The domain is characterised by linear belts of greenstone and a large (200m by 100m) fresh migmatitic tonalite platform. Outcrops are generally fresh in the north, becoming progressively weathered to the south until they merge into undifferentiated colluvium.

Two greenstone corridors 5-20m wide transect the domain from SSW to NNE and are separated by a 90-120m wide corridor of migmatitic tonalite. The western greenstone

corridor is composed of amphibolite and the eastern corridor is composed of BIF. S1 within the greenstones has a sub-vertical dip and trends parallel to the migmatitic tonalite contact ~020 º (Map: Fig. 5).

The migmatitic tonalite has type-one morphology (30-40 vol. % leucosome; Appendix A: Table 1). S1 is sub-vertical and parallel to the greenstone contact trending 022º. S2 is sub-parallel to S1. S3 trends SE-NW but is highly variable, ranging from 270-360º and displays sinistral and dextral shear senses. Due to lack of 3D exposure, only a handful of L1 and S3 dip measurements were taken, and were sub-vertical (70-90º)(Map: Fig. 5).

The relationship between S1 and S3 is well preserved on the fresh migmatitic tonalite platform in the NW of the domain. S1 has a strong orientation with an average of 024 (n=109). S3 has a variable orientation, and range of intensity from slight open folds of S1 fabric (Fig. 6.1C), to a strong oblique deflection into leucosome-filled shear bands (Fig. 6.1B). Shear bands offset S1 by as little as 1cm to around 30cm. They are between 40cm and 3m in length, and often rotate towards and merge with S1 at their tips. The leucosome in shear bands has a diffuse border with the host rock, is absent of schlieren and dies out along strike into a gentle fold. Careful observations of shear zones, revealed sinistral shear bands and related drag folds have a N-S orientation ranging from 332º to 356º, with an average of 297º (n=63). Dextral shear bands were orientated NW-SE with a larger range from 251º to 359º and an average of 337º (n=46)(Fig. 6.2A,B). Between 332º and 340º the two bands overlap (Fig. 6.2C). Shear bands have similar appearance in the field, including length, leucosome composition, drag fold geometry and diffusion into the host rock. However, dextral shear bands are orientated at a greater angle to S1 than sinistral shear bands. The averaged angle between S1 and S3 (dihedral angle - θ) for dextral shear bands is 83º compared to sinistral shear bands 46º.

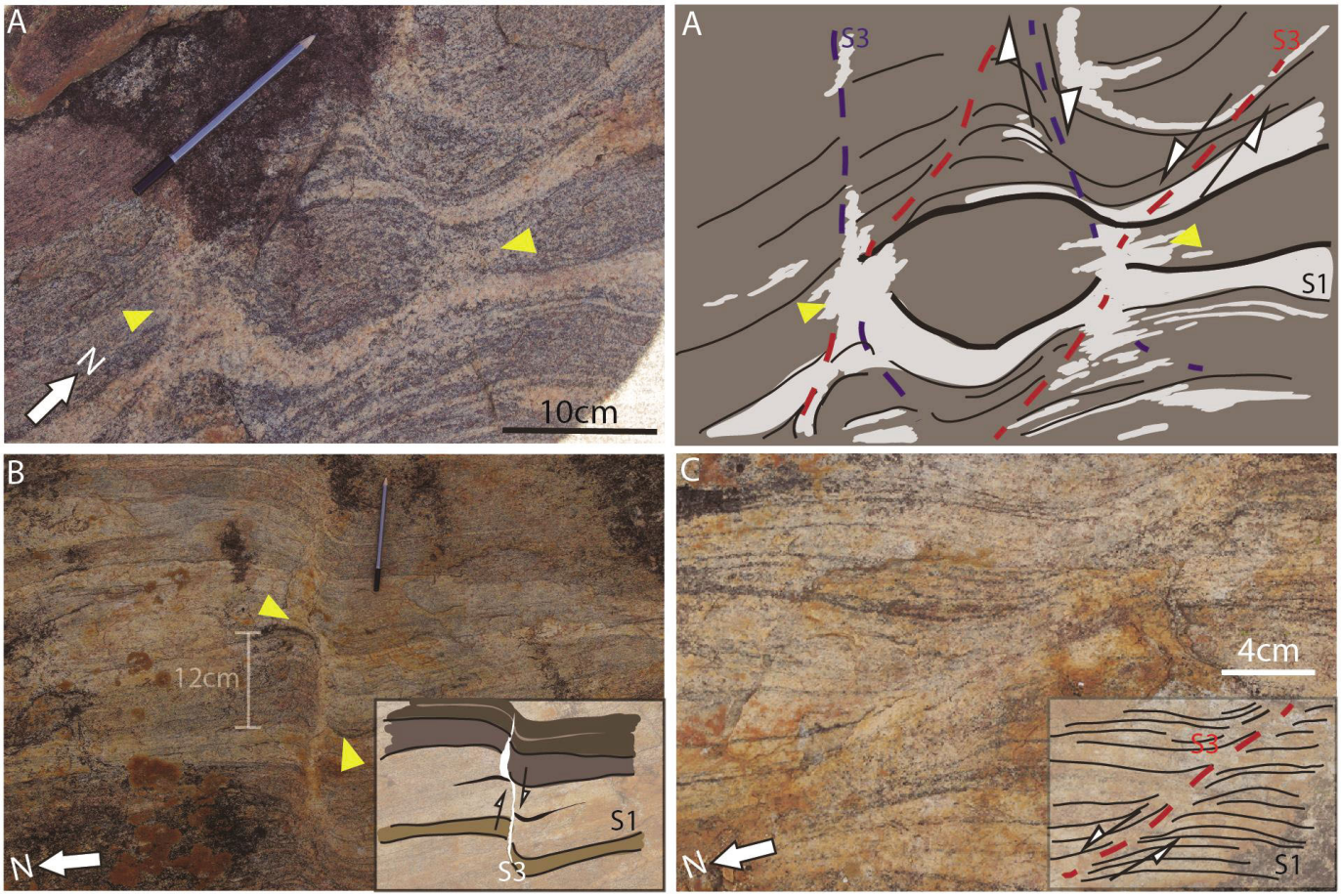

Figure 6.1: Migmatitic tonalite platform, NW of Western domain: A) Photograph and schematic sketch of foliation boudinage: Intersection of dextral and sinistral shear bands (S3) diffuses into melt patches (gold arrows). S1 thins and deflects into, and is continuous through the melt patch. **B)** Dextral S3 melt filled shear band: S1 fabric deflects into shear band. Note offset (12cm) can be seen between schlieren bands, at the top of the photograph offset has reduced to ~10cm and S1 fabric is continuous through the shear band. **C)** Sinistral S3 shear band causes slight open drag folds of S1 fabric.

The intersection of two S3 shear bands with opposite sense is rare. In most cases, they would stop short of intersecting by curving slightly towards the S1 fabric and diffuse out. On odd occasions (Fig. 6.1A) the intersection between two shear zones coincides with the presence of a leucosome where displacement on the shear zone dies out with no cross-cutting relationship. Adjacent S1 fabric becomes thinner and curved towards the intersection melt patch. The shear bands have similar morphology (but opposite sense) and the same composition. The lack of cross cutting relationships and their similar relationship to the leucosomes supports the interpretation that the sinistral and dextral shear zones are the same generation.

6.1.1 Preliminary Interpretations

S1 and S3 – Main platform

Fig. 6.2C is a rose diagram with superposed measurements of dextral and sinistral S3 shear band orientations. The angular relationship between the two bands represents a conjugate set. As stated in (Ramsay, 1980a), a conjugate set exists if the obtuse angle between the shear bands that faces the greatest shortening direction is between 90° and 130° (Fig. 6.2C). In order to evaluate this for the western domain, we took the highest sinistral orientation less the lowest dextral orientation. The shear sense between these angles defines the compressional domain of a strain ellipsoid (Fig. 6.2C). The obtuse angle between shear bands that face the greatest shortening direction is 105º (highest sinistral orientation less lowest dextral orientation), which is within the definition of Ramsay (1980). The shortening axis transects the centre of the obtuse angle and is orientated towards 304º, which is almost normal to the S1 (024º). The stretching axis is normal to the shortening axis, 034º.

Cobbold et al. (1971) investigated the development of internal structures in deformed anisotropic rocks. A number of models were made from plasticine (rock analogue) and subject to bulk pure shear. In a compressional experiment normal to the foliation (anisotropy), internal boudins initially formed. With progressive strain, conjugate normal kink bands developed at 45º to the foliation. The development of conjugate shear bands indicates the western domain was subject to pure shear. However the dextral and sinistral shear bands have a range of orientations (Fig. 6.2C), unlike the experiments in Cobbold (1979) where the dextral and sinistral shear bands were orientated in only one direction, 45º from each other. The larger range in orientation of the shear bands could be caused by an element of simple shear, which is described further below.

Thinning of S1 fabric and diffusion of S3 into melt patches upon the intersection of sinistral and dextral shear bands matches the description of internal boudinage in Ramsay (1980a), (Platt and Vissers, 1980) and Cobbold (1971)(Fig. 6.1A). As opposed to normal boudinage, internal boudinage does not form due to competency contrasts between two layers or lithologies. It forms in response to mechanical inhomogenities in an otherwise homogenous rock that are caused by internal anisotropy, such as a foliation plane (Platt & Vissers 1980). S1 melanocratic-leucocratic banding and S2 mineral and aggregate alignment represent anisotropies in the migmatitic tonalite. Thinning S1 fabric, and melt patches at the intersection between dextral and sinistral shear bands (Fig. 6.1A) is characteristic of internal boudin necks, which according to Ramsay (1980a), occur at 'chance' locations of intersecting shears.

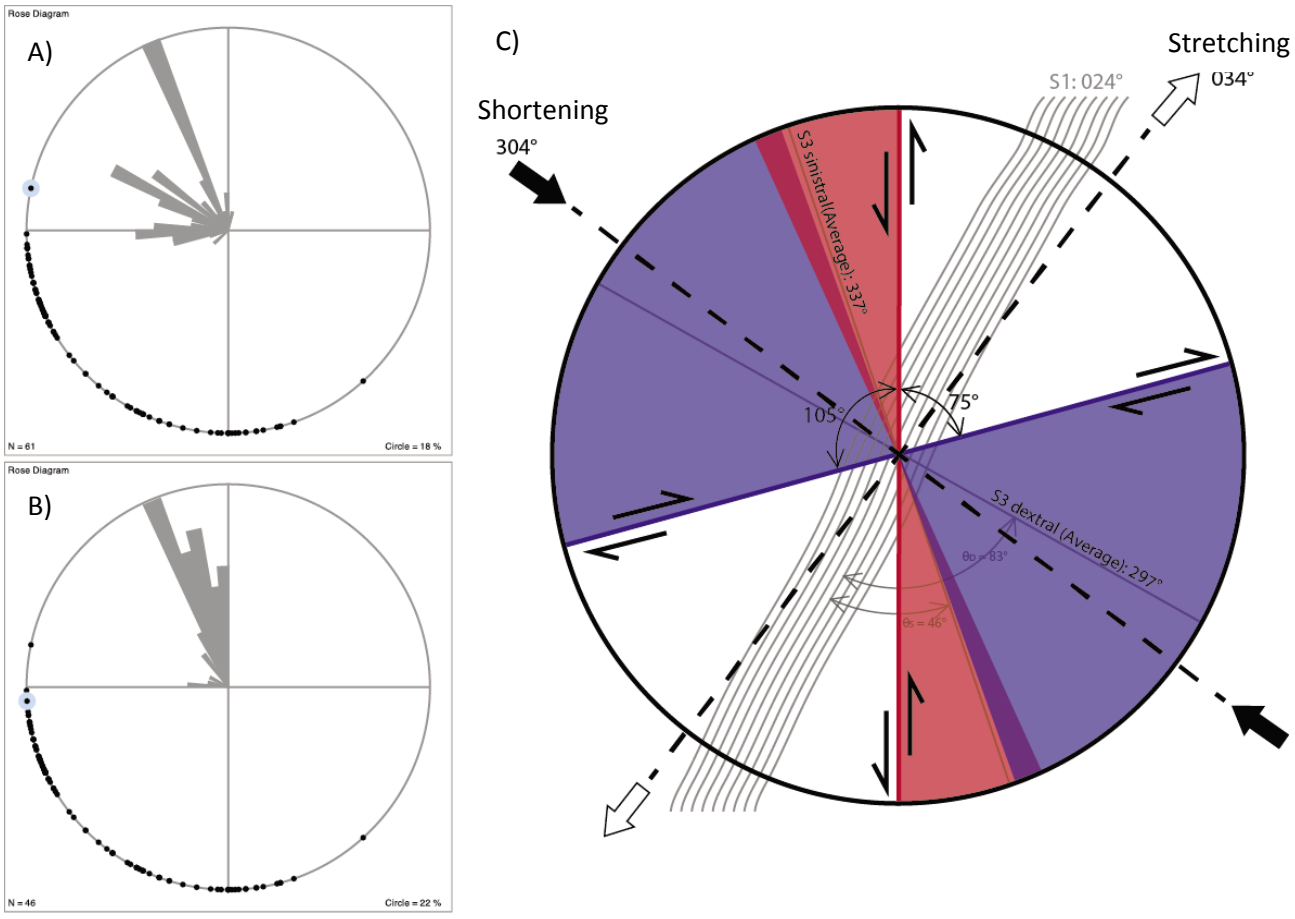

Figure 6.2: Conjugate set: A) Rose diagram: Dextral shear band have orientations between 251° and 359°. **B)** Rose Diagram: Sinistral shear band range between 332° and 356°, a narrower range than the dextral shear zones and a more prominent N-S orientation. **C)** Schematic representation of conjugate shear bands: dextral and rose diagrams are overlayed. Dextral is blue, sinistral is red. The main stretching axes (034°) is sub parallel to S1 (024°), and perpendicular to the main shortening axes (304°) – note obtuse angle between the shear band (105°) faces the greatest shortening direction, and the acute angle (75°) faces the greatest stretching direction.

Passchier (2001) defines 'flanking folds' as the deflection of host rock fabric into shear bands (Fig. 6.1B,C & 6.3A). S3 flanking folds observed on the migmatitic tonalite platform are adjacent to shear bands, and offset host rock fabric with a synthetic sense. Their formation can be attributed to mechanisms described in Passchier (2001) – shear bands formed during or after folding (Fig. 6.3B). They are initiated when non-coaxial flow causes deflection of the host fabric (S1). Progressive deformation causes a fracture to develop. The fracture is intruded by melt or aqueous fluids - which cause partial melting of the host rock. A melt filled shear band is formed. If movement along the shear band occurs during rotation the host rock fabric is offset with synthetic sense. Fig. 6.3A is a flanking fold that has been synthetically offset by a melt filled shear zone. This indicates the shear band has rotated with progressive deformation, or the shear band has accommodated slip without further folding of flanking structures (Fig. 6.3B)(Passchier 2000).

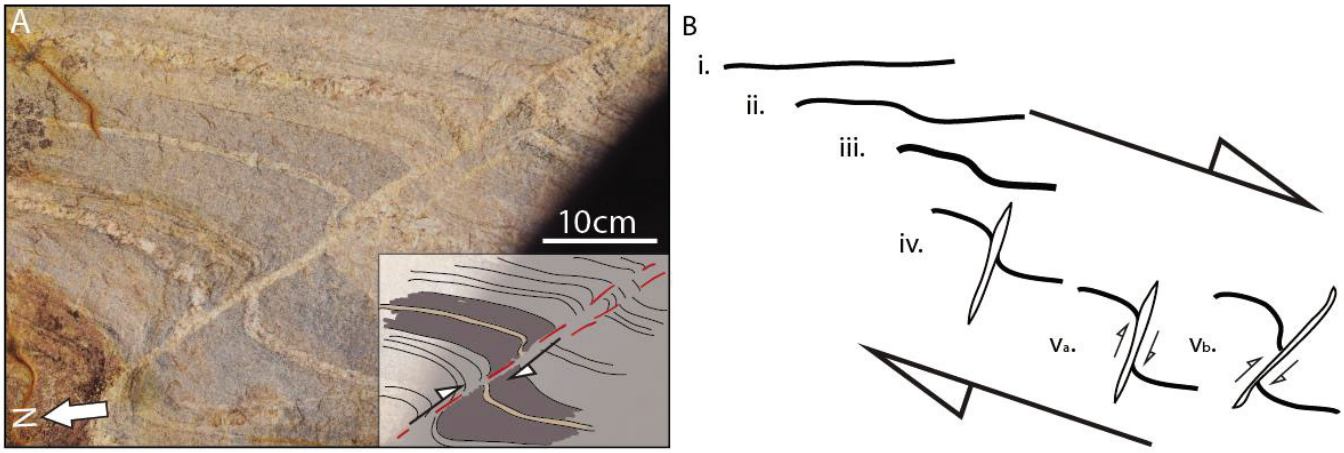

Figure 6.3: Flanking fold geometry around S3, migmatitic tonalite, main platform, Western domain: A) S1 deflects into dextral S3 shear band. S1 is deflected and offset (10cm) by the shear band. Note the shear band has a sharper boundary with the host rock compared to Figure 6.1A - B. **B) i. – iii.:** Dextral flow causes deflection of host rock fabric. **iv.** A fracture develops from progressive dextral movement, intruded by melt or aqueous fluid that causes melting. $\mathbf{v_a}$ – S1 is offset, the shear band has accommodated slip without further folding of flanking structures. $\mathbf{V_b}$ – Progressive deformation causes shear band rotation and S1 becomes offset. Diagram is based on Figure 8 in Passchier (2001).

Shear band rotation may also explain the large range in strike of dextral shear zones compared to sinistral (Fig. 6.2C). Before we proceed with this explanation a few terms

need to be defined: ‘angular velocity’ specifies the velocity at which a shear band rotates; ‘zero angular velocity’ specifies the axis (orientation) of which a shear band no longer rotates (Fig. 6.4A). During progressive deformation shear bands will rotate towards zero angular velocity of flow (Hanmer and Passchier, 1991). Shear bands may rotate at different rates depending on their original orientation (Platt and Vissers 1980; Passchier et al., 1990). Consider Fig. 6.4B, if the sinistral band rotates clockwise it will have an opposite sense to bulk rotation (shear direction) and become inactive. The dextral band has a synthetic sense compared to bulk rotation, and will rotate slowly. It will continue to provide movement for a longer amount of time (Platt and Vissers 1980). The wide spread of dextral shear bands in Fig. 6.2 suggest they have rotated in a clockwise direction. The sinistral shear bands have a narrow range because they have a smaller arc towards zero angular velocity (compared to dextral shear bands). As they rotate clockwise they will have an opposite sense to the bulk rotation direction and become increasingly inactive (Fig. 6.4C). The clockwise rotation of shear bands indicates the main platform of the West domain has undergone a larger scale dextral simple shear expressed by the formation of a conjugate set of shear bands and their rotation towards the zero angular velocity plane.

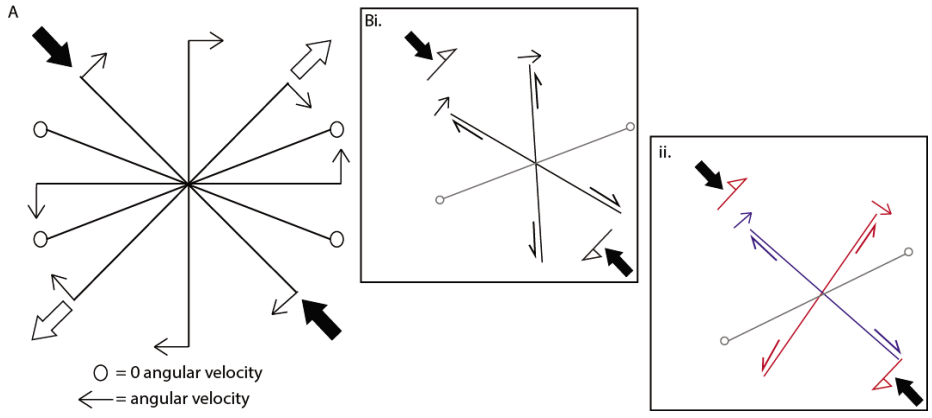

Figure 6.4: Progressive deformation (flow) in a volume of rock – general shear A) If we divide a rock into domains by drawing imaginary lines, and then apply outside deformation (black and white arrows), the lines have an angular velocity which will rotate towards zero angular velocity. General shear is a mixture of pure shear and simple shear therefore the axis that defines zero angular velocity is slightly oblique to the principle stretching axis (white arrows). Modified from Passchier et al. (1990). **B) i.** During progressive deformation, in this case general shear, the sinistral band has a smaller arc towards zero angular velocity. **ii.** As the sinistral band approaches zero angular velocity it becomes increasingly inactive because it has the opposite sense to the bulk shear direction.

To fully interpret the local kinematics, a vertical sense of the S3 shear bands is needed. This information may be obtained from lineation measured in planes parallel to the S3 plane, and kinematic indicators (such as sigmoidal clasts) parallel to the lineation and perpendicular to S3 (Passchier 1990). Unfortunately, this was not obtained during the study due to absence of 3D outcrop, and lack of clear kinematic indicators on S3 XZ thin sections. Dextral and sinistral shear bands of the same generation could occur in transtensional (dip-slip) or transpressional environments. An example is given is Fig. 5.4 where transtensional deformation has caused dextral extension. The resulting horst-and-graben structure has both sinistral and dextral faults on either side of the down-going block.

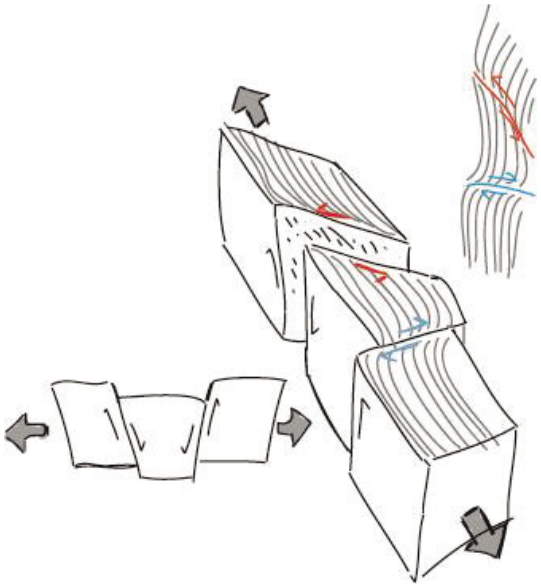

Figure 6.4: Transtentional 'horst and graben': Dextral and sinistral shear bands can occur on opposite sides of a down going graben.

In summary, the distribution of dextral and sinistral shear band orientations form a conjugate set, with a NE-SW stretching axis and a NW-SE shortening axis. Horizontal orientations of synthetic shear bands indicate pure shear, but the large range of dextral orientations suggest shear bands may have been rotated clockwise by a progressive broader dextral simple shear component. This suggests the area has undergone general shear - a mix of pure and dextral simple shear. Foliation boudinage is observed at the intersection between sinistral and dextral shear bands, which indicates extension along strike sub-parallel to S1 NE-SW (Fig. 6.2c). Caution must be exercised with this interpretation

because the absence of a vertical shear sense prevents a thorough interpretation of the local kinematics.

6.2 Central domain

The central domain consists of an area of 3.5km N-S by 3km E-W in the centre of the migmatitic tonalite core (Map: fig. 2). This study focused on a large elliptical structure resembling a 'squashed donut' towards the north of the domain. The ellipse, has a long axis orientated roughly E-W. It is composed of an outer greenstone ring that surrounds a central core of migmatitic tonalite. Outcrops are fresh in the eastern half and become weathered and lateritic rapidly into the western fold closure. Greenstone outcrops in the east are dominantly amphibolite and in the west they are dominantly BIF. Migmatitic tonalite morphology decreases from high-grade (40-50 vol. % leucosome) to medium-grade (30-40 vol. % leucosome; Appendix 1) with increasing distance away from the greenstone contact.

S1/S2 is predominantly ~E-W but curves 180º around the greenstone fold closures. Towards the centre of the ellipse, S1 becomes folded and displays a wide range of geometries, from open to isoclinal with upright to sub-vertical fold axis. In some areas S1 forms dome-and-basin patterns (Fig. 6.5). These are the patterns that Myers and Watkins (1985) observed and interpreted as fold interference. Foley (1997) and Caudery (2013) found they were formed through sheath folding. Sheath folds have irregular shapes but most are roughly elliptical. The long axis is sub-parallel to S2 and showed variable orientation but most were orientated roughly E-W (Map: Fig. 7). The hinge of the fold rotates and becomes sub-parallel to L1. L1 is sub-vertical and has a radial orientation (Map: Fig. 7).

S3 overprints sheath folds and is generally N-S throughout the area, although it does display some variation in the Eastern fold hinge (Map: Fig 5). It has both sinistral and

dextral sense and was observed shearing dome-and-basin structures.

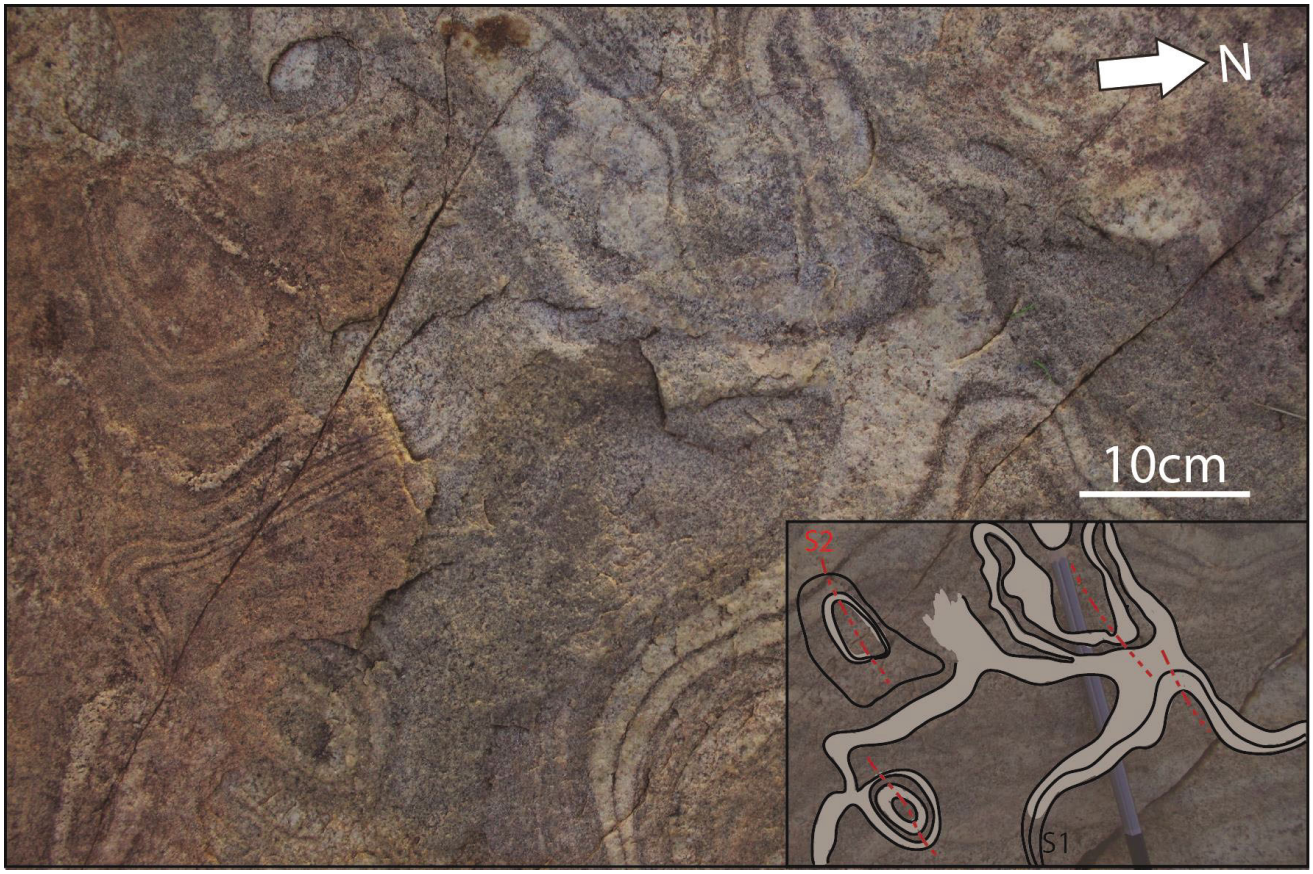

Figure 6.5: Migmatitic tonalite, Central Domain: Sheath folds create dome-and-basin patterns. Domes are elongate and irregular shaped with a ~E-W long axis.

Analysis of dome-and-basin patterns

A large block of migmatitic tonalite containing a sheath fold was retrieved from the central domain (Sample: MZF214306; Fig. 6.6). Unfortunately the sample was not in-situ, however it contains a biotite preferred orientation, and a quartz and feldspar aggregate alignment that is parallel to the long axis of the sheath fold and taken to represent S2. There is no foliation overprinting S2. The sheath fold has a sub-vertical axis, which was typically observed in the field.

A rock saw was used to section the sample into 1.5cm slabs, cut normal to the S2 foliation and parallel to L1 (XZ of S2)(Fig. 6.6A). The cross section reveals a synformal fold closure with an axial surface parallel to S2 (Fig. 6.6B). The hinge line of the fold closure is curvilinear and eventually becomes parallel to L1.

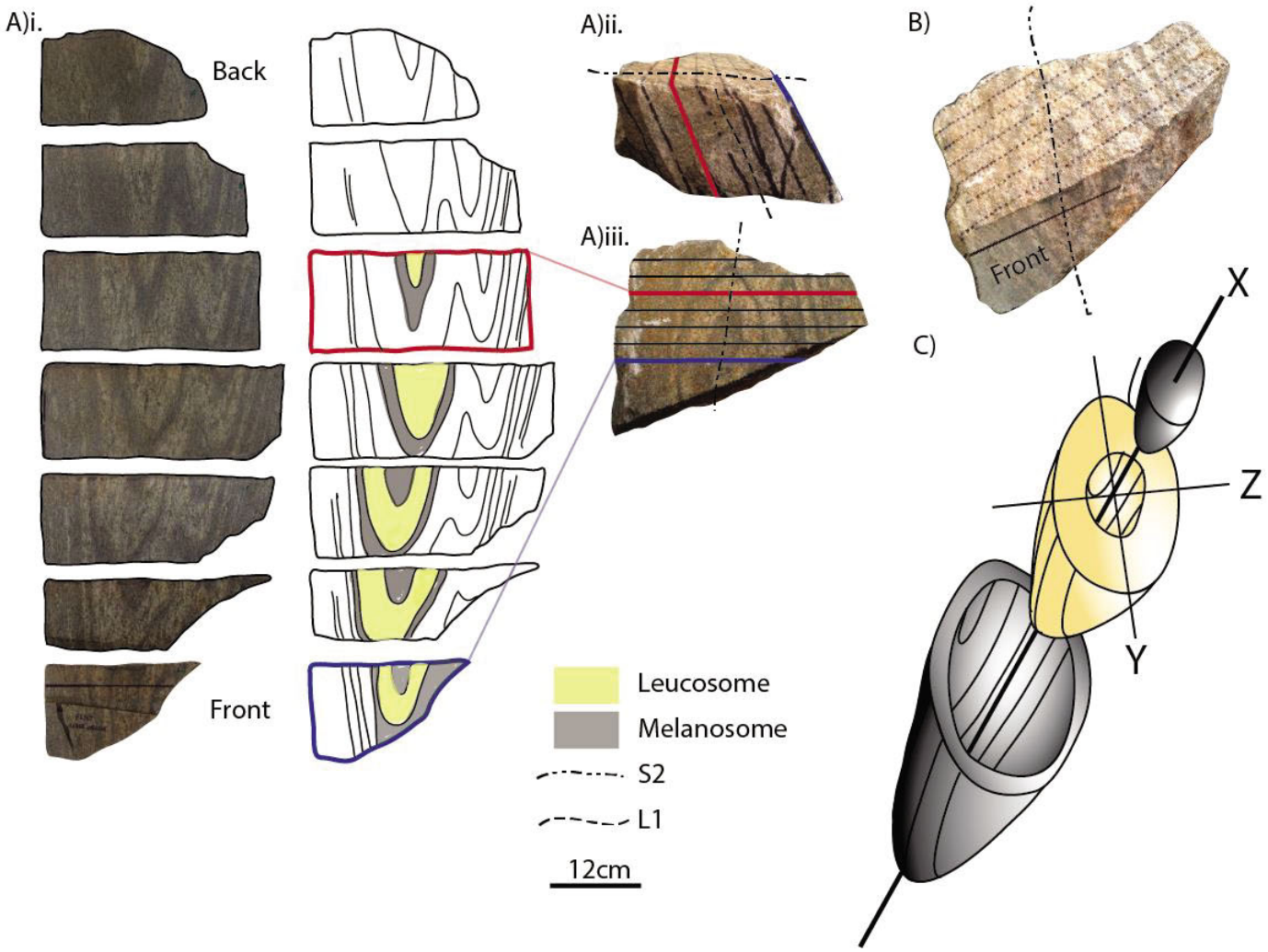

Figure 6.6: Cross section through sheath fold, cut parallel to L1 and perpendicular to S2, migmatitic tonalite (MZF214306), Central Domain: A) i. Photographs and schematic diagrams. The melanosome and leucosome were used as marker layers (schematic drawing) to trace the geometry of the sheath fold. **ii & iii.** Slabs parallel to L1 and perpendicular to S2, indicating the position of the cuts shown in (i). **B)** 3D perspective of sample. **C)** Exploded 3D perspective of sheath fold constructed from marker layers, the x-axis is parallel to L1. Note hinge of the fold becomes parallel with the L1 (X-axis).

6.2.1 Preliminary Interpretations

Sheath fold analysis

The sheath fold analysis revealed L1 is contained by the sub-vertical S2 foliation, which defines the axial plane of the sheath. This indicates L1 is a stretching lineation and is sub-vertical (X-axis)(Map: Fig. 6; Passchier et al. 1990). This is consistent with the

previous observations of this study area by Foley (1997) and Caudery (2013). Curvature of the fold hinge into parallelism with the stretching lineation is diagnostic of a sheath fold (Alsop and Holdsworth, 2012).

During non-coaxial deformation, a fold hinge will initially form at a high angle to the shear direction. As deformation progresses, a sheath fold forms when the hinge line rotates towards parallelism with the shear direction and becomes sub-parallel to the stretching lineation. The direction of the fold apex indicates the direction of non-coaxial flow (Fossen, 2010). The dome-and-basin patterns observed in the field are therefore attributed to one progressive non-coaxial shearing event, as opposed to a type-one interference pattern (Ramsay, 1980b) of two superposed upright folding events with normal axial surfaces suggested by Myers & Watkins (1985).

Sub-vertical non-coaxial deformation

The recognition of sheath folds and associated shear direction in the meso-scale can also be applied to the macro-scale. We interpret the 'squashed donut' to represent a map-scale sheath fold viewed in the yz plane. The x-axis of the sheath fold is sub-parallel to L1 (sub-vertical) and the hinge to the sheath fold may project either above or below the outcrop surface S1. is sub-parallel and continuous around the elliptical greenstone-tonalite contact.

Rheological contrasts between the greenstone and migmatitic tonalite have caused intense shearing adjacent to the contact, evidenced by strong vertical S1/S2. Towards the centre of the ellipse, the rheological contrasts within the migmatitic tonalite are low and accommodate a more passive style shearing. Deformation in the centre is not as intense compared to the margins and sheath fold geometry is preserved.

In summary, the dome-and-basin patterns interpreted previously to represent type-one interference patterns by Myers & Watkins (1985), was the result of sheath folding

during a single non-coaxial deformation event with maximum stretching in a sub-vertical direction, indicated by the association of the vertical lineation and the x-axis of the sheath fold.

6.3 East domain

The eastern domain is approximately 3km from the monzogranite contact. It is 1km N-S by 1km E-W, and characterised by small but plentiful outcrops of greenstone and migmatitic tonalite. Outcrops are generally fresh but discontinuous (Map: Fig. 4).

Greenstones are dominantly amphibolite and form narrow chains that transect the domain from SSE-NNW. S1 is sub-vertical and more intense in the migmatitic tonalite, expressed by repetitive leucocratic-melanocratic banding characteristic of type-one morphology (30-50 vol. % leucosome; appendix 1). S2 is sub-parallel to S1, similar to the other domains where migmatitic tonalite has an intense S1 foliation. S3 trends N-S (Map: Fig. 7) and is dominantly dextral on the horizontal plane, offsetting S1 fabric between 10 and 25cm (Fig. 6.7).

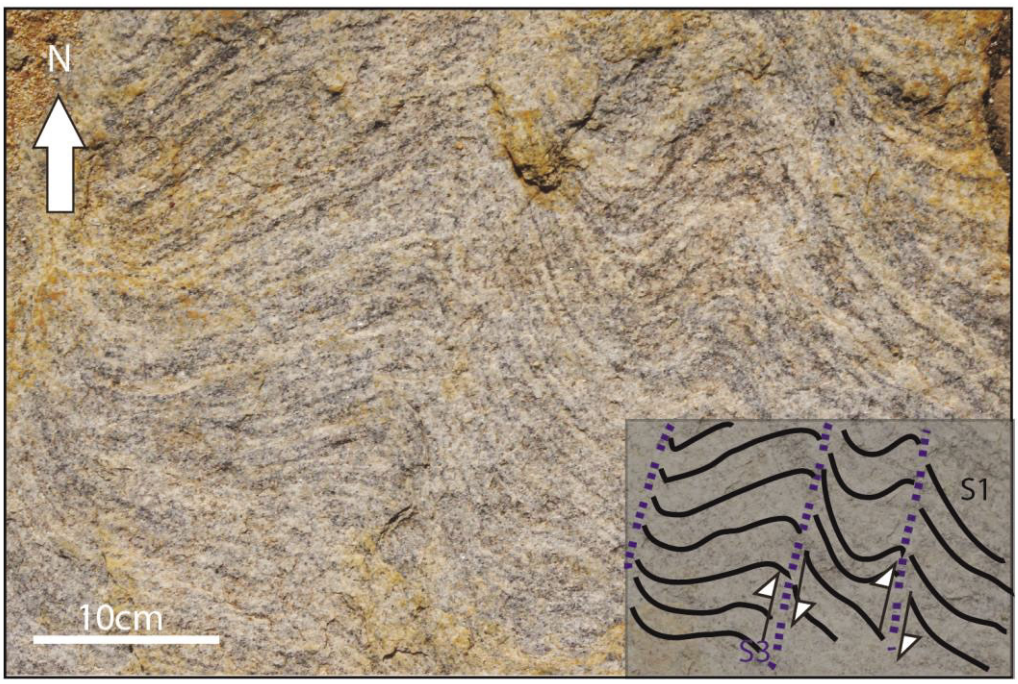

Figure 6.7: Eastern domain: S3 axial planar to S1 crenulations spacing is around 15cm, and S1 is almost E-W. Note faint leucosomes along S3 have a diffuse boundary with S1. S2 is sub-parallel to S1.

Due to lack of 3D exposure, dip measurements were not obtained for S3. An orientated hand sample was retrieved from the field and sliced with a rock saw perpendicular to a S3 dextral shear band (MZF314312). The shear band had a strike of 005º and a dip of 70W, vertical shear sense was top to the right indicated by deflection of S1 fabric. Only a handful of outcrops had a suitable surface for a L1 measurement, most were plunging between 70 and 80º towards 300º (Map: Fig. 7).

The relationship between S1 and S3 is preserved on the fresh tonalite platform in the centre of the domain. S3 has a bimodal spacing distribution: one set spaced between 10 and 20cm (Fig. 6.6), and a second set spaced between 20 and 50cm, where a set contains 3 or more S3 shear bands. When S3 is spaced closer together S1 has a more E-W orientation and a larger dihedral angle (angle between S3 and S1 (θ)=77º). When spaced further apart S1 is orientated NW-SE and has a smaller dihedral angle (average(θ)=54º). This creates asymmetric undulations in the bulk S1 fabric, and results in an overall trend of around 315º.

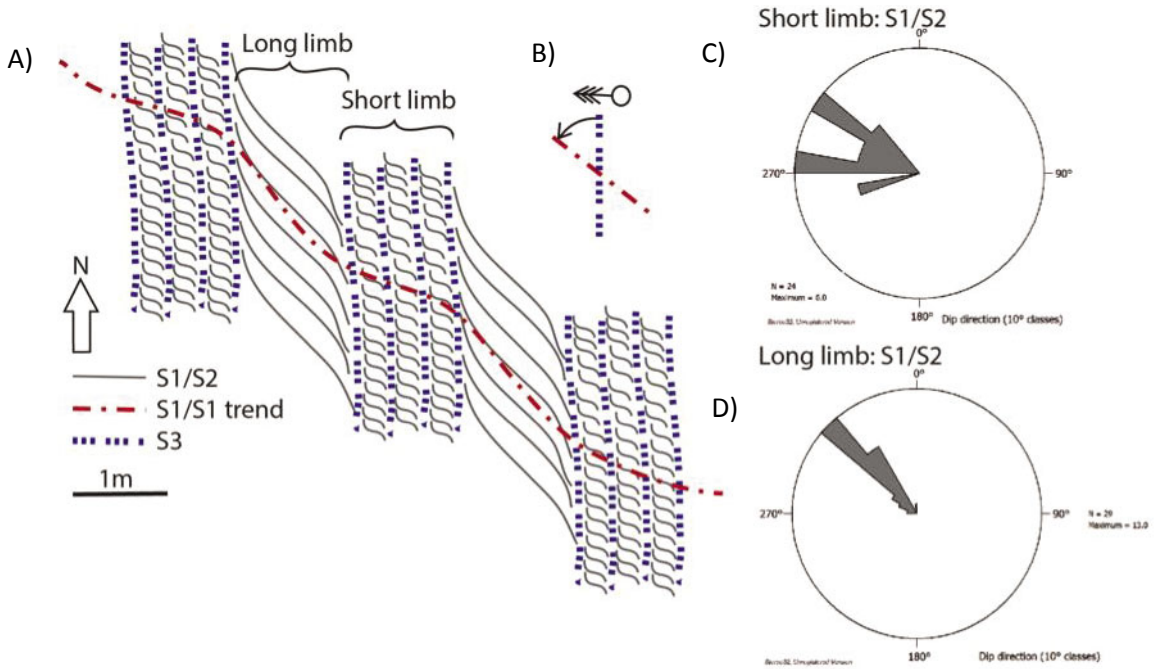

Figure 6.7: A) Bimodal distribution of S1. When S3 is closely spaced, S1 is orientated ~E-W (refer to C). When S3 is further apart S1 is SE-NW (refer to D). The two orientations create S-fold geometry. **B)**Vergence between S1 and S3 predicts a fold closure to the northwest. **C)** Rose diagram of S1 when S3 is between 10 and 20cm apart. **D)** Rose diagram of S1 when S3 is between 20 and 50cm apart.

6.3.1 Preliminary interpretations

The asymmetry of S1 indicates a large scale fold closure to the north-west, towards the Central Domain described in Section 6.2.

7. DISCUSSION

Overprinting foliations in the migmatitic core reveal a structural pattern that formed from partial melting, emplacement and subsequent deformation of the migmatitic tonalite. This section starts with a discussion on partial melting of tonalite which is attributed to the formation of the S1 and S3 leucosomes, followed by a discussion of the structural evolution of the migmatitic core.

7.1 Anatexis

Melting may involve the addition of aqueous fluids (water-fluxed melting) or the breakdown of hydrous minerals (dehydration melting). Addition of an aqueous phase will decrease the solidus of a rock and melting will begin at lower temperatures compared to dehydration melting. In a binary system, congruent melting occurs at a temperature where the solid phase and liquid phase have the same composition. Incongruent melting is when a solid phase melts to produce another solid phase and a liquid phase that have a different composition to the original. Products of water-flux melting reactions may be congruent or incongruent. Dehydration melting involves the incongruent breakdown of hydrous minerals such as biotite and hornblende to produce peritectic minerals such as pyroxene and garnet (Weinberg and Hasalová, 2014).

Reading back through microstructures to observe where melt first originated, where is has migrated to, and how it has crystallised can help to identify minerals involved in the melting reaction. Holness et al., 2011 described melting structures that specifically relate to the former presence of melt: corroded and embayed grain boundaries, thin films of minerals pseudomorphing melt along grain boundaries and crystallisation from melt

indicated by crystal faces against inferred patches of former melt, orientation of elongate euhedral minerals.

7.1.1 Partial melting of tonalite

Field and petrological observations of the migmatitic tonalite were used to determine conditions of partial melting during D1 (S1 leucosome) and D3 (S3 leucosome). A more detailed petrographic and geochemical analysis is needed to constrain potential P-T-t path, which is outside of the scope of this thesis. Mineralogy of leucosome and melanosome as well as melting microstructures in the melanosome are used to infer a potential melting reaction.

S1and S3 leucosomes are composed predominantly of plagioclase, quartz and minor K-feldspar. Magnetite was observed only in the leucosome (Fig. 5.2B). Titanite is also present as a minor phase in the migmatitic tonalite. As mentioned in the section 4.1, quartz grains have been affected by dynamic recrystallization. Melting and crystallisation microstructures described in Hollness et al. (2008) are difficult to distinguish, however the S1 and S3 leucosomes show evidence of crystallisation from melt: euhedral plagioclase grains with straight boundaries when in contact with quartz (Fig. 5.3C), straight edged-grains of quartz (Fig. 5.3C), and biotite inclusions within plagioclase and quartz grains (Fig. 4.2D). Plagioclase grains in the melanosome have embayed and corroded edges, indicative of partial melting (Fig. 4.2G).

Biotite concentration in low-grade migmatite melanosome (Appendix A) is around 20 vol. %, increasing to 40% in melanosome of a high-grade migmatite. Volume of leucosome in the high-grade migmatite also increases from 20 vol. % to 50%. Biotite has been partitioned to the melanosome. This indicates biotite is a not major reactant. However, some grains appear rounded and corroded in thin section, which indicates a small amount of biotite has melted.

The composition of the melanosome and leucosome suggests the major melt producing reaction involves a congruent reaction of quartz and plagioclase (and K-feldspar) with some small involvement of biotite. The absence of peritectic minerals or any evidence of their former presence such as pseudomorphs of garnet, indicate congruent melting has occurred. This together with the high volume of leucosome (20-50 vol. %) can be attributed to influx of aqueous fluids close to the H2O saturation solidus (wet solidus) of quartz and plagioclase (and K-feldspar):

Qtz + Pl(Ab) +/- Kfs(Or) + H2O = Melt (Vernon et al., 2004)

Influx of aqueous fluids may also cause a minor reaction of biotite:

Plg (Ab) + Qtz + Kfs (Or) + Bt + H2O = Ttn + melt (Sawyer, 2010)

Water present melting of common crustal rocks (including tonalite) begins at upper amphibolite facies at around 620-650°C at typical crustal pressures (Weinberg & Hassalova 2014).

7.1.2 Presence of magnetite in leucosomes

Magnetite is present as a minor phase in S1 and S2 leucosomes (Fig. 6.2B). It only occurs in the leucosome, which indicates it is a product of a melting reaction. In thin section it fills the interstitial spaces suggesting late stage crystallisation. Magnetite is an iron oxide (Fe3O4), in order to exist, as a product of a melting reaction a source of iron in the reactants is required. Iron may have come from the breakdown of biotite (discussed in 7.1.1). Iron may also be sourced from aqueous fluids that facilitate melting of tonalite. It is incompatible with plagioclase and quartz and may remain as dissolved ions until the later stages of crystallisation. Nearby BIF in greenstones could be a source of primary iron in the aqueous fluids.

7.2 Structural evolution of the migmatitic tonalite core

Our observations and preliminary interpretations show that the migmatitic tonalite

core evolved through three deformation events. The first event caused partial melting of a tonalite protolith and formed stromatic migmatites (S1). The second event folded and sheared S1 in a vertical direction. The third event caused partial melting and N-S orientated shear bands. S1 and S2 foliations define the emplacement stage of the migmatitic core, and S3 is an overprinting event caused by E-W compression.

D1

D1 is attributed to the formation of stromatic metatexite migmatites through water-fluxed partial melting of tonalite (discussed above). In the eastern and western domains, migmatitic tonalite has a 40-50 vol. % leucosome (high-grade, Appendix A) and S1 trends parallel to greenstone bodies. This was also observed in the central domain, where S1 trends the contact of a large elliptical amphibolite raft. Away from the raft, migmatitic tonalite has 30-40 vol. % leucosome (medium-grade) and variable orientation.

Sawyer (2008) explains that differential stress can drive the segregation of leucosome from melanosome. If stress is applied to a melting rock it will squeeze melt from the matrix and compact the residuum. The difference in migmatite morphology may indicate that high-grade migmatites (Appendix A) formed in a higher differential stress environment compared to medium and low-grade migmatites. We observed a larger volume of leucosome in the migmatitic tonalite near the greenstone contact, and a smaller volume away. The rheological differences between the greenstone and the migmatitic tonalite may cause strain localisation, and increase differential stress during melting.

D2

D2 gave rise to sheath folds (Fig. 6.5). The hinge of the sheath fold becomes parallel to L1, the stretching lineation, and therefore defines a vertical stretching.

The lack of association of leucosomes with F2 structures suggests that the migmatites formed during D1 had already solidified during this second event. When

migmatites are folded during melting, some of the melt can migrate to dilatant sites that develop as the fold grows. If melt migrates along fold limbs it can collect in the hinge zone and form an axial planar leucosome (Weinberg and Geordie 2008; Sawyer 2008). While this has been documented during D3, we did not observe an axial planar leucosome in F2 folds. The axial plane was defined by the S2 foliation - elongate aggregates of quartz and feldspar cross cutting the boundary between the leucosome and melanosome. This suggests that folding occurred after D1, after the leucosome crystallised and the migmatite was in a predominantly solid-state. However, folding may have occurred during D1 migmatisation and progressed into the solid-state (Gervais et al., 2004; Weinberg and Podladchikov, 1995)resulting in an S2 axial planar overprint. In this case S1 and S2 were formed during a progressive D1.

We interpret D2 to be a diapiric ascent phase of the migmatitic tonalite. This is supported by observations of a sub-vertical stretching lineation and sheath folding. We can also consider how the migmatitic tonalite body was deformed as it ascended. Strain regimes of an ascending diaper have been studied in Schmeling et al. (1988), Dixon (1975) and Cruden (1990). As a diapir rises, the upflow from its interior will push material out to its margins. The margins become sheared and flattened against the host rock. Towards the centre of the diapir, continuous vertical flow will progressively stretch the rocks. As mentioned above, type-one migmatites of the east and west domain may have been formed under higher differential stress than type-two and may correlate to high strain zones that occur at the margin of a diapir. Sheath folds in the central domain indicate a dominantly vertical sense of movement and may be correlated to the core of a diapir. By contrast, sheath folds are rare in the east and west domains and may have been transposed (flattened) towards the diapir's margins.

D3

The large scale distribution of features associated with D3 across the study area suggest a large scale fold, where the east and west domains define high strained limbs, and the central domain a less-deformed hinge area.

- In the western domain, the relationship between S1/S2 and S3 was interpreted to reflect general shear – a mix of NW-SE simple shear and dextral pure shear. S3 shear bands were rotated clockwise with progressive deformation, indicating a bulk sense of dextral shear. Dextral shear is associated with the west limb of a fold with a N-S axial plane in buckle and flexural flow fold models (Hudleston and Lan, 1993; Ghosh, 2013).
- In the eastern domain S3 caused asymmetric undulations of S1 fabric. Vergence between S3 and S1 indicates a large scale fold closure to the N-W.
- In the central domain, the main trend of S1/S2 is E-W, which is perpendicular to N-S S3 shear zones. This is expected in a hinge zone. The older fabric is wrapping around the fold.

We propose D3 is an E-W compressional event that caused folding and partial melting of the migmatitic core. N-S melt filled shear bands (S3 leucosome) define the axial plane. The absence of peritectic minerals in the leucosome suggest they were, like the S1 leucosome, formed by water-fluxed partial melting.

Aqueous fluids can exploit weakness in a rock, such as a foliation plane (Passchier 2000). Aqueous fluids may have exploited the S3 axial planar foliation and caused partial melting. The margins of the leucosomes are not sharp, they are diffuse and S1 fabric is deflected into them. This suggests melting occurred during progressive deformation, because there is continuity between the host rock and the melt filled shear bands.

8.0 CONCLUSION:

An east-west traverse across the core area revealed a progressive change in structures associated with D3 that suggest a large-scale fold. The east and west domains define high strained limbs, and the central domain a less deformed hinge area. E-W compression caused folding and partial melting. Shear bands (S3) are axial planar to the large-scale fold. Leucosomes in the shear bands were formed through water-fluxed partial melting of the migmatitic tonalite during deformation.

The earlier S1 and S2 foliations define emplacement fabric and yield information on the original emplacement of the core. Formation of S1 fabric is attributed to water-fluxed melting of tonalite (D1). S2 is a solid-state overprint of S1 and is axial planar to F2 sheath folds. It was formed during the diapiric ascent of the migmatitic tonalite body (D2). The central domain, marking the hinge zone of the large fold, contains sheath folds associated with vertical movement that correlate to the interior of a diapir. In the east and west domains sheath folds are rare, and the migmatites have more melt marked by leucosomes. Compressive strain at the margins of a diapir may have transposed the sheath folds, and segregated more melt by compacting the melanosome. Diapiric ascent may have occurred during D1, and progressed into the solid-state D2. In summary, we associate D2 with diapirism because of the strong vertical lineation (L1), the formation of sheath folds with a sub-vertical axial plane (S2) and the variation in migmatite morphology that was correlated to the strain regime of an ascending diaper.

Our field observations from the east, central and west domains were tied together to propose a model for the structural evolution of the migmatitic core of the Yalgoo dome. The core was formed by diapiric ascent of a migmatitic tonalite body (D1 and D2). After emplacement the core was subject to E-W compression (D3). We initially interpreted a large-scale fold with an apex to the north on the aeromagnetic image presented in Fig.1.3.

Our observations support this interpretation. This study supports the dome-wide non-uniformitarian model presented in Foley (1997) and Caudery (2013). It is a step forward in understanding a more thorough evolution of the Yalgoo dome. The next step is to investigate the structural relationship between the core and the younger monzogranite mantle and understand the 150Ma difference in crystallisation age.

REFERENCES

ALSOP, G.I., AND HOLDSWORTH, R.E. 2012. The three dimensional shape and localisation of deformation within multilayer sheath folds. *Journal of Structural Geology* **44**, 110–128.

ARCHIBALD, N.J., BETTENAY, L.F., BINNS, R. A., GROVES, D.I., AND GUNTHORPE, R.J. 1978. The evolution of Archaean greenstone terrains, Eastern Goldfields Province, Western Australia. *Precambrian Research* **6**, 103–131.

CHEN, S.F., RIGANTI, A., WYCHE, S., GREENFIELD, J.E., AND NELSON, D.R. 2003. Lithostratigraphy and tectonic evolution of contrasting greenstone successions in the central Yilgarn Craton, Western Australia. In Precambrian Research, pp. 249–266.

COBBOLD, P.R., COSGROVE, J.W., AND SUMMERS, J.M. 1971. Development of internal structures in deformed anisotropic rocks. *Tectonophysics* **12**, 23–53.

COLLINS, W.., VAN KRANENDONK, M.., AND TEYSSIER, C. 1998. Partial convective overturn of Archaean crust in the east Pilbara Craton, Western Australia: driving mechanisms and tectonic implications. *Journal of Structural Geology* **20**, 1405–1424.

CONDIE, K.C., AND BENN, K. 2006. Archean geodynamics: Similar to or
different from modern geodynamics? In Archean Geodynamics and Environments, pp. 47–59.

CRUDEN, A.R. 1990. Flow and Fabric Development during the Diapiric Rise of Magma. *The Journal of Geology* **98**, 681–698.

DIXON, J.M. 1975. Finite strain and progressive deformation in models of diapiric structures. *Tectonophysics* **28**, 89–124.

FOLEY, B.J. 1997. Reassessment of archaean tectonics in the Yalgoo district, Murchison Province, Western Australia. Abstracts - Geological Society of Australia **46**, 23..

FOSSEN, H. 2010. Structural Geology (Cambridge university press).

GEE, R.D. 1979. Structure and tectonic style of the Western Australian Shield. *Tectonophysics* **58**, 327–369.

GERVAIS, F., NADEAU, L., AND MALO, M. 2004. Migmatitic structures and solid-state diapirism in orthogneiss domes, eastern Grenville Province, Canada. In Gneiss Domes in Orogeny, D.L. Whitney, C. Teyssier, and C.S. Siddoway, eds. (Geological Society of America Special Paper 380),.

GERYA, T. 2014. Precambrian geodynamics: Concepts and models. *Gondwana Research* **25**, 442–463.

GHOSH, S.K. 2013. Structural geology: Fundamentals and modern developments (Elsevier).

GOODWIN, A.M. 1996. Principles of Precambrian Geology.

HANMER, S., AND PASSCHIER, C.W. 1991. Shear-sense indicators: a review. *Geological Society of Canada Paper* **90**, 72.

HOLNESS, M.B., CESARE, B., AND SAWYER, E.W. 2011. Melted rocks under the microscope: Microstructures and their interpretation. *Elements* **7**, 247–252.

HUDLESTON, P.J., AND LAN, L. 1993. Information from fold shapes. *Journal of Structural Geology* **15**, 253–264.

VAN KRANENDONK, M.J., COLLINS, W.J., HICKMAN, A., AND PAWLEY, M.J. 2004. Critical tests of vertical vs. horizontal tectonic models for the Archaean East Pilbara Granite–Greenstone Terrane, Pilbara Craton, Western Australia. *Precambrian Research* **131**, 173–211.

VAN KRANENDONK, M.J., HUGH SMITHIES, R., HICKMAN, A.H., AND CHAMPION, D.C. 2007. Review: Secular tectonic evolution of Archean continental crust: interplay between horizontal and vertical processes in the formation of the Pilbara Craton, Australia. *Terra Nova* **19**, 1–

38.
VAN KRANENDONK, M.J., IVANIC, T.J., WINGATE, M.T.D., KIRKLAND, C.L., AND WYCHE, S. 2013. Long-lived, autochthonous development of the Archean Murchison Domain, and implications for Yilgarn Craton tectonics. *Precambrian Research* **229**, 49–92.
MYERS, J.S., AND WATKINS, K.P. 1985. Origin of granite-greenstone patterns, Yilgarn Block, Western Australia. *Geology* **13**, 778.
PASSCHIER, C.W. 2001. Flanking structures. *Journal of Structural Geology* **23**, 951–962.
PASSCHIER, C.W., MYERS, J.S., AND KRONER, A. 1990. Field geology of high-grade gneiss terrains (Berlin: Springer-Verlag).
PATERSON, S.R., VERNON, R.H., AND TOBISCH, O.T. 1989. A review of criteria for the identification of magmatic and tectonic foliations in granitoids. *Journal of Structural Geology* **11**, 349–363.
PLATT, J.P., AND VISSERS, R.L.M. 1980. Extensional structures in anisotropic rocks. *Journal of Structural Geology* **2**, 397–410.
RAMSAY, J.G. 1980a. Shear zone geometry: A review. *Journal of Structural Geology* **2**, 83–99.
RAMSAY, J.G. 1980b. The techniques of modern structural geology Volume 1: Strain Analysis (Academic Press).
ROSENBAUM, G., WEINBERG, R.F., AND REGENAUER-LIEB, K. 2008. The geodynamics of lithospheric extension. *Tectonophysics* **458**, 1–8.
SAWYER, E.W. 2008. Atlas of migmatites (NRC Research press).
SAWYER, E.W. 2010. Migmatites formed by water-fluxed partial melting of a leucogranodiorite protolith: Microstructures in the residual rocks and source of the fluid. *Lithos* **116**, 273–286.
SCHMELING, H., CRUDEN, A.R., AND MARQUART, G. 1988. Finite deformation in and around a fluid sphere moving through a viscous medium: implications for diapiric ascent. *Tectonophysics* **149**, 17–34.
SWAGER, C.P., AND NELSON, D.R. 1997. Extensional emplacement of a high-grade granite gneiss complex into low-grade greenstones, Eastern Goldfields, Yilgarn Craton, Western Australia. *Precambrian Research* **83**, 203–219.
CAUDERY, J.N. 2013. Structural evolution of the Yalgoo Dome (unpublished honours thesis), Monash University.
VERNON, R.H. 2004. A practical guide to rock microstructure (Cambridge university press).
VERNON, R.H., JOHNSON, S.E., AND MELIS, E.A. 2004. Emplacement-related microstructures in the margin of a deformed pluton: The San Jose tonalite, Baja California, Mexico. *Journal of Structural Geology* **26**, 1867–1884.
WATKINS, K.P., AND HICKMAN, A.H. 1990. Geological Evolution and Mineralization of the Murchison Province, Western Australia. *Geological Survey of Western Australia, Bulletin*.
WEINBERG, R.F., AND GEORDIE, M. 2008. Magma migration, folding, and disaggregation of migmatites in the Karakoram Shear Zone, Ladakh, NW India. *Bulletin of the Geological Society of America* **120**, 994–1009.
WEINBERG, R.F., AND HASALOVÁ, P. 2014. Water-Fluxed Melting of the Continental Crust: A Review. *Lithos*.
WEINBERG, R.F., AND PODLADCHIKOV, Y.Y. 1995. The rise of solid-state diapirs. *Journal of Structural Geology* **17**, 1183–1195.
WILLIAMS, P.R., AND WHITAKER, A. J. 1993. Gneiss domes and extensional deformation in the highly mineralised Archaean Eastern Goldfields Province, Western Australia. *Ore Geology Reviews* **8**, 141–162.
DE WIT, M.J. 1998. On Archean granites, greenstones, cratons and tectonics: does the evidence demand a verdict? *Precambrian Research* **91**, 181–226.
ZIBRA, I. 2014. Yalgoo Dome, Yilgarn Craton. *Fieldnotes: A Geological Survey of Western Australia Newsletter,* **71**, 7.

APPENDIX A

Table 1: MIGMATITE MORPHOLOGY OF THE YALGOO CORE AREA

Grade	Leucosome	Melanosome	Characteristics
Low			
Bulk Volume	20%	80%	
Grain Size	2-3mm	<2mm	
Mineralogy	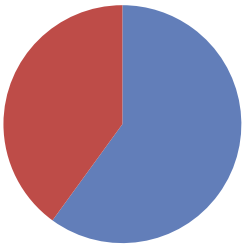	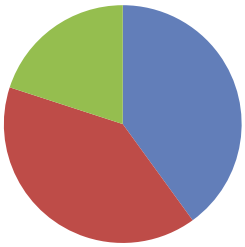	
Texture	Minor k-feldspar. Multiple bands between 2mm and 15mm, thinner bands have diffuse contact with melanosome, thicker have a sharper contact.	Minor hornblende. Contains small diffuse patches of leucosome (<3mm) that create a sugury texture. More homogenous than higher grades.	Straight layer parallel leucosomes disrupt and otherwise homogenous melanousome. Some open to moderate folding.
Medium			
Bulk Volume	40%	60%	
Grain Size	2-3mm	<3mm	
Mineralogy	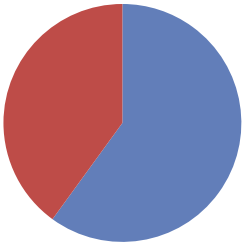	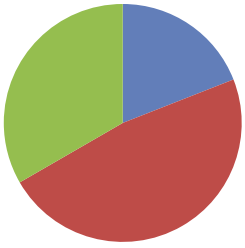	
Texture	Minor k-feldspar. Multiple, continuous bands between 2mm and 20mm. Patchy leucosomes within the melanosome begin to link up and form bands.	Minor hornblende. Darker than low grade, sugary texture. Dark bands begin to form that resemble schlieren.	Bands are folded, displaying sheath geometry in some areas. Found away from greenstone contacts.
High			
Bulk Volume	50%	50%	
Grain Size	2-3mm	<3mm	
Mineralogy	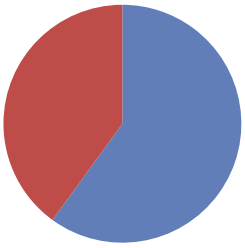	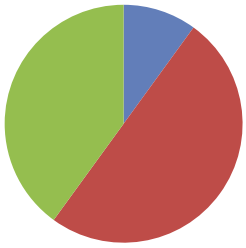	
Texture	Minor k-feldspar. Multiple continuous bands. Bands are pervasive, linking up an anastomosing around schlieren layers	Minor hornblende. Trails of biotite form discontinuos schlieren layers	Sub-vertical foliation and lineation, predominantly adjacent to greenstone contacts. Sheath fold patterns rare.

APPENDIX B

Michael Fenwick

Literature Review 1:

STRUCTURAL EVOLUTION OF MIGMATITES AND TECTONIC CONTROLS OF MAGMA

INTRODUCTION

The currently accepted definition of a migmatite is taken from Sawyer (2008b):

"Migmatite is a metamorphic rock formed by partial melting"

A migmatite is made up of a neosome and a paleosome. The **neosome** forms the part of the rock that has been affected by partial melting. The **paleosome** remains unaffected and preserves structures older than the melting event. The neosome is further divided into the **leucosome** and **melanosome**. The leucosome is lighter coloured and derived from segregation of partial melt consisting (predominantly) of feldspar and quartz. The **melanosome (residuum)** is the darker coloured solid residual fraction remaining from the segregation of partial melt, consisting of minerals such as biotite, garnet and pyroxene. For a more detailed explanation of migmatite nomenclature, please refer to Sawyer 2008b.

Structural evolution of migmatites is controlled by the percentage melt fraction reached during partial melting, and the various mechanisms of melt segregation that act upon the partially melted rocks. This review aims to discuss the mechanisms of partial melting that lead to the progression from solid to melt

dominated rheology, and identify migmatitic structures on the microscopic and mesoscopic scale through the progression.

MELTING

There are two types of melting:

Wet Melting

The addition of H_2O lowers the melting point of a rock at a given temperature and pressure (Thompson & Connolly 1995). Examples of a metapelite and a quartz-feldspathic wet melting reaction are:

$$\text{i) Ms + Bt + Pl + Qtz + } \mathbf{H_2O} \text{ = Melt}$$

$$\text{ii) K-spar + Qtz + Pl + } \mathbf{H_2O} \text{ = Melt}$$

Wet melting reactions are usually the first to produce melt in a system that is increasing in temperature, ~650˚C (Winter 2009). Figure 1 illustrates a simplified P-T phase diagram, with a H_2O saturated solidus. The amount of melt produced is limited to the amount of H_2O present or until one of the other reactants is exhausted.

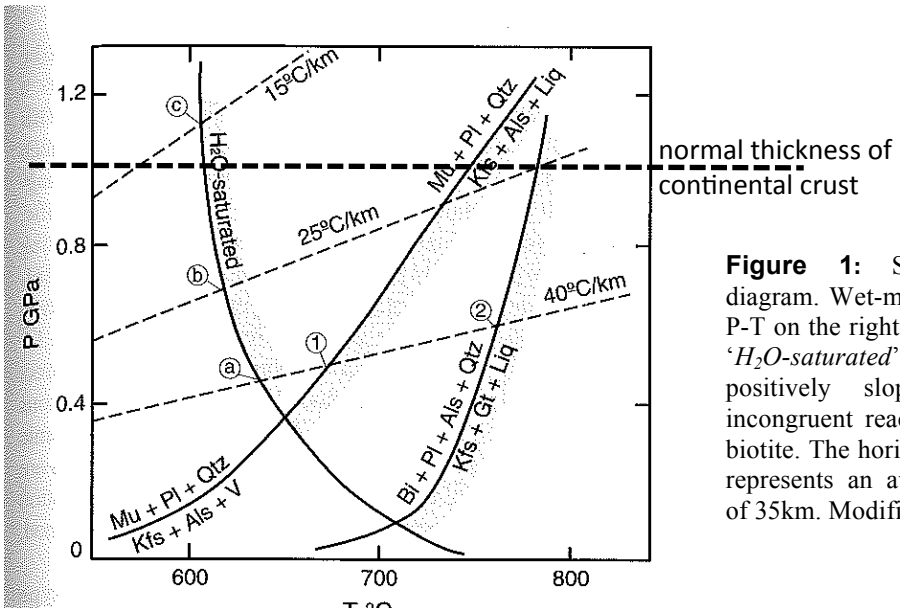

Figure 1: Simplified P-T phase diagram. Wet-melting reactions begin at P-T on the right of the negatively sloped '*H_2O-saturated*' solidus curve. Two positively sloped curves represent incongruent reactions of muscovite and biotite. The horizontal heavy dashed line represents an average crustal thickness of 35km. Modified from Winter, 2009.

Wet melting generates only a small amount of melt without additional influx of water from external sources. Crystalline rocks have limited porosity and contain little water at mid to lower crustal levels (<1 vol %) (Brown 2007). External sources of water may find pathways through the crust locally via contact aureoles, or regionally via infiltration from adjacent rock units and along shear zones. This is referred to as water-assisted melting (Berger et al. 2008) or fluid influx melting (Brown 2007) and leads to the generation of large volumes of melt. Sawyer (2010) investigated partially melted orthogneiss in the Opatica Subprovince of the Canadian Shield and proposed fluid influx melting occurred. In partially melted rocks, a micro-structural analysis of quartz, microcline (k-feldspar) and plagioclase revealed evidence of melting. Quartz and microcline decreased in abundance and biotite increased in abundance compared to the protolith (paleosome). The protolith did not contain enough biotite to produce the amount of melt present (25-30%) by incongruent reactions (see below), a reaction similar to reaction ii) above occurred.

Incongruent melting (hydrate breakdown)

The main hydrous minerals that participate in incongruent reactions are biotite and muscovite in metasediments and also amphibole in meta-igneous and metabasic rocks. Examples of hydrate breakdown reactions are (in order of increasing activation temperature):

iii) Ms + Pl + Qtz = Als + Kfs + Melt

iv) Bt + Als + Qtz = Grd/Crd + Kfs + Melt

v) Hbl + Qtz = Pl + Opx + Cpx (+/- Grt) + Melt

The amount of melt produced depends on the amount of reactants available (Brown 2007). Hydrate breakdown reactions occur at different temperatures, dependant on pressure and rock fertility (see "Partial melting in the continental crust"). Mica will generally begin to breakdown between 700 and 900˚C (figure 1; Sawyer 2011).

PARTIAL MELTING OF THE CONTINENTAL CRUST

The average thickness of the continental crust is around 35km (Cruden 2000). At a typical geothermal gradient of 25˚C/km, the mid to lower crust may generate small increments of wet melting (figure 1), however a thermal perturbation is needed for incongruent melting to commence. Additional sources of heat supply include (from Thompson 2000):

i. Intrusions – plutons, dykes and basaltic magma (local)
ii. Thickening of the continental crust - the lower crust is subject to higher temperatures through advection from the mantle
iii. Concentration of radiogenic elements in thickened crust
iv. Exhumation of thickened crust causing decompressional dehydration melting
v. Basaltic underplating of continental crust
vi. Asthenosphere upwelling beneath thinned lithosphere

The source of external heat is a product of the tectonic environment. The amount of heat/energy produced will determine the volume of melt generated – melt fraction (Rushmer 1996; Brown 2001). Vanderhaeghe (2001) reviewed a number of studies that constrain the pressure and temperature conditions required to melt common crustal protoliths. Relatively fertile crustal rocks were found to generate from 20 to 60% of melt in the range of 700 to 900˚C. Thompson (1999) identified three internal controls of crustal melting that determine the melt fraction:

i. Rock fertility – potential amount of reactants available to yield melt at a minimum temperature (Winters 2009). For example incongruent melting of interbedded metapelite, when temperature surpasses the biotite subsolidus (700-900˚C) metapelite layers with more biotite produce more melt. Vernon (2003) investigated anatexis of interbedded metapelites and metaspammites in the Cooma Complex, in south eastern Australia, and found melt formed in the metapelite layers and not in the metaspammitic layers because the latter did not contain the reactant minerals to form melt under the local pressure and temperature conditions.

ii. H_2O content – refer to '*Wet melting'*.

iii. Magnitude, duration and temperature of heat source and country rock – comparable to melting chocolate in sunlight vs. in the shade. Sunlight has more energy (larger magnitude) and delivers higher temperatures than shade; chocolate will melt at a faster rate in the sun. In either environment, an increase in exposure time will increase the amount of melt produced.

ONSET OF PARTIAL MELTING

When a rock starts melting droplets form at the junction of mineral grains. As melting progresses, droplets join together and create an interconnected network through the solid rock framework. Laporte (1994)(figure 2) summarised an ideal dihedral angle[1] (θ) model for monomineralic rocks with similar interfacial energy (surface tension) between the melt and minerals:

$0^\circ < \theta < 60^\circ$ - melt forms a continuous network along grain edges

[1] Angle between melt droplets formed at grain junctions

$\theta > 60^{\circ}$ - melt occurs as isolated pockets, if the melt fraction exceeds a critical value (Φ_c) ~1 vol. % (mafic rocks), at $\theta = 60^{\circ}$ connectivity can be established. With increasing θ (60°+), Φ_c must also increase to establish connectivity.

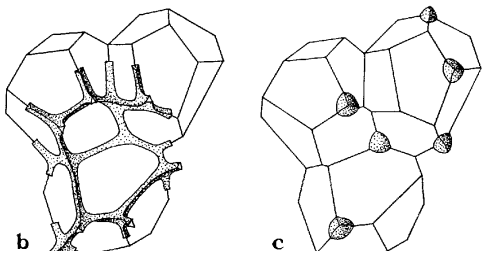

Figure 2: b) when the $\theta<60^{\circ}$ melt connectivity is achieved. **c)** $\theta>60^{\circ}$ melt forms isolated pockets at grain corners. Modified from Laporte, 1994.

Rushmer (1996) contended that the application of the ideal dihedral angle model is minimal because of the "polymineralic non-ideal nature of the lower crust" and the critical melt fraction (Φ_c) also depends upon mineral melting reactions, depth, viscosity, volatile content, composition and deformation.

Brown (2007) refers to the critical melt fraction (Φ_c) as the "melt connectivity transition", Vigneresse et al. (1996) uses "liquid percolation threshold" as part of the percolation theory. Both authors suggest connectivity occurs at a melt fraction of around 5-8 vol. % for felsic melts, and lower for mafic melts. When the critical melt fraction is reached the partially melted rock becomes permeable, and melt can move through and away from its former solid framework. A driving force is needed to move the melt through the permeable matrix, and a dilatant site for it to collect in (Sawyer 1999). When this is achieved, the melt (leucosome) becomes segregated from its residuum (melanosome) and a migmatite is formed.

MELT SEGREGATION

There are three main forces that drive the segregation of melt (leucosome) from residuum (melanosome):

i. Gravity/buoyancy – When melt connectivity has been established and a density difference exists between the solid and the melt, the matrix will compact and expel melt (figure 3; Brown et al. 1995; Wickham 1987).

ii. Volume changes associated with melting (Rutter & Mecklenburgh 2006; Brown 1995) –

    a. Wet melting causes a volume reduction because residuum and melt occupy a smaller volume than the original solid protolith. The volume reduction is accommodated by permanent deformation of the solid framework through compaction (compaction convection).

    b. Dehydration melting causes a volume increase. Excess melt will dilate the rock and infiltrate space between grains. Mesoscopic cracks eventually form and foliation surfaces open.

iii. Applied differential stress – In an open system melt will be expelled from areas of high pressure and migrate to areas of low pressure. At grain scale, melt will migrate along grain boundaries to areas of lower pressure. At the mesoscale, melt migrates to structural sites such as fractures and shear zones, pressure shadows of peritectic minerals, or boudin necks developed from competency contrasts between rock layers (Brown 1995, Vigniresse 1996).

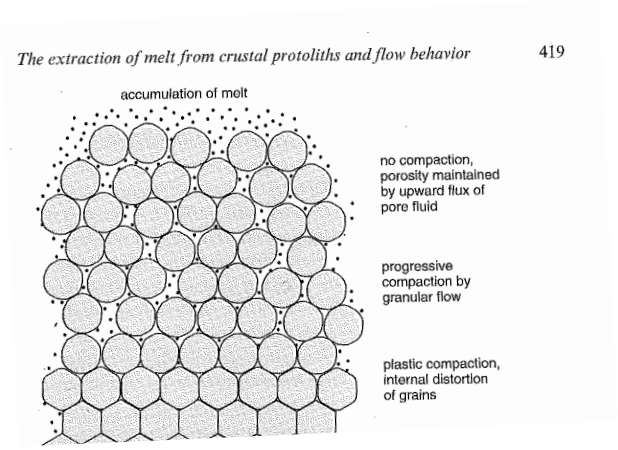

Figure 3: Buoyancy driven melt segregation. When melt connectivity is established, the more buoyant melt will begin to separate from the matrix. An increase in fluid pressure will compact the matrix and squeeze out any remaining melt. This illustrates the path of the green arrow on figure 8 (from Rutter & Mecklenburgh, 2006).

Weinberg (2006) explained segregation is mostly controlled by deformation and rock anisotropy, and 'Cryptic segregation' (segregation driven primarily by pressure gradients such as points i. and ii. above) is less efficient at lower melt fractions. Anisotropy refers to properties of a rock (such as strength) that vary with applied directional stress. Rocks preferentially deform along planes of weakness such as stratigraphic competency contrasts, cleavage and foliation. Vernon (2003) found leucosomes in the Cooma Complex of southeastern Australia were confined to the metapelitic layers, and did not impinge on metaspammitic layers. The anisotropy between the two stratigraphic layers resulted in the preferential partitioning of deformation into the less competent metapelitic layer. Deformation of the metapelitic layers also provided dilation space for the melt to occupy.

Rutter & Mecklenburg (2006) used a yield surface curve (effective mean stress vs. differential stress, Figure 4) to illustrate a melting rock responding to the drivers of melt segregation. Inside the yield surface the melting rock behaves elastically; on and outside the yield surface it behaves plastically through non-reversible changes in shape. The way a rock responds to applied stress, or the way it is deformed, is reflected in its structure and geometry created during melt segregation. Deformation is accommodated by dilation or compaction of the rock, as detailed in table 1.

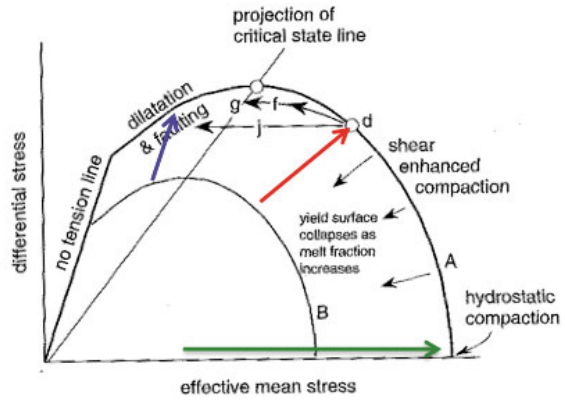

Figure 4: Yield surface of a melting rock, x(effective mean stress)=($\sigma_1+\sigma_2+\sigma_3/3$)-p, where p=pore fluid pressure; y(differential stress)=$\sigma_1-\sigma_3$. The critical state line crosses through the crest of each curve where dilatancy and compaction are in balance. Blue arrow shows an increase in yield surface due to dilatancy hardening. Red arrow shows an increase in yield surface due to strain hardening. The green arrow shows increasing effective mean stress without differential stress, caused by hydrostatic compaction under increasing melt fraction, similar to buoyancy driven segregation mechanism discussed above. Modified from Rutter & Mecklenburg, 2006.

Critical State Line		
	Left *(Hvorslev region)*	**Right *(Roscoe region)***
Deformation mechanism:	Dilation	Compaction
Deformation accommodation:	Strain localisation, vein networks and shear bands	Ductile flow and melt expulsion
Effect on matrix/rock:	Melt pressure reduced, effective mean stress increased	
Yield surface:	B ➔A increase	B ➔A increase
	Both require higher differential stress or pore fluid pressure for deformation to continue	
	= dilatancy hardening	**= strain hardening**
	Fluid pressure is restored by melt migration/drainage into dilation areas (matrix)	Porosity decreases, increasing the strength of the rock

Table 1: Regions along the yield curve – synthesised from explanations contained in Rutter & Mecklenburg (2006), and Brown (2007).

MELT STRUCTURES AND MIGMATITE MORPHOLOGY

Melt structures define how melt was distributed through the host rock, Sawyer (2001) identified 4 controlling factors:

i. Amount and rate of melt produced

ii. Host rock fabric

iii. Intensity of syn-tectonic deformation (discussed in *"Melt segregation"*)

iv. Melt residence time

i. a) Amount of melt produced

With the onset of partial melting (very low melt fraction), melt structures that develop differ in response to the melting environment. A melting rock may be exposed to hydrostatic stress (contact aureole) or a combination of hydrostatic and differential stress (regional deformation). These differing physical environments are referred to as *static* and *dynamic* (Sawyer 2001). Hollness et al. (2011) explained static melting microstructures are controlled by the dihedral angle; at relatively low melt fractions melt will form thin films along grain boundaries (see '*Onset of partial melting*'; figure 5a). Dynamic melting structures are similar, but melt connectivity is accelerated under differential stress, which initiates at progressively smaller fractions. Sawyer (2001) identified two structures that represent the start of melting:

i. Reactant minerals, such as muscovite, biotite and hornblende (in incongruent reactions) become rounded, decrease in size, appear as inclusions in melt patches or may be absent altogether (figure 5a,b).
ii. Solid product minerals have larger grain sizes with crystal faces adjacent to melt pockets (figure 5b).

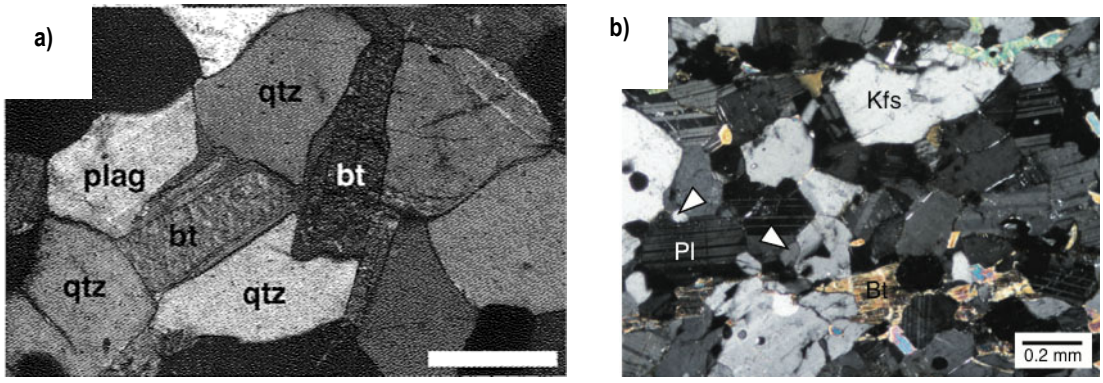

Figure 5: a) Photomicrograph of a granulite phase metapelite, with the melting reaction bt + qtz + pl = opx + kfs (melt). Films of kfs (product of melting reaction) occur on grain boundaries between reactant phases (qtz + bt), reactant phases are also more rounded when in contact with kfs (from Holness, 2008). **b)** Banded orthogneiss with similar melting reaction to a). White triangles point to interstitial qtz; pl and kfs have straight grain boundaries (from Hasalova et al. 2008).

At mesoscopic scale, an increase in melt fraction in a static or a very low differential stress environment will cause melt to coalesce into patches of small rounded neosomes, termed ‘patch migmatites’ (Sawyer 2008b; figure 6a & b). The segregation mechanism follows the green arrow on the yield curve to ‘hydrostatic compaction’ (figure 4). The contrast in viscosity between the melt and the residual solid causes pore fluid pressure to build with increasing melt fraction until the yield surface is reached, upon which the solid matrix will compact and expel the melt. The neosome remains in contact with the melanosome (residuum), therefore the migmatite remains *in situ* (Sawyer 2008b).

A further increase in melt fraction under static (or very low differential stress) will cause in-situ patch leucosomes to expand and to link up. During expansion, the neosome damages and consumes pre-anatectic structures of the paleosome, such as fabric and bedding. In doing so a space is created for melt to occupy. A large patch of neosome is formed (leucosome + melanosome), with intermittent ‘ghost-like’ remnants of paleosome. This is known as a ‘nebulitic migmatite’ (Sawyer 2008b)(Figure 6c).

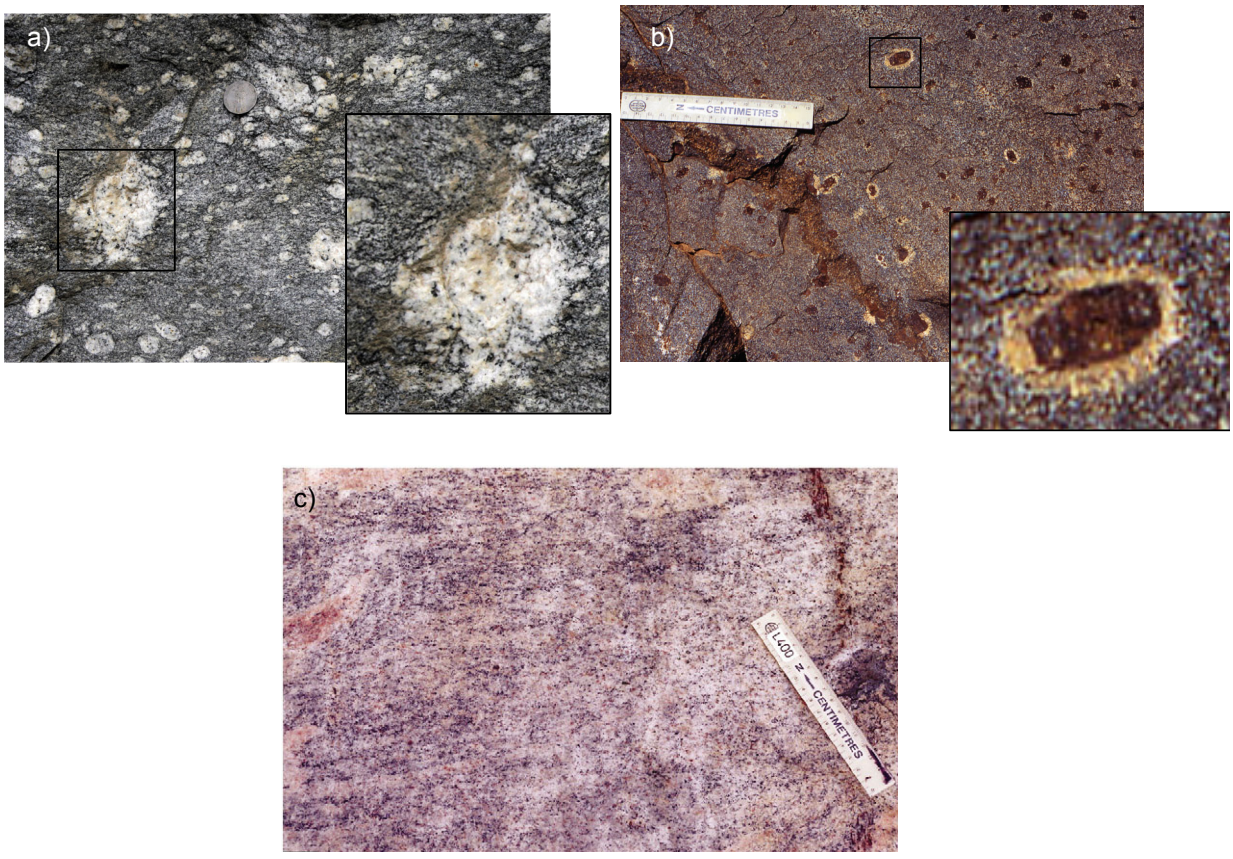

Figure 6: Patch migmatites – mineral grains are coarser than the protolith. **a)** Patch metatexite migmatite – dark melanosome (residuum) occurs as outer rim to a lighter leucosome (see inset), pre-anatectic structures are preserved in surrounding paleosome (from Roberto's geosite, 2014) **b)** Patch metatexite migmatite – residual peritectic phase (garnet) is surrounded by a 'moat' of leucosome (from Sawyer, 2008a). **c)** Nebulitic diatexite migmatite – On the right hand side is a large patch of unsegregated leucosome with diffuse borders. The light grey protolith appears as 'ghostlike' rafts within the patch (from Sawyer, 2010).
http://users.monash.edu.au/~weinberg/Pages/Zanskar_Leucosomes_Malung_Tokpo/Zanskar_2011_leucosome.htm

A migmatite dominated by melt, with pre-partial melting structures present as 'rafts', 'ghost like' or lost altogether is referred to as a **diatexite migmatite.** If pre-partial melting structures are present in a coherent manner the migmatite is called a **metatexite** migmatite (figure 7). Both may occur in the same terrane, however a metatexite will typically occur in the lower temperature terrane, and the diatexite in the higher temperature terrane. A transitional terrane may or may not exist in-between (Sawyer 2008b, [illegible] *'in situ metatexite patch migmatites'*, and figure 6c [illegible] *te'*.

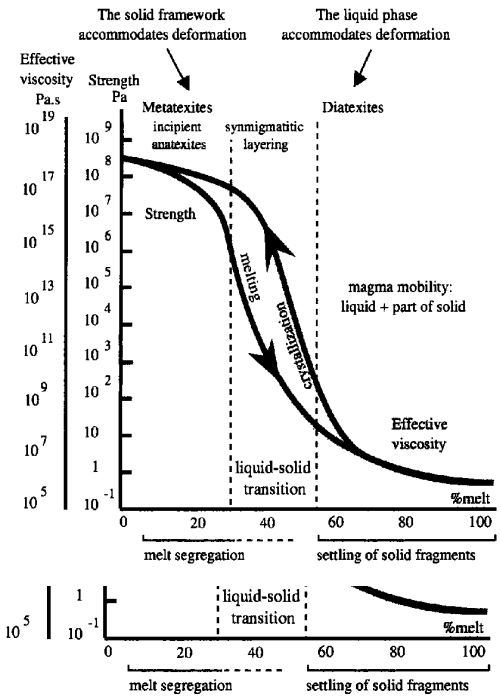

Figure 7: Transition from metatexite to diatexite with increasing melt fraction (x-axis). The transition causes a decrease in strength of the rock (Y-axis) – solid framework accommodates deformation in metatexite migmatites, the melt phase accommodates deformation in diatexite migmatites. Viscosity also decreases, as the solid framework is progressively lost with increasing melt fraction. Modified from Vanderhaeghe, 2001.

The melt fraction that marks the transition from a solid-dominated metatexite, to a liquid dominated diatexite is referred to as the "rheological critical melt percentage" (Brown et al. 1995; Rosenberg & Handy 2005). Vanderhaeghe (2001) suggests this

transition occurs in the range of 30 to 50 vol. % melt, illustrated in figure 7 (melt fraction derived from numerous experimental data).

b) Rate of melt production

A slow rate of melt generation will allow melt to drain from residuum, preserving pre-anatectic (pre-melt) structures. A migmatite may undergo high degrees of partial melting and still remain a metatexite if efficient drainage pathways exist to transport melt elsewhere. If melt rate exceeds drainage rate, it will have a longer residency time within the matrix, and begin to deform and consume pre-anatectic structures (Thompson 2000).

ii. Host rock fabric

From the onset of partial melting, a rock with relatively isotropic fabric such as granite will produce different migmatite structures compared to an anisotropic rock with foliations and competency contrasts, such as a metapelite. Leucosomes exploit weakness within the rock and initially grow parallel to foliations (or bedding contacts; figure 8) (Weinberg 2006; Sawyer 2001).

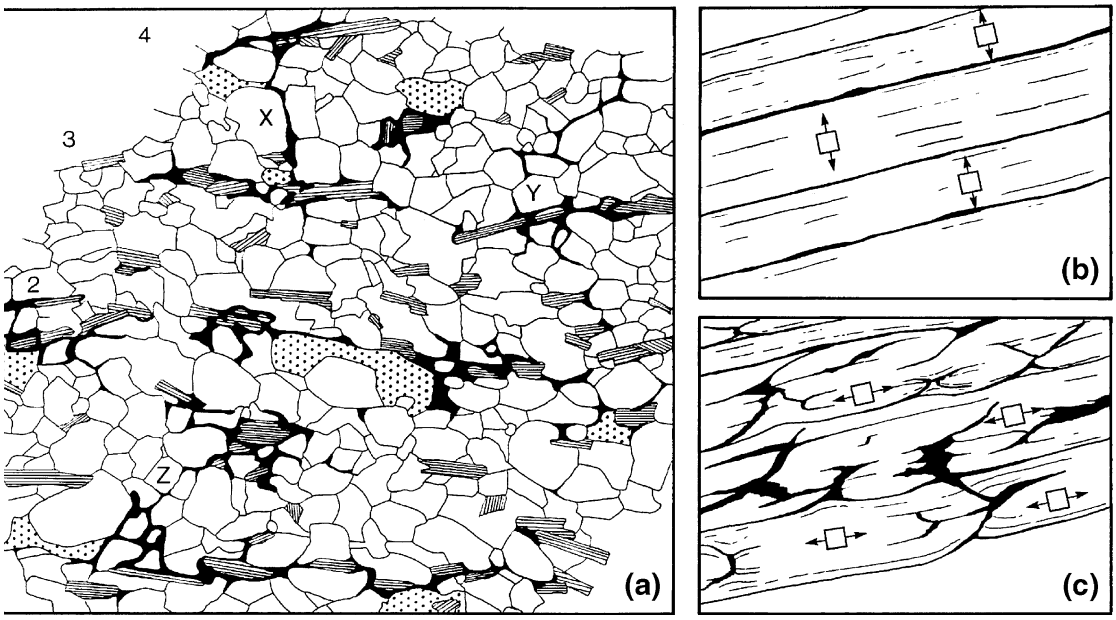

Figure 8: Foliation defined by preferred orientation of biotite grains. Biotite – striped, orthopyroxene – dotted, plagioclase and quartz – white. Melt is black. **a)** Melt forms and connects along aligned biotite grains; fluid pressure may result in connections normal to the foliation (X). **b)** Melt moves across and accumulates in dilational spaces between fabric and layering. **c)** Increasing differential stress (syn-

At the grainscale, melt distribution is determined by textures within the matrix (Sawyer 2001). For example melt will pool along aligned grains of biotite (reactant mineral) in a metapelite, as melting progresses the melt will link to adjacent grains, and eventually form linear arrays that trace an existing foliation (figure 8a). When a melt develops during a period of low differential stress, pressure gradients will exist normal to the fabric or layering. Melt moves across and accumulates in dilational spaces between adjacent fabrics or layers (figure 8b).

Host rock fabric could exist in the rock prior to anatexis (pre-anatectic), or it could form during anatexis (syn-anatectic, syn-tectonic). If syn-tectonic deformation increases, strain incompatibilities will develop and exploit host rock anisotropy (Guernina & Sawyer 2003).

iii. Intensity of syn-tectonic deformation

An increase differential stress can create a pressure gradient and drive melt from high to low-pressure sites. Melt segregation follows the blue arrow in the Hvorslev region on figure 8. Melt migration occurs parallel to the foliation because the degree of connectivity is higher (aligned reactant grains; Laporte 1994) and critical melt fraction (Φ_c) is lower as applied directional stress increases. Initial melt pathways exploit pre-existing host rock fabric. The pathways dilate as melt drains leaving stronger residuum behind. Fluid pressure builds within the melt channels because the stronger residuum becomes strain-hardened and increasingly resistant to further compaction (figure 4 – point d to point g). Fluid pressure may also build if the imposed strain rate is higher than the rate at which melt can escape (Brown 1995). The increase in pressure will eventually open dilation spaces where

melt can migrate and pool, relieving pressure in other areas of the system (figure 8c). Host rock anisotropy determines where dilatancy structures will occur, exploiting competency contrasts and planes of weakness within rock fabric and stratigraphy (Sawyer 2008b).

When a leucosome forms in a dilation site, the melt has moved away from its point of origin and is no longer in contact with its melanosome. A leucosome that has migrated away from is origin, but is still within its source layer is called an *in-source* migmatite (Sawyer 2008b). Figure 9 details a number of structures that can occur in an '*in-source dilatant structured metatexite migmatite'*.

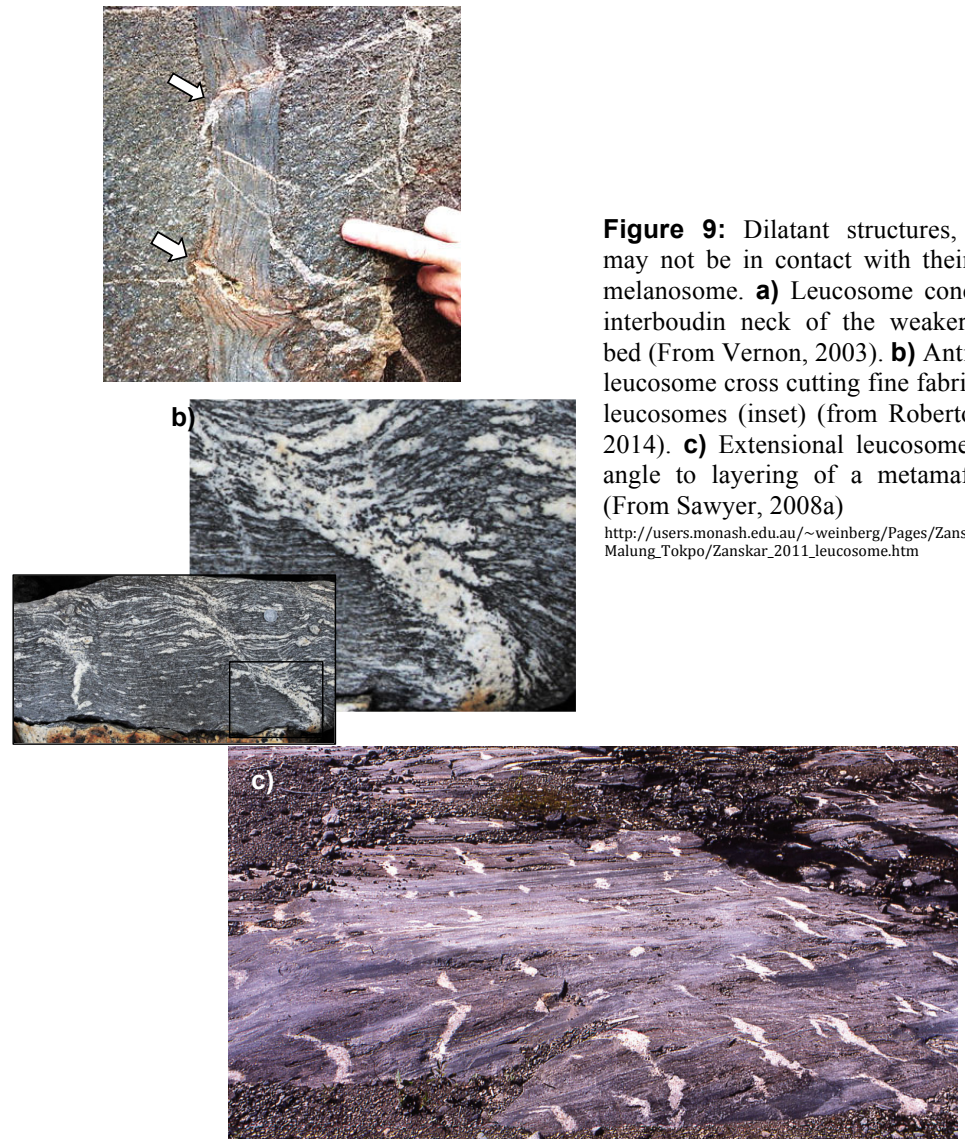

Figure 9: Dilatant structures, migmatites may not be in contact with their associated melanosome. **a)** Leucosome concentrated in interboudin neck of the weaker metapelite bed (From Vernon, 2003). **b)** Antithetic shear leucosome cross cutting fine fabric orientated leucosomes (inset) (from Roberto's Geosite, 2014). **c)** Extensional leucosomes at a high angle to layering of a metamafic outcrop. (From Sawyer, 2008a)
http://users.monash.edu.au/~weinberg/Pages/Zanskar_Leucosomes_Malung_Tokpo/Zanskar_2011_leucosome.htm

Progressive deformation will accelerate the creation and number of dilatant structures, and subsequently increase melt fraction. Eventually the rock will become weaker and approach the rheological critical melt transition (Figure 7). Melt filled channels, shear bands and dilation bands interconnect, with an orientation determined by the direction of applied stress (figure 10a). When two sets of leucosomes intersect, such as parallel and oblique to compositional layering, they form a '*net structure'* (figure 10b; Sawyer 2008b). Weinberg & Mark (2006) investigated the intricate relationship between melt-enhanced deformation and melt migration in migmatites within the Karakoram Shear Zone, India. During folding, magma drained from layer parallel leucosomes (*in-situ*) into axial planar (*in-source*) leucosomes. Melt enhanced deformation because slip was preferentially accommodated along layer parallel and axial planar foliations. The build up of pore pressure in fold hinges allowed melt to penetrate through rock layering (figure 11).

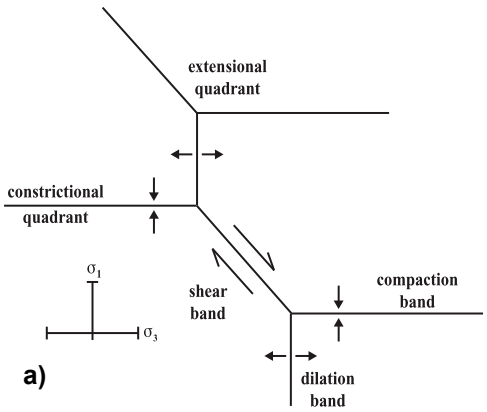

Figure 10: a) Melt pathways. Melt is squeezed from the matrix into channels orientated perpendicular to σ^1 (constrictional). Melt is transported through shear bands to dilational spaces that open perpendicular to σ^3 (extension) (from Brown, 2007). **b)** Net structure – fabric orientated leucosomes (constructional) are crosscut by a second set of shear/dilational leucosomes (from Sawyer, 2008a).

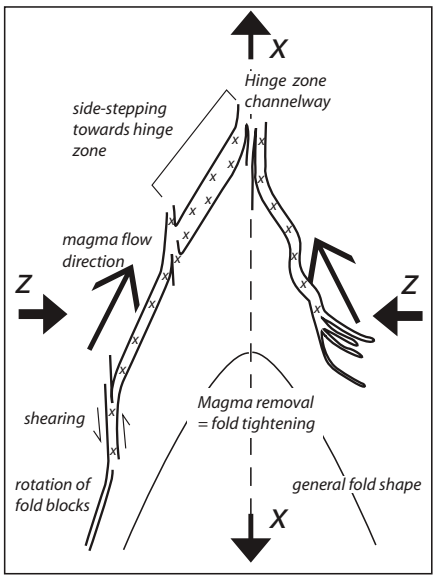

Figure 11: a) Melt enhanced deformation (σ^1=z σ^3=x) – Axial planar leucosomes cross cut layer parallel leucosomes, accommodating slip. Melt bursts through the hinge zone and is transported away (from Weinberg & Mark, 2008).

A *'stromatic migmatite'* is dominated by thin, parallel and laterally persistent leucosomes (figure 12) and contains a large proportion of melt. Pre-partial melting structures are retained in melanocratic layers. This structure accommodates the most amount of strain within the metatexite migmatite group. A further increase in melt fraction destroys the remaining pre-partial melting fabric and begins the transition to a diatexite migmatite (Sawyer 2008b).

http://users.monash.edu.au/~weinberg/Pages/Czech_2013/Banded_gneiss_migmatites.htm

Figure 11: Banded gneiss - stromatic migmatite. Sheared axial planar leucosomes are the dominant. The paleosome is preserved in dark melanocratic bands. It could be argued that these dark bands represents *schlieren* (if there was further evidence of magmatic flow) making this a diatexite migmatite. Photo taken Parallel to lineation and perpendicular to foliation (from Roberto's Geosite, 2014).

During the transitional phase between diatexite and metatexite tabular fragments of competent neosome can become completely surrounded by melt. The melt phase accommodates most of the deformation and fragments (called "*schollen" or "rafts")* can become orientated by the applied differential stress (Sawyer 2008b). A competency contrast exists between schollen fragments and the surrounding melt producing syn-magmatic structures that provide an indication of shear sense and magmatic flow, including pressure shadows and deflection of sub-magmatic or magmatic foliations (figure 12).

http://users.monash.edu.au/~weinberg/Pages/DomFeliciano_belt/Diatexite_Itapema.htm

Figure 12: Giant amphibolite schollen surrounded by sheared diatexite. Notice preferred orientation of smaller schollen around the large raft, an indication of shear flow (from Roberto's Geosite, 2014)

Schollen structures decrease in size and frequency as melt fraction increases. Melt will begin to flow in response to local and regional deformation and flow bands may

develop. '*Schlieren'* are darker bands rich in platy or blocky minerals consisting principally biotite and accessory phases (figure 13). Although the origin of schlieren is not fully understood, Milord & Sawyer (2003) list four potential origins:

i. Unmelted residuum – mineral phases that have not participated in melting reactions
ii. Mineral accumulations formed during magma flow – Milord & Sawyer (2003) found St.Malo schlieren were developed from the separation of biotite and plagioclase through grain dispersive pressure during melt flow.
iii. Compositional layering
iv. Sites of melt loss – highly residual remains of fertile layers

Loss or absence of schlieric structures produce homogenised diatexites. With further and complete separation of neosome from the protolith, the crystallised melt (magma) can be classified as anatectic granite (D'Lemos 1992).

Figure 13: Schlieren Diatexite Migmatite – Schlieren are thin, dark, subparallel bands with a preferred orientation. Sub to euhedral, coarse plagioclase grains define a magmatic foliation in the leucosome (From Sawyer, 2008a).

iv. Melt residence time

A Migmatite seen in the field is a snap shot, frozen in time, of a melt system that evolved through many stages. High strain metatexite and diatexite structures develop and evolve because melt is driven out of the matrix towards low-pressure sites. If reactant(s) are exhausted, melt production ceases and pore pressure decreases. Melt pathways subsequently deflate and collapse, leaving just melanocratic remnants. Alternatively, if the heat source is exhausted and temperature decreases, melt crystallises in the pathway before drainage can occur (figure 14; Sawyer 2001).

Figure 14: Stromatic metatexite with a collapsed melt escape channel. The collapsed channel is visible as a melanocratic lamination across the middle of the photograph, left to right. The collapse structure truncates the vertical dilatant leucosomes and foliation/layer parallel leucosomes (Roberto's Geosite, 2014).

http://users.monash.edu.au/~weinberg/Pages/Zanskar_Leucosomes_Malung_Tokpo/Zanskar

DISCUSSION

Plate tectonics provide the thermal perturbations required to initiate melting. It is also the main driver of deformation. A positive feedback mechanism exists between deformation and melting. Rock strength decreases exponentially with increasing melt fraction (Figure 7; Vanderhaeghe 2001). Rock anisotropy is increased when there is a viscosity difference between the leucosome and melanosome. Leucocratic layers are more viscous, and weaker than melanocratic layers and preferentially partition strain to accommodate deformation.

This was demonstrated in Weinberg & Mark (2006); melt facilitated strain localisation (along leucosome pathways and fold hinges), which may have been more homogenous if melt was absent.

On a tectonic scale, a 'chicken or egg' dilemma exists between melt and deformation. Rosenburg et al. (2007) explored the question of whether melt induced strain localisation (local deformation) or if strain localisation created pathways for melt. On a crustal scale, large bodies of melt in the mid to lower crust localise strain and spread laterally to form weak sub-horizontal channels which drive the transformation of topography above. A good example is explained in Rosenburg et al (2007) with the formation of melt-weakened intracrustal channel in the Himalayas. On a regional scale, in the mid to upper crust, shear zones accommodate the emplacement of buoyant, partially melted crust (magma). D'lemos (1992) proposed thermal softening of country rocks during magma ascent through a shear zone enhanced ductile deformation and strain localisation (within the shear zone). Therefore regional tectonics and granite generation and emplacement may be a contemporaneous process.

D'Lemos (1992) investigated a correlation between granitic plutons and shear zones and proposed a model of emplacement. Magma was generated in an anatectic zone and entered a ductile extensional jog within a mid crustal shear zone. It then rose through the crust via buoyancy and build up and release of pressure in dilatant zones (dilatancy pumping) along 'megadyke' channelways within the shear zone. Upon reaching the upper crust, it is emplaced in an extensional jog in a brittle, anastomosing strike slip fault system (figure 20a). It is interesting to consider how this larger crustal scale process can be compared to the mesoscale process of migmatite formation. Both scales operate under basic principle of expulsion of melt from the matrix into drainage channels and migration towards low pressure dilatant sites.

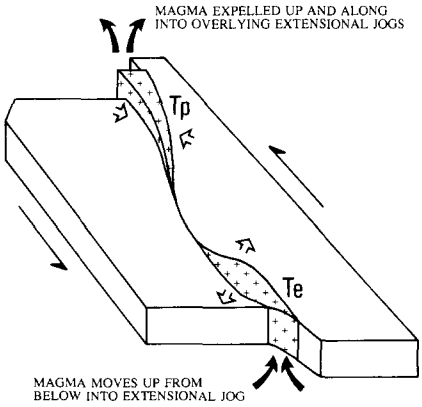

Figure 20: Upper crustal shear zone creating extensional jogs for magma to migrate to. Similar to mesoscale shear band structures in migmatites (From D'Lemos, 1992).

CONCLUSION

The different forms of geometry and structure a migmatite can have are due to the high number of variables that determine how it is created. From the beginning of migmatite formation, initial partial melting microstructures are determined by the depth and type of melt reaction that takes place. Increasing the partial melt fraction achieves melt connectivity, and allows melt to begin to flow within the rock. Segregation mechanisms will squeeze melt out of the matrix into drainage channels parallel to any weakness in the rock as a result of anisotropy (foliations, layering). Syn-tectonic deformation will accelerate melt connectivity, but doesn't initially influence melt flow pathways until higher strain rates are achieved and lower pressure dilation spaces and shear bands develop. Increasing the melt fraction further causes a rheological transition from metatexite (solid framework accommodates deformation) to diatexite (liquid framework accommodates deformation).

A migmatite resembles a frozen network of structures that facilitated the segregation of melt (leucosome) from residuum (melanosome). Morphology classification is based upon three divisions:

- The amount of melt present in the rocks
- The degree to which leucosome and melanosome are separated from each other and the protolith
- The degree of deformation the migmatite has endured

Migmatic structures progress from simple patch neosomes, to moderate melt fraction and moderate strain stromatic metatexite migmatites to homogenous diatexites. Rock strength decreases during the transition from metatexite to diatexite. The weaker melt phase has an enhanced ability to localise strain, which may enhance local deformation.

REFERENCES

BERGER A.*, et al.* 2008 Tectonically controlled fluid flow and water-assisted melting in the middle crust: an example from the Central Alps, *Lithos,* vol. 102, no. 3, pp. 598-615.

BROWN M. 2001 Crustal melting and granite magmatism: Key issues, *Physics and Chemistry of the Earth, Part A: Solid Earth and Geodesy,* vol. 26, no. 4-5, pp. 201-212.

--- 2007 Crustal melting and melt extraction, ascent and emplacement in orogens: Mechanisms and consequences, *Journal of the Geological Society,* vol. 164, no. 4, pp. 709-730.

BROWN M.*, et al.* 1995 Melt segregation in migmatites, *Journal of Geophysical Research,* vol. 100, no. B8, pp. 15,655-15,679.

D'LEMOS R. S., BROWN M. & STRACHAN R. A. 1992 Granite magma generation, ascent and emplacement within a transpressional orogen, *Journal - Geological Society (London),* vol. 149, no. 4, pp. 487-490.

GUERNINA S. & SAWYER E. W. 2003 Large-scale melt-depletion in granulite terranes: An example from the Archean Ashuanipi subprovince of Quebec, *Journal of Metamorphic Geology,* vol. 21, no. 2, pp. 181-201.

HASALOVÁ P.*, et al.* 2008 Origin of migmatites by deformation-enhanced melt infiltration of orthogneiss: A new model based on quantitative microstructural analysis, *Journal of Metamorphic Geology,* vol. 26, no. 1, pp. 29-53.

HOLNESS M. 2008 Decoding Migmatite Microstructures, *Working with migmatites. Mineral Assoc Canada Short Course,* vol. 38, pp. 56-75.

HOLNESS M. B., CESARE B. & SAWYER E. W. 2011 Melted rocks under the microscope: Microstructures and their interpretation, *Elements,* vol. 7, no. 4, pp. 247-252.

LAPORTE D. 1994 Wetting behavior of partial melts during crustal anatexis: the distribution of hydrous silicic melts in polycrystalline aggregates of quartz, *Contributions to Mineralogy and Petrology,* vol. 116, no. 4, pp. 486-499.

MILORD I. & SAWYER E. W. 2003 Schlieren formation in diatexite migmatite: Examples from the St Malo migmatite terrane, France, *Journal of Metamorphic Geology,* vol. 21, no. 4, pp. 347-362.

PETFORD N.*, et al.* 2000 Granite magma formation, transport and emplacement in the Earth's crust, *Nature,* vol. 408, no. 6813, pp. 669-673.

ROBERTO'S GEOSITE, 2014. School of Geosciences, Monash University, Australia. http://users.monash.edu.au/~weinberg, accessed April 2014.

ROSENBERG C. L. & HANDY M. R. 2005 Experimental deformation of partially melted granite revisited: Implications for the continental crust, *Journal of Metamorphic Geology,* vol. 23, no. 1, pp. 19-28.

ROSENBERG C. L., MEDVEDEV S. & HANDY M. R. 2007 Chapter 13: Effect of Melting on Faulting and Continental Deformation. Dahlem University Press.

RUSHMER T. 1996 Melt segregation in the lower crust: How have experiments helped us?, *Transactions of the Royal Society of Edinburgh, Earth Sciences,* vol. 87, no. 1-2, pp. 73-83.

RUTTER E. & MECKLENBURGH J. 2006 The extraction of melt from crustal protoliths and the flow behavior of partially molten crustal rocks: an experimental perspective, *Evolution and differentiation of the continental crust. Edited by M. Brown and T. Rushmer. Cambridge University Press, Cambridge, UK*, pp. 386-429.

SAWYER E. W. 1999 Criteria for the recognition of partial melting, *Physics and Chemistry of the Earth, Part A: Solid Earth and Geodesy,* vol. 24, no. 3, pp. 269-279.

--- 2001 Melt segregation in the continental crust: Distribution and movement of melt in anatectic rocks, *Journal of Metamorphic Geology,* vol. 19, no. 3, pp. 291-309.

SAWYER E. W. 2008a Atlas of migmatites. NRC Research press.

SAWYER E. W. 2008b Working with Migmatites: Nomenclature for the Constituent Parts, *Working with migmatites. Mineral Assoc Canada Short Course,* vol. 38, pp. 1-27.

SAWYER E. W. 2010 Migmatites formed by water-fluxed partial melting of a leucogranodiorite protolith: Microstructures in the residual rocks and source of the fluid, *Lithos,* vol. 116, no. 3-4, pp. 273-286.

SAWYER E. W., CESARE B. & BROWN M. 2011 When the continental crust melts, *Elements,* vol. 7, no. 4, pp. 229-234.

THOMPSON A. B. 2000 Some time-space relationships for crustal melting and granitic intrusion at various depths. pp. 7-25.

THOMPSON A. B. & CONNOLLY J. A. D. 1995 Melting of the continental crust: some thermal and petrological constraints on anatexis in continental collision zones and other tectonic settings, *Journal of Geophysical Research,* vol. 100, no. B8, pp. 15,565-15,579.

VANDERHAEGHE O. 2001 Melt segregation, pervasive melt migration and magma mobility in the continental crust: The structural record from pores to orogens, *Physics and Chemistry of the Earth, Part A: Solid Earth and Geodesy,* vol. 26, no. 4-5, pp. 213-223.

VERNON R. H. 2003 Contrasting magmas in metapelitic and metapsammitic migmatites in the Cooma Complex, Australia, *Visual Geosciences,* vol. 8.

VIGNERESSE J. L., BARBEY P. & CUNEY M. 1996 Rheological transitions during partial melting and crystallization with application to felsic magma segregation and transfer, *Journal of Petrology,* vol. 37, no. 6, pp. 1579-1600.

WEINBERG R. F. 2006 Melt segregation structures in granitic plutons, *Geology,* vol. 34, no. 4, pp. 305-308.

WEINBERG R. F. & MARK G. 2008 Magma migration, folding, and disaggregation of migmatites in the Karakoram Shear Zone, Ladakh, NW India, *Bulletin of the Geological Society of America,* vol. 120, no. 7-8, pp. 994-1009.

WICKHAM S. M. 1987 The segregation and emplacement of granitic magmas, *Journal of Geological Society,* vol. 144, no. 2, pp. 281-297.

WINTER J. D. 2009 An introduction to igneous and metamorphic petrology. (2nd ed. edition). Prentice Hall, Upper Saddle River, N.J.

APPENDIX C

Field Area: Yalgoo (Badja), Murchison Domain, Youanmi Provence, Yilgarn Craton, Western Australia. South of the small township of Yalgoo, "The Yalgoo Dome" a 30x90km archean granitic dome bordered by archean greenstone belts. Co-ordinates: 28˚46'38"S; 116˚37'27"E (Google Earth Figure 1).

GSWA Map sheets: 1:100,000 - Wuraga 2141, Yalgoo 2241, Mellenbye 2140, Badja 2240, Perenjori 2139, Rothsay 2239.

Figure 1: The Yalgoo Dome – Granite intrusions are flanked by linear green stone belts (denoted by grey arrows). Image taken from Google Earth.

Geological setting and previous work

Two ancient cratons form the backbone of Western Australia, the Pilbara craton in the north, and the larger and younger Yilgarn Craton in the south (Yilgarn – 1,000,000km^2). The latter accounts for most of the land in the south half of the state. Previous research has estimated that most of the Yilgarn was formed between the meso- and neo-archean, 3.1 and 2.6Ga (Champion & Cassidy 2007), however ongoing research by the Western Australia Geological Survey is continually constraining formation dates and evolutionary stages with renewed precision (see Van Kranendonk et al. 2013, Ivanic et al. 2012). The Yilgarn is dominated by N-S trending linear greenstone belts separated by granitic bodies. Granites comprise of around 70% of rock types per surface area, greenstones make up less than 30% (Figure 2). The granite-greenstone association is a pattern consistent with other similar aged terranes around the world, for example the Slave Province (Canada), Zimbabwe Craton and the Dharwar craton in India (Kusky & Polat 1999).

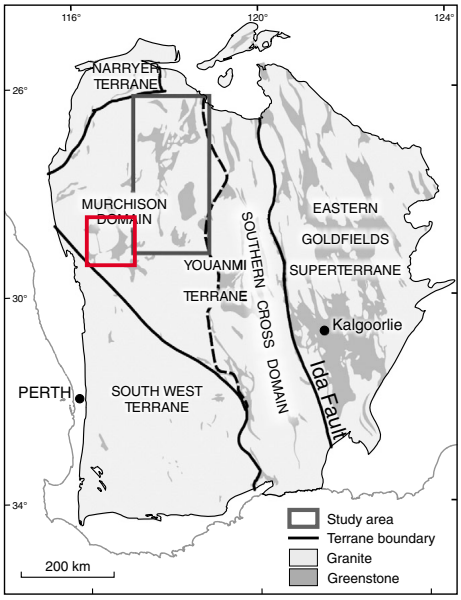

Figure 2: Yilgarn craton with terrane subdivisions. Note the linear ~north-south granite/greenstone pattern in the top half of the craton. The red box encloses the field area. Modified from Ivanic, 2012.

The Yilgarn is divided into three terranes – the Eastern Goldfields Superterrane (EGST), the Youanmi and Southwest Terranes (YT), and the Narryer Terrane (figure 2). The north-south trending Ida fault system separates the EGST from the Youanmi Terrain.

The Youanmi Terrane is ~300,000km^2 encompassing the bulk part of the western Yilgarn. It is differentiated from the eastern Yilgarn (EGST) based on its higher metamorphic grade, older and more fragmented greenstone belts, and presence of banded iron formations (BIF) (Van Kranendonk et al. 2013). The Youanmi Terrane is further divided into the Murchison Domain in the west and the Southern Cross Domain in the east. This division is based on the differing lithostratigraphic assemblages of greenstone belts. A north-south anastomosing strike slip shear zone separates the domains. Ivanic et al. (2012) propose the Murchison Domain was developed between 2.81-2.72Ga through melting and reworking of existing crust.

The Yalgoo Dome[1] is positioned slightly southeast from the centre of the Murchison Domain. It is a lozenge shape granitic intrusion with a long axis orientated north-south and approximate dimensions of 90x30km. North-south orientated synformal greenstone belts flank the dome, easily identified on the google earth satellite image as dark patches on either side of the lighter granite outcrops (figure 1). There is limited literature specifically addressing the formation of the Yalgoo dome, namely Rey et al. (1999) and Myers & Watkins (1985). Watkins & Hickman catalogued the stratigraphy of the area in their 1990 publication and proposed a tectonic model for the Murchison Domain. Subsequent studies conducted in the Murchison Domain have increased the amount of geochemical and geochronology data available. This has resulted in modifications to the original stratigraphic scheme of Watkins & Hickman (1990) by Pidgeon & Hallberg (2000) and Champion & Cassidy (2002 & 2007). Van Kranendonk et al. (2013) developed a new stratigraphic scheme and tectonic evolution model for the

[1] Interestingly, Foley (1997) refers to the 'Yalgoo Dome' as the 'Badja Granitoid Dome', Badja is also the name of the GSWA map sheet at the centre of the dome and mayve its original name.

Murchison domain, however the study area was in the north-east of the Murchison Domain, it did not envelope the Yalgoo Dome.

Geology of Yalgoo

Watkins & Hickman (1990) presented a detailed description of the stratigraphy in the Murchison Domain, the data collected in the Yalgoo region is presented in figure 3 (below) and table A1 in appendix A. This emphasised geochemical analysis to determine possible origins of intrusive and extrusive magmatism and detailed descriptions of volcanic sequences within greenstone belts. There have been subsequent modifications to the Murchison domain stratigraphic scheme, the original descriptions and chemical analysis of the rocks are still applicable.

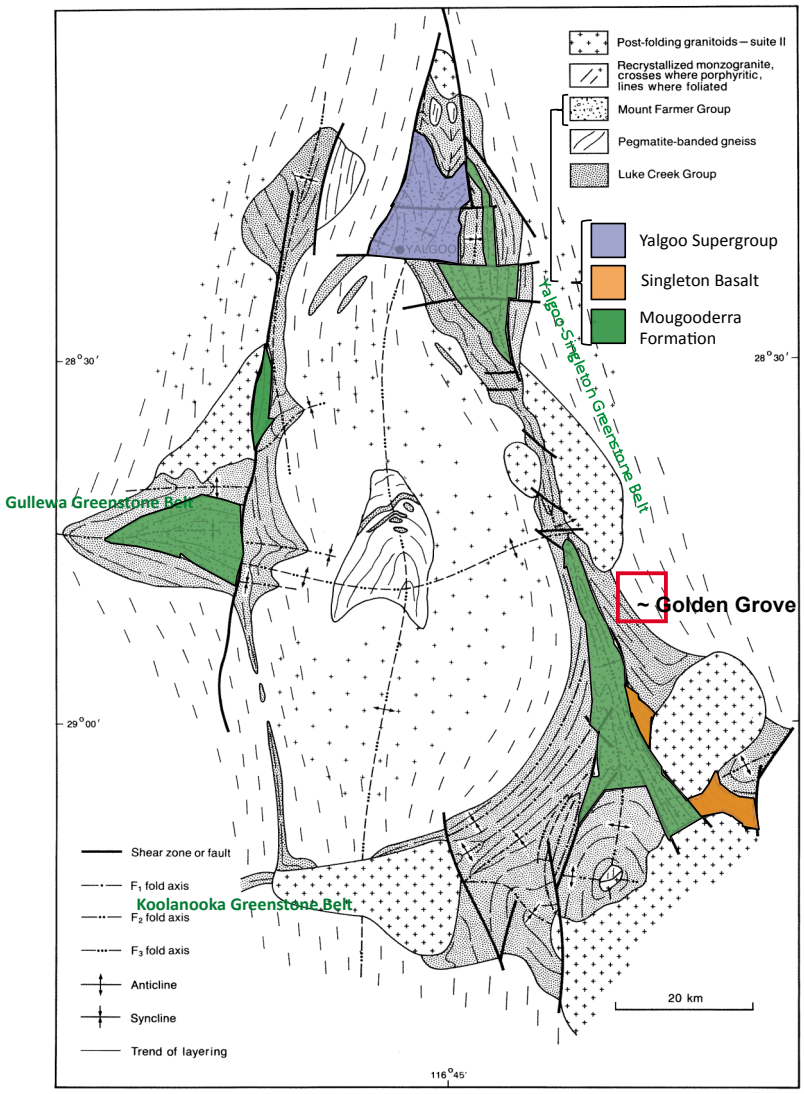

Figure 3: Map synthesised from data presented in Watkins & Hickman (1990). Refer to appendix A for detailed description of rock units.

In the new stratigraphic scheme for the Murchison domain presented by Van Kranendonk et al. 2013, comment was made about older greenstones in Golden Grove, on the eastern edge of the Yalgoo-Singleton Greenstone Belt (red box, figure 3). It is possible to compare Van Kranendonk et al 2013 and Watkins & Hickman (1990) in this area. Similarities exist between the bimodal basal units of the Norie Group in Van Kranendonk (2013), and the upper Luke Creek Windaning Fomation and the base of the Mount Farmer Mougooderra formation in Watkins and Hickman (1990). Watkins & Hickman (1990) divided the upper greenstone sequences into formations unique to individual greenstone belts. Van Kronendonk & Ivanic (209) used available geochronology data to group together rocks of similar composition and age that were previously divided into different units by Watkins & Hickman (1990), and to also divide units that grouped rocks of different ages together. The stratigraphic scheme is applicable to the northeast Murchison field area of Vankronendonk et al. (2013) (appendix A2), and it is suggested that it may be applicable to the entire Murchison Area. This suggestion may be proved or modified with information from current studies that are being conducted in the Yalgoo area.

Watkins & Myer (1990)	Van Kronendonk et al. (2013)
Basal Mount Farmer Mougoderra Formation Sedimentary rocks and minor basalt ~2000m. Upward-fining sequence of epiclastic sedimentary rocks - Basal: medium to coarse grained, poorly sorted lithic wacke, with lenticular conglomerate clasts.	**Golden Grove Greenstones** 2.5km thick package of felsic and intermediate volcanic, felsic volcaniclastic and chemical sedimentary rocks. Unconformably overlain by a unit of banded iron formation and volcaniclastic mass flow sedimentary rocks containing
Upper Luke Creek Windaning Formation Abundant jaspilitic BIF and grey-white chert units interlayered with felsic volcanic, volcaniclastic and volcanogenic rocks, minor basalts. BIF's a few cms to 150m	

Table 2: Comparison between Watkins & Hickman (1990) and Van Kranendonk et al. (2013) of greenstone sequences in the Golden Grove area of the Yalgoo-Singletone greenstone belt.

Watkins and Hickman (1990) divided granitoid rocks into three units:

i. Pegmatite banded gneiss: two phases of monzogranite, and one phase of granodiorite sourced from partial melting of lower crustal mafics, subsequently deformed creating the gneissosity.
ii. Recrystallised monzogranite: Compositionally similar to pegmatite banded gneiss (similar source). Metamorphosed and recrystallised by post emplacement deformation.
iii. Post Folding Granitoids: Proximal to greenstone belts, never intrude wholly within older granitoids. Partial melting of lower crustal mafics with subsequent crustal assimilation.

Champion & Cassidy (2007) investigated granitoids in further detail and found the original stratigraphic scheme to be inconsistent with new geochronology data. For example pegmatite-banded gneiss, the oldest felsic intrusive from Watkins & Hickman (1990), contains younger material and evidence of magma mingling (Champion & Cassidy 2007; Van Kranendon & Ivanic 2009). The modification proposed 5 granite groups for the entire Yilgarn Craton, based on geochemical characteristics (table 2).

Group Area %	Lithologies	Field Characteristics	Geochemistry	Youanmi Terrane	Eastern Goldfields Superterrane	Comments
High-Ca >60%	**granodiorite, granite, trondhjemite.** distributed both within and external to greenstone belts	strongly deformed to gneissic to mildly deformed; typically ovoid plutons (elongate parallel to structural grain); minor dykes/sills and small bodies; some allanite or sphene	high Na_2O, Na_2O/K_2O, low Th, LREE, Zr; mostly Y-depleted, Sr-undepleted; range of LILE, LREE and Th contents; younger rocks extend to more LILE-enriched compositions	>3.0 Ga-2.9? Ga, ca. 2.81 Ga, ca. 2.76 to 2.68 Ga; mostly 2.73-2.68 Ga	ca. 2.8 Ga (minor remnants); 2.74-2.65 Ga; majority 2.685 to 2.655 Ga; youngest members appear to occur within Kalgoorlie Terrane	high pressure partial melting of basaltic protoliths
Low-Ca >20%	**granodiorite, granite** mostly external to greenstone belts	mildly deformed to undeformed, locally strongly deformed; large intrusions (sheet-like) to small pods and dykes; biotite-dominant; allanite, sphene and fluorite-bearing	high K_2O, low Na_2O, high Rb, Th, LREE, Zr; moderately fractionated end-members	2.65-2.6? Ga; mostly 2.65 to 2.63 Ga; possibly also 2.685 Ga	2.655 to 2.63 Ga	partial melting of High-Ca type source rocks
High-HFSE 5-10%	**granite, minor granodiorite** mostly internal or marginal to greenstone belts	variably deformed, high-level intrusives, commonly spatially associated with volcanic rocks and volcanic complexes; presence of amphibole in a very felsic rock is diagnostic	distinctive combination of high FeO*, MgO, TiO_2, Y, Zr with low Rb, Pb, Sr, Al_2O_3	3.01 to 2.92 Ga?, ca. 2.81 Ga, 2.76 Ga to 2.45 & younger?; also 2655-2620 Ma	>2.72 Ga to 2.665 Ga; 2.7 to 2.68 Ga most common; mostly geographically restricted to Kurnalpi Terrane & north-east Kalgoorlie Terrane	spatial association with VHMS mineral systems
Mafic 5-10%	**diorite, granodiorite, granite, tonalite & trondhjemite**	variably deformed, distinctive dark-looking granites; form moderate to small sized plutons and common dikes and sills; common amphibole ± biotite ± pyroxene	low SiO_2 (55-70+%), moderate to high Ni, Cr, MgO; range of LILE, LREE and Th; subdivided into high- and low-LILE	3.01 to 2.92 Ga?, ca. 2.81 Ga, 2.76 Ga to 2.10 Ga	>2.72 Ga to 2.65 Ga; possibly younger? LILE-enriched members tend to be ca. 2.665 and younger	common spatial association with gold mineralisation, especially high-LILE members
Syenitic <5%	**syenite, quartz syenite** internal or marginal to greenstone belt	commonly undeformed; distinctive red granites with green pyroxene (or amphibole); K-feldspar-rich, little or no quartz	high total alkalis (Na_2O + K_2O) 10-12%; commonly low MgO, FeO*, TiO_2	none	ca. 2.65 Ga, and 2.655-2.645 Ga	some spatial association with gold mineralisation

Table 2: Champion & Cassidy (2007) – Granite classifications according to craton wide geochronology and geochemistry. Coloured blocks in "Group / Area %" indicates granites present in Yalgoo field area (see figure 3).

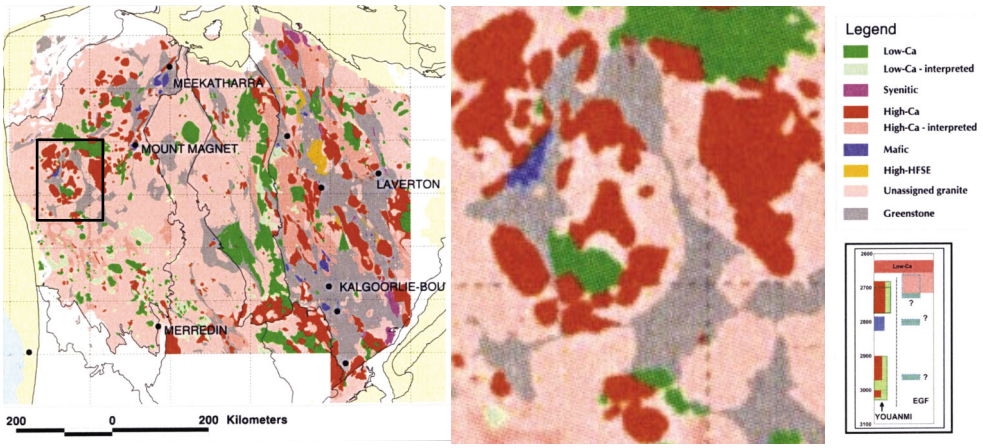

Figure 3: Left: distribution of granites in the Yilgarn Craton. Centre: Distribution of granites in Yalgoo area. Modified from Champion & Cassidy, 2007.

Structural geology

Table 3 comprises a comparison of deformation events according to Watkins & Hickman (1990), Van Kranendonk (2013), Watkins & Myers (1985) and Stewart (2013). There is consistent evidence for regional D_2 tight, upright folding with east-west axial surfaces, D_3 folds with north-south axial surfaces and D_3 north-south trending shear zones. Stewart (2013) proposed a tectonic history of the Golden Grove area using detailed mapping of the

Zn-Cu deposit at Gossan Hill, detailed local structural observations and regional correlations. Rocks at Golden grove did not undergo regional folding events recorded in other greenstone belts by the other authors.

To diapir or not to diapir - how did the Yalgoo dome come into being?

Of the limited studies focused specifically on the Yalgoo dome, there has been controversy surrounding its formation. Early models explained granite/greenstone patterns in the Yilgarn Craton to be the result of by intrusive deformation of greenstones by syn-kinematic diapirs and post kinematic plutons and batholiths (Archibald 1978). Myers and Watkins (1985) dismissed diapirism as a mechanism for granitoid emplacement. Instead they proposed the granite/greenstone patterns of the Yilgarn Craton developed from erosion of fold interference patterns (type 0), based on the following evidence:

- D_2 folds with steep east-west axial surfaces refolded by tight D_3 folds with steep north-south axial surfaces.
- No radial extension lineations, most foliations are parallel to axial surfaces of F_2 and F_3. F_3 foliations are at a high angle to the east-west contacts.
- Lack of concordant foliations at greenstone and monzogranite contacts, the few that were detected were taken to be formed from sheared limbs of F_3 folds (along the contact zone).

Rey et al. (1995) concluded against the horizontal tectonics model of Myers & Watkins (1985), based on the following evidence:

- Steeply dipping regional foliation with a large variation in strike (50-90˚) (radial). Foliation wraps around hinges of greenstone synforms and trends parallel to granitoid/greenstone contacts.

	Watkins & Hickman 1990	van Kranendonk 2013	Walkins & Myers 1985	Stewart 2013
D1	Subhorizontal banding of Pegmatite banded gneiss, large isoclinal folds in the Luke Creek Group. Pegmatite banded gneiss protoliths intrude Luke Creek Group	Tilting of 2950Ma greenstones at golden grove prior to being uncomformably overlain by 2810 Ma sedimentary rocks.	Formation of gneissose layering in the pegmatite banded gneiss and layer-parallel foliation in some greenstones. These planar fabrics are cut by intrusions of monzogranite.	N-S extension and deposition/volcanism 2950, and tilting towards the south. Deposition of Windang Group rocks (2810Ma), uncomformably capping Gossan Hill Group.
D2	Upright east-west trending tight folds, with vertical axial planes and subhorizontal fold axes	Older greenstones of Polelle and Norie (>2735Ma) are tilted, locally folded and uncomformably overalin by basal coarse clastic sedimentary rocks of the 2730Ma Glen Group.	Folding with steep east-west axial surfaces and subhorizontal fold axes in the gneiss and greenstones, and a foliation partallel to these axial surfaces in monzogranite.	Tilting towards the south. Deposition of Windang Group rocks (2810Ma), uncomformably capping Gossan Hill Group. Ductile shear bands develop at low angles to stratigraphic contacts.
D3	Development of north-northwesterly trending tight and isoclinal folds, upright, with vertical axial planes. Formation of stong penetrative fabrics. Dome and basin patterns developed and form granite-greenstone pattern	Tight east-west trending folds of greenstones of the 2735-2700Ma Glen Group and 2735-2710Ma Yalgowra Suite	D3 folds D2 structures. Tight folds with steep north-south axial surfaces. Foliation parallel to D3 axial surfaces, intersection lineations seen in rocks with older fabrics. Prominent steep north-south foliation developed in monzogranite, parallel to axial surfaces of D3 folds in greenstones and pegmatite banded gneiss.	Tilting to the west. ENE-WSW orientated shortening. NNW crenulation clevage, related to regional folding.
D4	System of shear zones and faults debelop, trending north-northeast to north-northwest. Related to D3 folding, responding to E-W compression. F3folds become isoclinal towards shear zones and some sheath folding develops. Verticle and horizontal displacement within shear zones, possible controlling intrusion of post folding granitoids.	North to north-notheast trending folds and strike slipe shear zones, foliations and metamorphic mineral elongation lineations - overprint D3 structures.		

Table 4: Summary of Deformation. Coloured cells indicate correlating events. Note D2 and D3 folding events are evidenced throughout the region (green and pink).

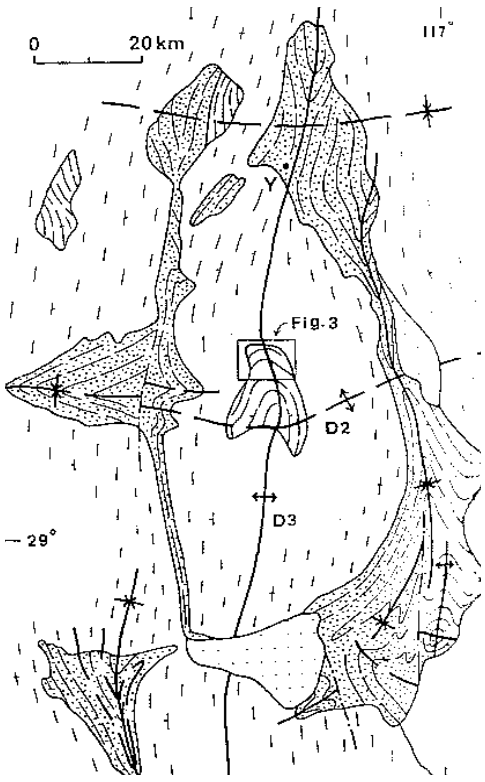

Figure 4: Simplified map from Watkins & Myers (1985) showing east-west D_2 folds intersected by north-south D_3 folds.

- Lineations dip and become more coherent towards greenstone contacts. Kinematic indicators suggest downward movement of greenstones relative to granitoids.
- Fold interference patterns only occur locally.
- Decrease in temperature from greenstones/granite contact toward the core of the greenstone.

Van Krandendonk et al (2013) investigated geometrical relationships between granitoids and greenstone synclines and found foliations oblique to bedding in the fold hinges. Axial planar foliations were present only in the innermost part of the fold hinge. This supports Rey et al. (1995) fold formation through sinking (downward movement) of greenstones into the granitoid rocks (figure 5).

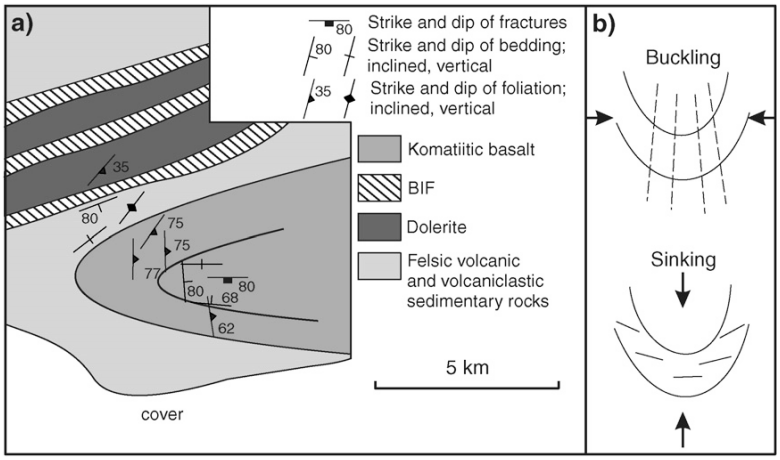

Figure 5: Bedding and cleavage relationships supporting downwards movement of granite with respect to greenstones. Horizontal compression would develop vertical axial planar foliations; the principle stress axis is orientated vertically during sinking and produces a foliation oblique to bedding (Van Kranendonk, 2013).

The Rey et al (1995) publication was based on an earlier masters manuscript by Foley (1995) (co-author of Rey et al 1995). Foley (1995) applied more recent techniques of identifying syn-magmatic deformation and closely examined the fabrics within the granitoid and greenstone rocks. A criterion was developed to discriminate between the two models (table 4). Foley (1995) concluded field evidence supported the diapiric model. In

particular, fabric wrapping around hinges of greenstone synformal troughs and trending parallel at the contacts (figure 6).

	Diapiric model	**Fold interference model**
At contacts	Magmatic to solid-state fabrics should trend parallel to granitoid/greenstone margins	North-south solid state fabric overprinting an east-west fabric. Continuous through both greenstone and granitoid rocks, regardless of orientation of contact
At hinges of greenstone synforms	Magmatic to solids-state fabrics within granitoids should wrap around hinges of greenstone and conform with contacts. There should be a greater number of fabrics within the greenstones, the main fabric axial planar.	Solid-state fabric should trend roughly north-south and may overprint earlier east-west fabric. Fabric should trend perpendicular to granitoid/greenstone contacts in hinges and become subparallel in limbs.
Within granitoids	Radial (variable) magmatic to submagmatic foliation	Penetrative north-south solid-state fabric overprinting east-west solid state fabric

Table 4: Criteria to distinguish between diapirism and Type 0 fold interference patterns (from Foley (1995).

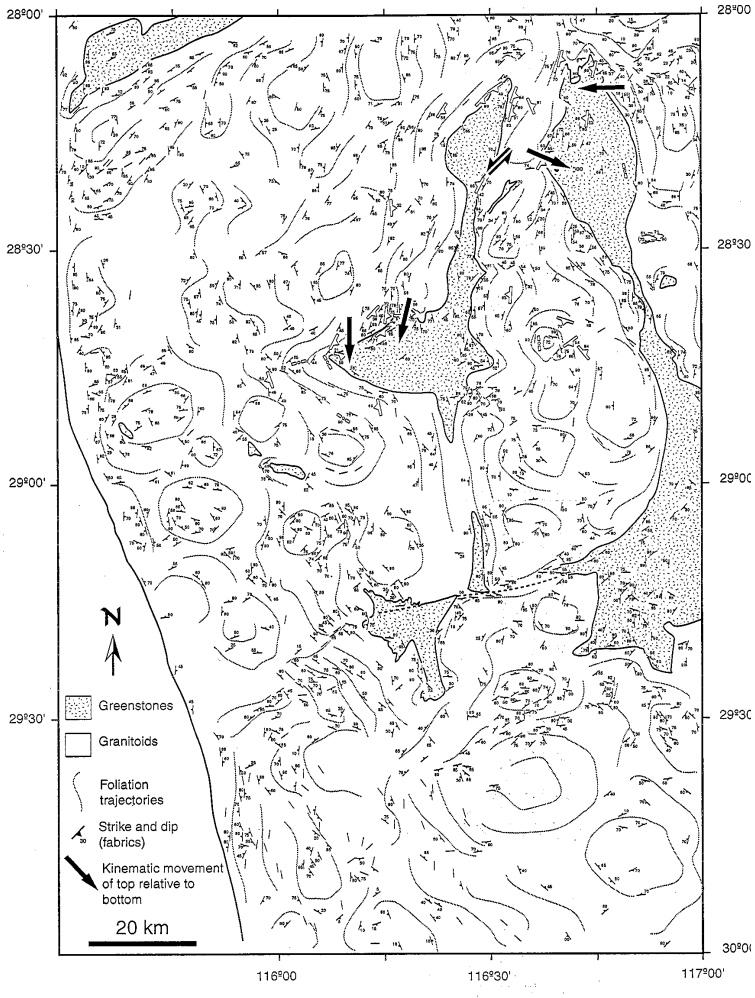

Figure 6: Map from Foley (1995) displaying strike and dip off fabrics (with trend lines) and kinematic sense of greenstones relative to granitoids (bold arrows).

(Other models of granite emplacement within the Yilgarn and Pilbara Cratons)

Tectonic Models

Van Kranendonk et al. (2013) reviewed and assessed two currently accepted tectonic models for the formation of the Murchison Domain and Yilgarn craton. Rock age data and stratigraphy were correlated across the Yilgarn craton, and crustal evolution was divided into a number of specific events.

Arc accretion model (figure 7)

Early accretion of the EGST onto the YT (2740-2730Ma) is consistent with the earliest extensional environments (back arc basins) and the later occurrence of plume-related komatiitic volcanism common to both terranes (2730-2720Ma). However, Van Kranendonk highlight the following points that do not support this model:

- Lack of structural features that indicate accretion.
- The model does not account for widespread granitic rocks dated prior to accretion and after accretion across the entire Yilgarn.
- Lack of high pressure mineral assemblages in the assumed foreland of accreted arcs.
- Lack of low grade rocks in assumed back-arc basins in later accreted arcs.

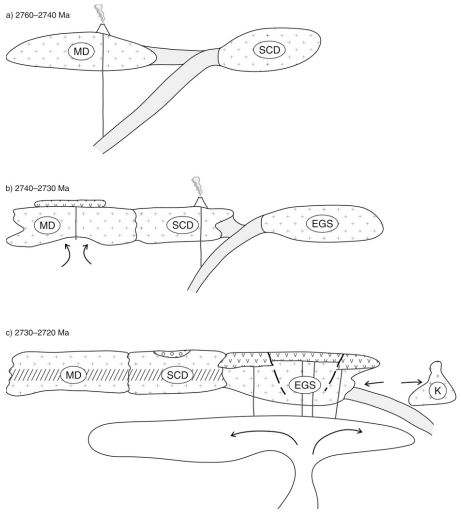

Figure 7: Arc accretion model from Van Kranendonk et al. (2013). MD – Murchison Domain, SCD – Southerncross Domain (Youanmi Terrane); EGS – Eastern Goldfields Superterrane. Note addition of mantle plume after accretion.

Plume Model *(figure 8)*

Van Kranendonk et al. (2013) explains that the rate of plume conduction through the crust can be correlated to the temporal change from mafic to felsic volcanism and widespread partial melting observed throughout the Yilgarn craton. This model does not account for the complex compositional change from mafic to felsic volcanism in different terranes. However Van Kranendonk et al (2013) note the change is possible in plume related volcanism by assimilation of crustal sources upon ascent and by different depths of partial melting, therefore this is the currently favoured model.

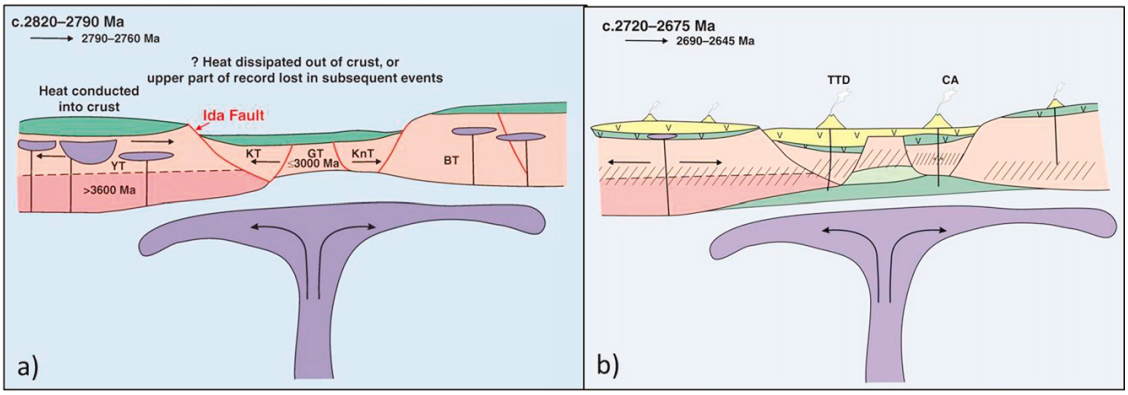

Figure 8: Plume model from Van Kroanendonk et al. (1995). Note widespread plutonism across the craton frm 2820-2790Ma. Basaltic underplating creates a reservoir for evolved magma generation, and the transition to widespread felsic volcanism 2720-2675Ma

It is interesting to compare the two contemporary models explained in Van Kranendonk et al. (2013) with the 5 stage horizontal tectonics model presented in Watkins & Hickman (1990), which supports the Watkins & Myers (1985) explanation of the granite/greenstone pattern throughout the Yilgarn Craton (figure 9).

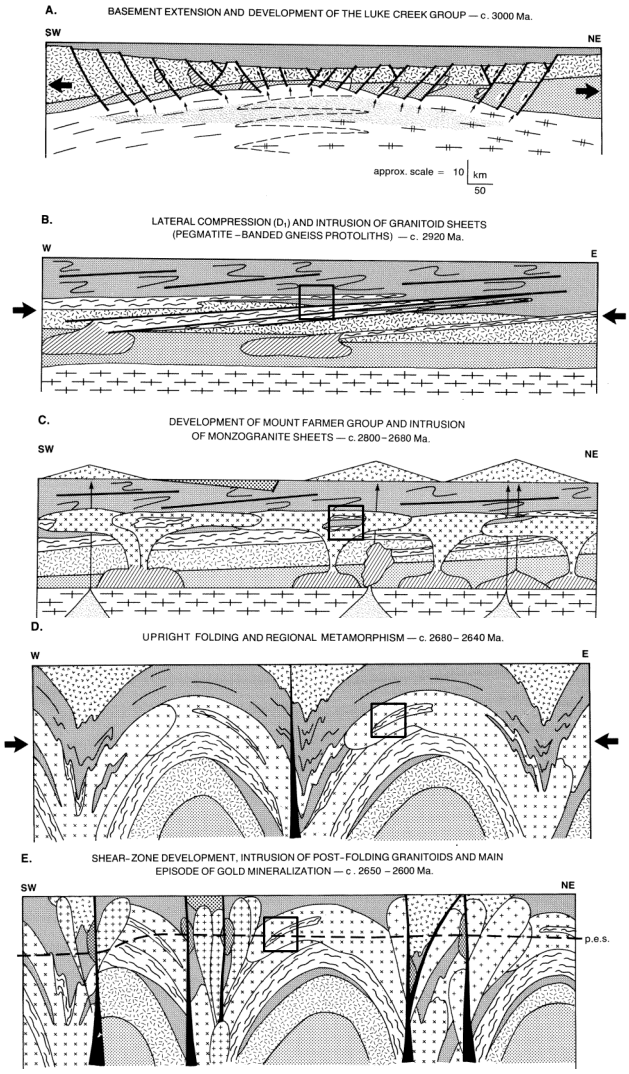

Figure 9: Horizontal tectonic model presented in Watkins & Hickman 1990.
a) Stage 1: 3000Ma - Basement extension and development of the Luke Creek Group (lowest volcanic sequence). Felsic volcanics resulted from partial melting of lower crust.
b) Stage 2: 2920Ma - Lateral compression and intrusion of pegmatite banded gneiss protolith.
c) Stage 3: 2800-2680Ma - Development of the Mount Farmer Group (upper volcanic sequence) and intrusion of Monzogranite sheets. Box highlights a raft of pegmatite banded gneiss interlayered with greenstone within a monzogranite sheet, this will later become the core of the Yalgoo Dome.
d) Stage 4: 2680-2640Ma - Upright folding and regional metamorphism, resulting in type 0 fold interference pattern. Box highlights core of Yalgoo Dome.
e) Stage 5: Shear zone development, intrusion of post folding granitoids. Subsequent erosion produces the granite/greenstone pattern throughout the yilgarn craton. Box highlights core of Yalgoo Dome.

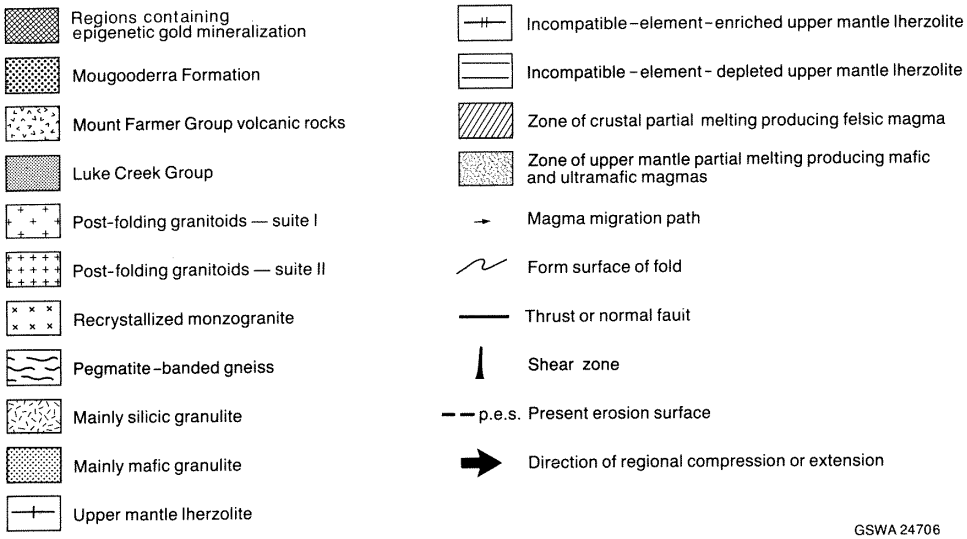

Conclusion

Van Kranendonk et al. (2013) synthesised primary data, and data from studies completed elsewhere in the in the Yilgarn Craton (for example Champion & Cassidy 2007, Ivanic & Van Kranendonk 2012) to create the new stratigraphic sequence and evolution for the Murchison Domain. The Yalgoo Dome was not encompassed in their field area. Few studies have been completed primarily focusing on the Yalgoo Dome. The Horizontal tectonic model used to explain the emplacement of the Yalgoo Dome and the granite greenstone pattern of the Yilgarn Craton in Watkins & Hickman (1990) and Watkins & Myers (1985) have been disproved by Rey et al. (1995), Foley (1995), Champion & Cassidy (2007) and the numerous papers from the Geological Survey of Western Australia. Plume and arc accretion models have been proposed that account for inconsistencies in the horizontal tectonics model, but they have their own flaws.

Within the Murchison Domain there is a consistent observation of upright folds with an axial plane trending east-west, and upright folds with an axial plane and related shear zones trending north-south. Regionally this has been caused by D_2 and D_3, but locally, the sequence of deformation events may differ (Stewart 2013). Ivanic & Van Kranendonk (2012) suggest D_2 and D_3 type 0 interference patterns are observable on a local level but not on a regional scale.

Although the work of Watkins & Hickman (1990) and Watkins & Myers (1985) has been outdated, their local stratigraphic descriptions, rock fabric descriptions, overprinting relationships and geochemical data have been extremely useful in subsequent studies. The current study being undertaken in the Yalgoo Area (in the south west quadrant of the Murchison Domain) and specifically on the Yalgoo Dome may lead to modifications and/or additions to the new stratigraphic scheme and deformation history of the region, it

could also provide insights that could correct inconsistencies in the current tectonic models.

References

ARCHIBALD N.J., BETTENAY L.F., BINNS R.A., GROVES D.I. & GUNTHORPE, R.J. 1978. The evolution of Archean greenstone terrains. Eastern Goldfields Province, Western Australia. *Precambrian Research* 6, 103-131.

CHAMPION D. C. & CASSIDY K. F. 2002. Granites of the Northern Murchison Province their distribution, age, geochemistry, petrogenesis, relationship with mineralisation, and I implications for tectonic environment. *In: Characterisation and metallogenic significance of archean granitoids of the Yilgarn Craton, Western Australia* pp. 1-54. 222.

CHAMPION D. C. & CASSIDY K. F. 2007. An overview of the Yilgarn craton and its crustal evolution. *Kalgoorlie '07 - Old Ground, New Knowledge, Geoscience Australia.* pp. 8-13.

FOLEY B. 1997. Reassessment of the archean tectonics in the Murchison Province, Western Australia. *ABSTRACTS - GEOLOGICAL SOCIETY OF AUSTRALIA* 46, 23.

IVANIC T. J., VAN KRANENDONK M. J., KIRKLAND C. L., WYCHE S., WINGATE M. T. D. & BELOUSOVA E. A. 2012. Zircon Lu–Hf isotopes and granite geochemistry of the Murchison Domain of the Yilgarn Craton: Evidence for reworking of Eoarchean crust during Meso-Neoarchean plume-driven magmatism. *Lithos* 148, 112-127.

KUSKY T.M. POLAT, A 1999. Growth of granite-greenstone terranes at convergent margins, and stabilization of Archean cratons. *Tectonophysics* 305, 43-73.

MYERS J.S. & WATKINS K.P. 1985. Origin of granite-greenstone patterns, Yilgarn Block, Western Australia. *Geology* 13, 778-780.

PIDGEON R. T. & Hallberg J. A. 2000. Age relationships in supracrustal sequences of the northern part of the Murchison Terrane, Archean Yilgarn Craton, Western Australia; a combined field and zircon U-Pb study. *Australian Journal of Earth Sciences* 47, 153-165.

REY P., COSTA S., VANDERHEAGUE O. & FOLEY, B. 1995. Archean regional strain field in the Yilgarn craton (WA): fold superposition or incremental strain field interferences. *Halls Gap SGTSG Conference Abstract Volume* pp. 221-222.

STEWART J. 2013. Golden Grove structural project, Western Australia (PGN geoscience). *MMG Mining Report*.

VAN KRANENDONK M. J. & IVANIC T. J. 2009. A new lithostratigraphic scheme for the northeastern Murchison Domain, Yilgarn Carton. *Geological Survey of Western Australia. Annual Review 2007-08*, 34-53.

VAN KRANENDONK M. J., IVANIC T. J., WINGATEA M. T. D., KIRKLAND C. L. & WYCHE S. 2013. Long-lived, autochthonous development of the Archean Murchison Domain, and implications for Yilgarn Craton tectonics. *Precambrian research* 229, 49-92.

WATKINS K. P. & HICKMAN A. H. 1990. Excursion No. 2: Murchison Granite-greenstone terrain.

Appendix A1: Rocks in the Yalgoo Area (from Watkins & Hickman 1990)

Name **Rocks that exist in the Yalgoo area**	Type	Description	Mineralogy	Deformation	Metamorphic Grade	Textures	Age	Geochemistry summary	Notes
Mount Farmer	Greenstone								
Yalgoo Supergroup									Confined to one greenstone belt - Yalgoo-Singleton GB. Represents an individual volcanic centre on an infrastructure of Luke Creek Group. Similar to *Porlell Subgroup*
Camberathunun Fomation		Sheared and weathered felsic volcanics, with small amounts of basalt and peridotite	Banded quartz-oligoclase-hornblende-chlorite. Felsic - Andesitic and probably pyroclastic	Sheared during D3 & D4, intensly deformed		Fragmental textures, altered		No data	
Singletone Basalt		Tholeiitic and high-Mg basalts, mafic pyroclastics, ultramafic rocks, gabbro, dolerite						Tholeiitic and high-Mg basalts: 10-20% partial melting of plagioclase/lherzolite source. Olivine and pyroxene crystllisation.	
Wadgingarra Basalt		Interlayered high-Mg and tholeiitic basalts, with minor amounts of ultramafics. Intruded by sills of gabbro, felsic porphyry and peridotite (now serpentine)	Tremoline-actinolite and oligoclase-andesine, minor chlorite, biotite, Fe-Ti oxides, sphene and quartz. Hornblende replacement of tremolite-actinolite in amphibolites.		Greeschist to lower amphibolite.	Lower 1800m is dominantly spinifex-textured, Upper 2200m is mainly tholeiitic basalt. Pillow lava occurs in the lower part 300-400m above base, elsewhere flow features are rare.		10-20% partial melting of upper mantle plagioclase-lherzolite, contaminated by felsic crustal material, crystal fractionation of olivine and pyroxenes	Spinifex textures are found in Komatiites. Occurs in the west of the hinge zone in the anticline north of Yalgoo
Mougooderra Formation		Sedimentary rocks and minor basalt ~2000m. Upward-fining sequence of epiclastic sedimentary rocks - Basal: medium to coarse grained, poorly sorted lithic wacke, with lenticular comglomerate beds (<10m thick). Clasts derived from underlying formations, no granitoid clasts. Middle: thin to thick beeded lithic wack, quartz arenite and shale, ripple marks. Upper: turbidite successions, siltstone and shale.		Extensive folding and faulting	Basalt - lower amphibolite: hornblende, olgolclase, biotite, chlorite, opaques. Synmetamorphic quartz segregations and post metamorphic quartz grains.	Basalt unit is strongly foliated, fine-grained featureless amphibolite. 200m thick in sandstone and shale layers. Spinifex texture and some pillow basalts		Seds - derived from underlying Windaning and upper Gabanintha formations. Basalt - 15% partial melting of a plagioclase/lherzolite source, crystal fractionation of olivine and pyroxene (+ crustal contamination).	Overlies Luke creek group (uncomformably) in Yalgoo area, occupies core of synclinal greenstone belts. Sheared contact with singleton basalt. Sed succession represent transition from shallow marine shelf to deeper distal sedimentary environments.
Luke Creek	Greenstone								
Upper volcanic sequence									
Windaning Formation		Abundant jaspilitic BIF and grey-white chert units interlayered with felsic volcanic, volcaniclastic and volcanogenic rocks, minor basalts. BIF's a few cms to 150m. Intruded by gabbro and dolerite sills, making up ~90% of sequence in the central part of the Yalgoo-Singleton GB.	Jasperlitic BIF - interlayered red jasper bands, black hematite and/or magnetite rich bands, white chert bands a few mm to cm's thick.		Greenschist BIF - quarts (crypto-grano), magnetite, hematite, siderite, pyrite, ankerite, calcite. Felsic interlayers - very fine grained, laminated, distal tuff with sedimentary structures;			BIF - chemical precipitation; Fesic volcanics - likely derived from crustal amphibolite source followed by crystral fractionation, some samples suggest low degrees of partial melting of a fracitonated crustal source (ganulite); Basalt tholeiite - ~20% partial melting of plagoclase-lherzolite source	Thick at Yalgoo-singleton GB. BIF distinguishable from lower volcanic sequence by its colour (red, white and black chert, Fe oxide bands), thickness (a few m to 150m) and associated rocks (dominantly felsics).BIF's form topographic prominent ridges and ranges of hills.
Gabanintha		Bimodal succession. Intrusive and extrusive ultramafics at base 1400m, overlain by high-Mg and tholeiitic basalt 1100m, and felsic volcanics and volcaniclastics 400m. Intruded by a layered gabbro sill 1000m,causing contact metamorphism to granulite facies. Felsic volcanic sequences throughout the provence represent individual volcanic compleses. Mafic and Felsic volcanism interlays indicate they were contemporaneous.	Felsics - Quartz, k-feldspar, plagioclase, epidote, biotite, amphibole, chlorite, sphene.	Cut by NW trending shear zones.		Felsics are strongly foliated and thoroughly recrystallised schists, with rare igneous textures.	2980+/-120 (Sm-Nd) Fletcher et al (1984)	Two types of basalts from source regions enriched and depleted prior to or during partial melting, fractional crystallised. Felsics - Two types - Low-(Zr+Y) formed from hydrous partial melting of crustal amphibolite, followed by fractional crystallisation, basaltic source rocks from upper mantle. High-(Zr+Y) from more mafic sources.	Most voluminous in Murchison, lowest stratigraphic formation south of latitude 28˚50', ~5000m thick.Felsic units represent individual volcanic centres. Epiclastic and sedimentary units underlie felsics at golden grove
Lower volcanic sequence									
Golconda Formation									Not in western most greenston belts or south of 28˚50'S
Murrouli Basalts		Succession of tholeiitic and high-Mg basalts, minor ultramafics, associated gabbro and dolerite sills. Up to 4,4000m thick. Base of basalt is always intrusive or tectonic contact with granitoid. Basement formation not recognised.		In high strain zones mafic rocks have become amphibolites.	Tholeiitic, basalt and gabbro - Greenschist - actinolite, albite-oligoclase, epidote, sphene, opaques. Amphibolite - hornblende, clinopyroxene, oligoclase-andesine, sphene, opaques. In unfoliated rocks metamorphic phases pseudomorph igneous textures. In foliated rocks they are aligned and overgrow tectonic fabric.	Tholeiitic basalt - dark green to grey, fine grained to aphanitic, featureless. High-Mg - Dark green with spinifex texture. Gabbro and Dolerite - medium to coars grained, massive. Pillow lava present at a few localities. Strong foliation, in particular next to monzo intrusions.		Theolites - 15-20% partial melting of upper mantle source - plagioclase/lherzolite with residual garnet and clinopyroxene, then fractionation of olivine and pyroxene and spinel probably during ascent to upper crust. High-Mg - partial melting of depleted mantle, olivine and spinel fractionation.	Two thin volcaniclastic units - lower breccia of basalt in a tuff matrix, upper heavilly altered tuff.
Name	**Type**	**Description**	**Mineralogy**	**Deformation**	**Metamorphic Grade**	**Textures**	**Age**	**Geochemistry summary**	**Notes**
Post Folding Granitoids (PFG) Suite II	Granitoid	Occur in three situations - interiors of GB's, contacts between recrystallised MZG and GB's, apices of GB's in RMG. Non within RMG (wholly).	Quartz rich monzogranite and syenogranite - quartz, k-feld, plagioclase, biotite (hornblended, muscovite)	Subcircular, discordant outcrop patterns that truncate stratigraphic units. Cut by D_4 shear zones.	Sharp contacts, contact aureoles a few hundred metres wide in albit-epidote and hornblende hornfels facies.	Appear texturally homogenous (apart from abundant xenoliths. Parting clevage paallel to granitoid contact in some aureoles.	U-Pb: 2641-2617; Sm-Nd: 3153, 3301Ma - much older than emplacement ages - older source with different composition relative to Type I. Rb-Sr: 2600Ma - corresponds to metamorphic event	Two distinct sources for type I and type II.	Higher proportions of ferromagnesium phases than RMG and PBG; occur in interior of GB's, contacts between RMG, apices of GB's in RMG
Recrystallised Monzogranite (RMG)	Granitoid	Most voluminous, recrystallised during regional metamorphism. Abundant cognate inclusions and xenoliths. Pegmatites and aplites are abundant, particularly adjacent to GB's.	Quartz, oligoclase, k-feldspar, biotite; minor chlorite, epidote, amphibole, muscovite, opaques, sphene, apatite, zircon, cabonates.		Secondary mobilisation during regional metamorphism evidenced by biotite retrograded to chlorite, loss of K/Rb, albitisation of calcic oligoclase grain rims	Three textural varieties - equigranular, porphyritic, sparsely porphyritic (all medium-coarse grained). Igneous textures recrystallised, crystalloblastic textures. Original magmatic phenocrysts pseudomorphed by microcline.	U-Pb: Equigranular foliated - 2681Ma; Porphyritic unfoliated - 2690Ma. Sm-Nd - 2837, 2827, 2794 & 2846Ma - two fractionation events from mantle sources. Rb-Sr: 2535 - 2706Ma	Porphyritic monzogranite is slightly more fractionated then equigranular. Less fractionated REE patterns relative to PBG - representing residual garnet/or amphibole sources - smaller degrees of partial melting of more fractionated source rocks.	Igneous textures obliteratd to granoblastic and lepidoblastic in unfoliated and foliated rocks. Intrusive contact and crosscutting relationships indicate porphyritic monzogranite intruded medium-grained equigranular monzogranite, the rare fine-grained phase intruded other 'textural variants'. Close compositional similarities between MZG and PBG suggest an association "It is unlikely MZG was derived by anatexis of PBG would require F=0.9" - maybe derived at different times by similar processes and from similar sources.
Pegmatite Banded Gneiss	Granitoid	Three components - 2 monzogranite-granodiorite phases and a pegmatite phase.	1st Monzogranite-granodiorite: medium-grained, finely banded, biotite rich and quartz-feldspar-rich layers, a fem mm to 1cm thick. Pegmatite: medium-to-coarse-grained quartz-feldspar bands a few cm thick, interlayered parallel to gneissosity. 2nd phase: intrudes earlier components as veins and dykes during deformation which forms gneissosity. (quartz-oligoclase-microcline-biotite, minor opaques, epidote, sphene, apatite, zircon) Perthitic microcline, oligolcase rimmed by albite.	Gneissosity reflects intense deformation. Planar elements rotated subparallel.	Biotite retrograded to aggegates of chlorite and rutile.	Pegmatite bands - microcline-oligoclase, quarzt - granoblastic and lepidoblastic. No remnenats of igneous texture.	Boungnoo 2933; Badja 3171, 2932. Sm-Nd indicate two fractionation events, derivation of source rock from mantle and partial melting.	Geniss protolith crystallised with plagioclase and quartz on liquidus, K-felds later. Biotite crystallised after intial plag crystallisation. Fluid pressure may have resulted in the abundance of pegmatites.	Large enclaves, rafts and partially absorbed remnants in RMG. Pegmatite bands intrude gneiss.

Appendix A1: Stratigraphic scheme proposed by Van Kranendonk et al. (2013)

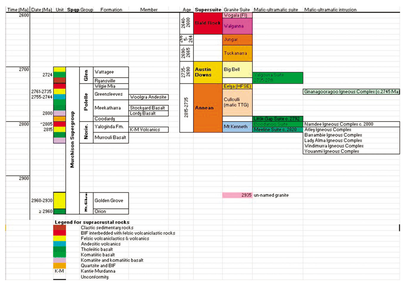

APPENDIX D

STRUCTURAL AND LITHOLOGICAL MAP OF THE YALGOO DOME CORE

MONASH University

Northeast Murchison Province, Yilgarn Craton, Western Australia

M. J. Fenwick

School of Earth, Atmosphere and Environment, Monash University, Victoria, Australia

Government of Western Australia
Department of Mines and Petroleum

Figure 1: Regional and Local setting

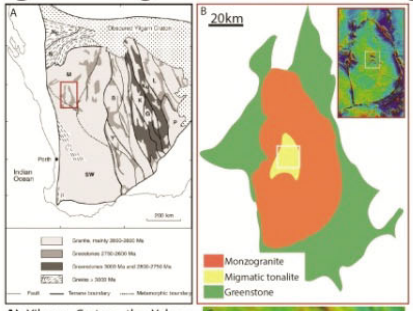

A) Yilgarn Craton, the Yalgoo Dome is in the red square. Modified from Chen & Wyche (2001).
B) Simplified geological map of the Yalgoo dome. Study area is inside the white box, refer to C). **Inset:** aeromagnetic image of the Yalgoo dome from the 2013 GSWA geophysical survey.
C) Aeromagnetic image of the core with the location of each study area.

Figure 2: Central Domain

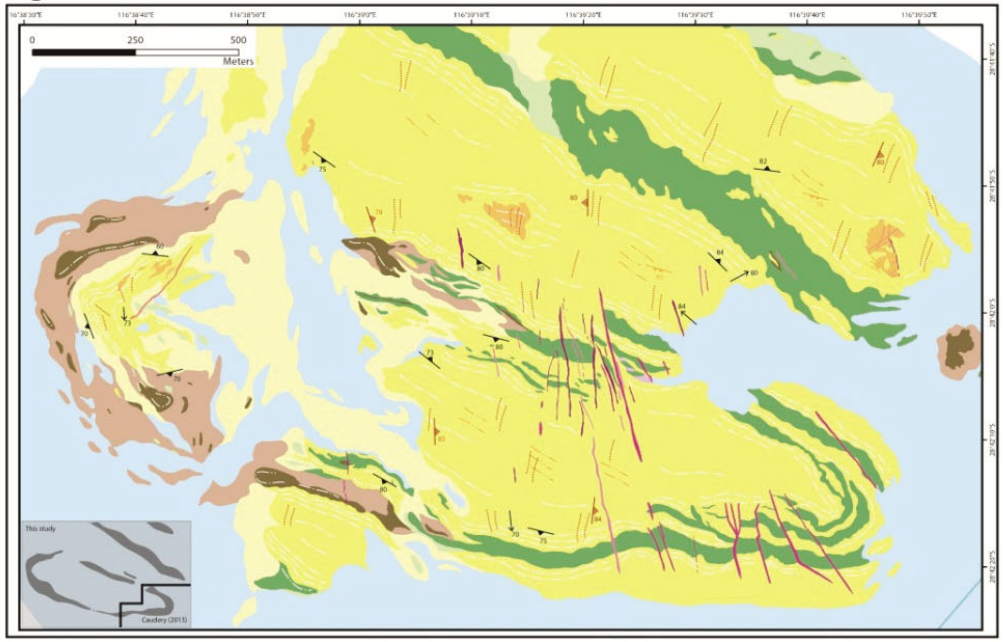

Figure 3: Western Domain

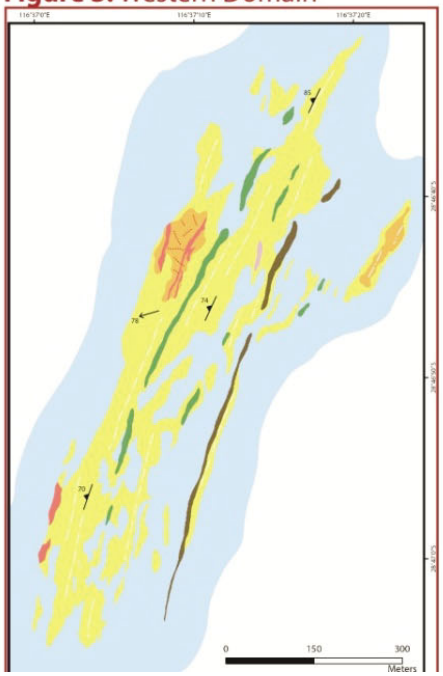

Figure 4: Eastern Domain

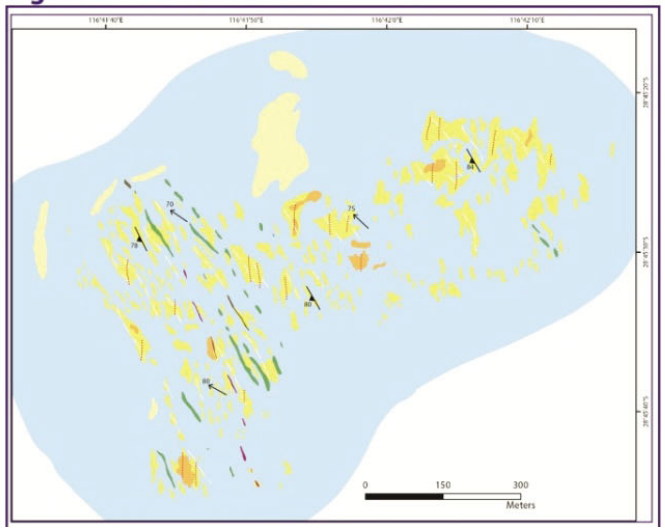

Legend

LITHOLOGIES

Colluvium (undifferentiated) and regolith

CROSS-CUTTING DYKES

SCHLIERIC: granitic (Kfs, Pl, Qtz, Bt). Equigranular (0.2<2mm). Contains discontinuous schlieric *'ghost layering'*.

SCHLIERIC - PORPHYRITIC: granitic (Kfs, Pl, Qtz, Bt). Kfs phenocrysts (1<3mm). Contains discontinuous schlieric *'ghost layering'*.

PORPHYRITIC: granitic (Kfs, Pl, Qtz, Bt). Kfs phenocrysts (1<8mm). Equigranular groundmass (0.2<2mm).

PEGMATITIC: Pl, Qtz, Kfs. coarse grained (8<15mm)

MIGMATITIC TONALITE

Stromatic metatexite migmatite. Fine-medium grained (0.2<4mm). Pl, Qtz, Bt, Kfs, Hbl, Mag, ±Ep, ±Ttn, ±Zrn, ±Mnz.

Well preserved platform

Very weathered - lateritic. In-situ and loose rubble.

GREENSTONES: BANDED IRON FORMATION

Interlayered ferruginous and siliceous aphanitic bands (1<4mm). Weakly magnetic.

Very weathered - lateritic. In situ and loose rubble. Lacks siliceous banding. Not magnetic.

AMPHIBOLITE

Fine grained (1<3mm). Hrn, Pl, ±Cpx. Contains felsic bands 2<20mm thick (Qtz, Pl, Kfs, ±Hrn). Ranges in texture from 'salt & pepper' to homogenous black.

Outcrop of disaggregated amphibolite in migmatitic tonalite. Dark layers of medium-coarse grained 0.4< 5mm amp aggregates interlayered

Very weathered - lateritic. In-situ and loose rubble.

SYMBOLS

S1/S2: foliation trace

S2: axial planar foliation to F2 sheath folds

S3: foliation, shear band trend

S1/S2 foliation

S2 axial planar-foliation

S3 foliation

L1 lineation

N

Figure 5: Western Domain structural data

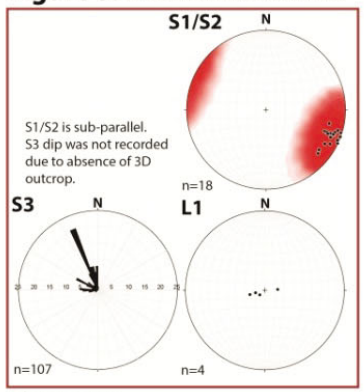

Figure 6: Central Domain structural data

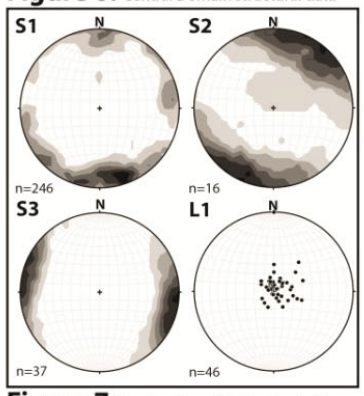

Figure 7: Eastern Domain structural data

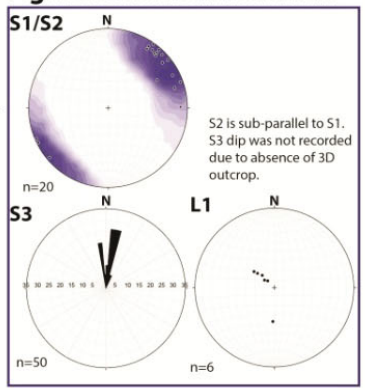

RECORD 2014/16

STRUCTURAL EVOLUTION OF THE YALGOO DOME, YILGARN CRATON, WESTERN AUSTRALIA: A CORE PERSPECTIVE

This Record is published in digital format (PDF), is available on USB and as a free download from the DMP website at <www.dmp.wa.gov.au/GSWApublications>.

Further details of geological products produced by the Geological Survey of Western Australia can be obtained by contacting:

Information Centre
Department of Mines and Petroleum
100 Plain Street
EAST PERTH WESTERN AUSTRALIA 6004
Phone: (08) 9222 3459 Fax: (08) 9222 3444
www.dmp.wa.gov.au/GSWApublications

Fenwick